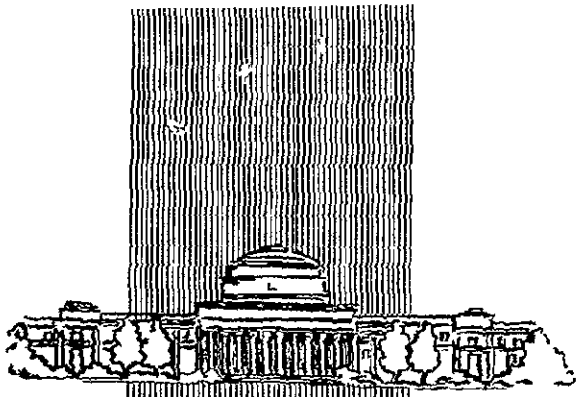

MASSACHUSETTS INSTITUTE OF TECHNOLOGY

NGR-22-009-207

TE-39

PRECISION TARGETING FOR MULTIPLE SWINGBY INTERPLANETARY TRAJECTORIES

by

Stephen S. Bayliss

MEASUREMENT SYSTEMS LABORATORY

MASSACHUSETTS INSTITUTE OF TECHNOLOGY

CAMBRIDGE 39, MASSACHUSETTS

TE-39

PRECISION TARGETING FOR MULTIPLE SWINGBY INTERPLANETARY TRAJECTORIES

by

Stephen S. Bayliss

June, 1970

Measurement Systems Laboratory
Massachusetts Institute of Technology
Cambridge, Massachusetts 02139

Approved: 

Director
Measurement Systems Laboratory

PRECISION TARGETING FOR MULTIPLE SWINGBY INTERPLANETARY TRAJECTORIES

by

Stephen Summers Bayliss

S.B., Massachusetts Institute of Technology, 1965

S.M., Massachusetts Institute of Technology, 1966

SUBMITTED IN PARTIAL FULFILLMENT

OF THE REQUIREMENTS FOR THE

DEGREE OF DOCTOR OF PHILOSOPHY

at the

MASSACHUSETTS INSTITUTE OF TECHNOLOGY

May 1970

Signature of Author Stephen Summers Bayliss
Department of Aeronautics and Astronautics
May 1970

Certified by R. Battin
Thesis Supervisor

Certified by Wallace E. Vander Velde
Thesis Supervisor

Certified by H. Miller
Thesis Supervisor

Certified by Walter McKay
Thesis Supervisor

Accepted by Judson R. Baron
Chairman, Departmental Graduate Committee

PRECISION TARGETING FOR MULTIPLE SWINGBY

INTERPLANETARY TRAJECTORIES

by

Stephen Summers Bayliss

Submitted to the Department of Aeronautics and Astronautics on May 11, 1970 in partial fulfillment of the requirements for the degree of Doctor of Philosophy.

ABSTRACT

Most recent studies involving multiple swingby interplanetary trajectories have been made using a simplified model consisting of a sequence of heliocentric conic arcs matched in relative hyperbolic exess velocity at each planetary encounter. This model provides adequate results for preliminary mission planning and analysis but as more advanced investigations are undertaken, an accurate N-body reference trajectory becomes necessary. This thesis presents a technique for the rapid determination of such a reference trajectory.

The gap between the simple conic model and the integrated N-body trajectory is bridged in two steps. The first of these utilizes a model of the trajectory consisting of alternating planetocentric and heliocentric conic legs corresponding to trajectory segments inside and outside of the planetary spheres of influence. The trajectory legs are constrained to match in position and time but are initially mismatched in velocity. An iteration scheme is developed to drive this mis-match to zero. As the second step, N-body perturbed trajectories are calculated which have the same end conditions in position and time as the conic legs in the previous step but have slight offsets in initial and final velocities. The same iteration scheme utilized in the first step is employed to match these perturbed segments in velocity as well as position and time. Finally, the accuracy of each trajectory leg is checked by numerical integration.

Three examples are considered in detail. They are.

1) a dual planet reconnaissance trajectory (Earth-Venus-Mars-Earth
2) Grand tour trajectory (Earth-Jupiter-Saturn-Uranus-Neptune)
3) periodic trajectory (a repeating Earth-Venus shuttle trajectory)

Free-fall trajectories are determined for the first two of these examples. Comparison with numerically integrated trajectory legs has shown these solutions to be accurate to better than 0.4 m/sec in initial and final velocity for heliocentric trajectory legs and better than 0.1 m/sec for planetocentric legs. No free-fall trajectory was found for the third example but a powered trajectory (with a total Δv of 220.5 m/sec) is presented. In general, accuracies comparable with the results of the preceding two examples are obtained.

Thesis Supervisors:

Professor Walter M. Hollister
Title: Associate Professor of Aeronautics and Astronautics, M.I.T

Professor Wallace E. Vander Velde
Title: Professor of Aeronautics and Astronautics, M.I.T.

Professor Walter McKay
Title: Professor of Aeronautics and Astronautics, M.I.T.

Professor Rene H. Miller
Title: H. N. Slater Professor of Flight Transportation, M.I.T.

ACKNOWLEDGEMENTS

The author wishes to thank his Doctoral Thesis Committee, Prof. Walter Hollister, Committee Chairman, Prof. Wallace Vander Velde, Prof. Walter McKay, and Prof. Rene Miller for their continued understanding, support, and encouragement throughout his doctoral program and thesis research. He would particularly like to express his appreciation to Prof. Hollister whose suggestions and criticisms were of great help in the completion of this thesis. He would also like to mention the assistance of Dr. Robert Stern and his other associates at the Measurement Systems Laboratory.

Acknowledgement is also made to the M.I.T. Computation Center for work performed under Problem Number M4131.

The author also wishes to thank his wife Diane not only for her typing of the early drafts of this thesis but also for her continued patience and understanding.

The final draft of this thesis was prepared by Miss Ann Archer and Mrs. Margarete Palazzi. Their efforts are gratefully acknowledged.

This research was sponsored in part by grant NGR-22-009-207 from the National Aeronautics and Space Administration. The publication of this report does not constitute approval by the National Aeronautics and Space Administration of the findings or the conclusions contained therein. It is published only for the exchange and stimulation of ideas.

TABLE OF CONTENTS

LIST OF FIGURES

LIST OF TABLES

Chapter 1
Introduction

1.0 Objectives of the Thesis

This thesis describes a technique for the determination of accurate reference trajectories for multiple swingby interplanetary trajectories. The main objectives of the research are the following:

1) To develop a basically analytic technique for the determination of multiple swingby reference trajectories which will converge rapidly from a wide range of initial guesses to a solution with a high level of accuracy.

2) To provide a means of specifying a multiple swingby trajectory with uniform accuracy along its entire length by providing a sequence of guidance aiming points spaced along the trajectory

3) To provide a simple, accurate and economical means for performing detailed mission analysis for multiple swingby trajectories.

4) To demonstrate the feasibility, accuracy, and generality of the technique by its application to three examples; a dual planet reconnaissance trajectory, a Grand Tour trajectory, and a periodic trajectory segment.

1.1 Definition of the Problem

The determination of space trajectories is usually posed as a two-point boundary value problem. The initial and final position vectors and the time of flight between them are given along with the equations of motion for the trajectory. The calculation of the reference trajectory which satisfies these conditions is the targeting problem. This thesis deals with the problem of targeting for trajectories charaterized

by one or more close planetary encounters between their launch and arrival points.

1.2 Existing Targeting Techniques and Their Application to Multiple Swingby Trajectories

The use of multiple swingby trajectories to substantially reduce the launch energy and flight time for a number of highly interesting missions has long been recognized [1,2]. Each close planetary encounter provides an opportunity to alter the energy of the trajectory with respect to the sun by use of the planetary gravitational field. In effect, the spacecraft exchanges energy with the planet. This ability to make major heliocentric velocity changes along the trajectory without fuel expenditure allows considerable flexibility in mission planning. Examples of some of the missions which have proposed are

1) Earth-Mars-Earth [3,4]
2) Earth-Venus-Earth [3]
3) Deep Space, Solar Probe and Out-of-Ecliptic [5,6]
4) Earth-Venus-Mercury [7,8,9]
5) Earth-Venus-Mars-Earth [3,10,11,12,13,14,15]
6) Outer Planets Missions [16,17,18,19,20,21]
7) Earth-Venus and Earth-Mars Periodic Orbits [22,23,24,25]

The majority of these studies have been concerned primarily with preliminary mission planning and guidance requirements studies using simplified models for targeting. To the author's knowledge, the only multiple swingby mission for which precision reference trajectories have been generated is the Earth-Venus-Mercury flight [7,8].

Present targeting techniques for multiple swingby interplanetary trajectories fall into two general classes. The first of these uses an approximate model for the mission consisting of a sequence of heliocentric conic arcs running from the center of one massless planet to

the next. Thus, the trajectory is determined by giving the order in which the specific planets are encountered along with the launch, arrival, and encounter dates. The effects of the planets on the trajectory are approximated as impulsive changes in velocity with respect to the Sun at each planetary encounter. Using this model, a search is made over a range of departure, arrival, and intermediate encounter dates to determine combinations which yield trajectories which are matched in hyperbolic excess velocity relative to the planet at each intermediate encounter and which are physically realizable in the sense that they do not require the trajectory to pass beneath the surface of any planet. This search may be carried out exhaustively to determine all possible swingby trajectories within the range of dates specified, [1,19] or may use an iterative technique to converge on a single set of dates [22]. The advantage of this technique lies in the speed with which each trajectory may be calculated.. Since the model assumes the trajectory to be a sequence of two-body legs, each may be determined as the solution to Lambert's Problem. The disadvantages of this technique are

1) The large number of trajectories which must be generated. For an exhaustive search procedure, large numbers of date combinations must be examined. An iterative technique mitigates this difficulty but may not provide all possible solutions.

2) The inaccuracies of the model. Both numerical [7,8,28] and analytic [27] studies have indicated that while the above model is acceptable for preliminary studies, it does not have sufficient accuracy for precise trajectory prediction for close planetary encounters.

In general, approximate targeting schemes presently employed for multiple swingby trajectories are most useful for preliminary mission

studies and for the generation of initial conditions for more accurate targeting techniques.

The other class of targeting procedures which have been applied to multiple swingby trajectories utilize numerical integration techniques to generate precision reference trajectories. An example of this procedure as applied to an Earth-Venus-Mercury trajectory in [8] is as follows,

1) Initialize the launch conditions at Earth and the aiming point at Venus with the conic values from an approximate targeting technique.

2) Search over the injection conditions at Earth until a numerically integrated trajectory hits the desired aiming point at Venus.

3) Continue the converged case from 2) on to Mercury and note the resulting miss of the desired target point there.

4) Perturb the aiming point at Venus and repeat steps 2) and 3).

5) From the results of step 4), construct partials of the miss at Mercury with respect to changes in the aiming ppint at Venus.

6) Compute and apply differential corrections to the aiming point at Venus.

7) Repeat steps 2) 3), and 6) until convergence at Mercury is obtained.

The average running time for a convergence criterion of $\pm$ 1000 km at Mercury was about 45 minutes on the IBM 7094. A variation on this technique employs a many-body state transition matrix obtained by the numerical integration of the variational equations to determine the

differential corrections in the targeting process. This latter method has been used [26] for the targeting of single leg trajectories (e.g. Earth-Venus or Earth-Mars) but to the author's knowledge has not been applied successfully to multiple swingby trajectories.

The advantage of the numerical integration technique is that it gives a completely defined accurate reference trajectory. All significant disturbing forces may be included to the degree of precision available on the computer used. The disadvantages of the technique are the large amount of time consumed by the repeated numerical integration of the trajectory legs and the question of its feasibility for trajectories involving more than one intermediate swingby. This latter difficulty arises from the strong sensitivity of the trajectory to small changes in swingby conditions for planetary encounters earlier in the trajectory. Thus, as more swingbys are added to the trajectory, the accuracy requirement for the determination of the earlier swingbys increases greatly. For the same reason, the linearity region for the differential correction process shrinks. Both of these reasons lead to a large increase in the number of numerical integrations of trajectory legs needed. This difficulty did not arise in the approximate targeting schemes since the trajectory was modeled as a set of shorter arcs to be matched dynamically at a number of intermediate points rather than as a single arc determined entirely by its initial conditions.

The targeting procedure developed in this thesis attempts to combine the advantages of both the approximate and the numerical integration techniques while minimizing the disadvantages of both.

1.3 Synopsis of Thesis

In Chapter 2, two patched conic models and their application to multiple swingby trajectories are described. The first corresponds to

the approximate model described in the preceding section. The second (the advanced patched conic model) adds planetocentric conic legs between the heliocentric conic legs to describe the swingby maneuver more completely and accurately. The conic legs are constrained initially to match only in position and time. Then, an iterative process is employed to vary the matching points until the legs also match in velocity.

Chapter 3 describes a basically analytic method for computing the perturbations of conic legs due to the disturbing accelerations of other bodies. A technique is developed for calculating the initial and final velocity offsets for each conic leg needed to produce a perturbed trajectory having the same initial and final conditions in position and time as the unperturbed conic reference leg.

Chapter 4 deals with the iterative techniques of matching the individual trajectory legs (either perturbed or unperturbed) in velocity as well as position and time. Both first-order and second-order techniques are developed.

Chapter 5 presents numerical results for a dual planet reconnaissance trajectory. The reference trajectory is specified by the position, velocity, and time at the sphere of influence entry and exit points for the launch, arrival, and swingby planets. Comparison with numerically integrated trajectory legs indicates that the analytically calculated trajectory legs match to within a total error in velocity of 0.2263 m/sec.

Chapter 6 presents the same results for a Grand Tour trajectory example. Here the trajectory segments were matched analytically to within a total error of 2.652 m/sec.

Chapter 7 discusses a segment of a periodic trajectory that shuttles between Earth and Venus. No free-fall trajectory was found

for this example but a powered trajectory requiring a total impulse of 220.534 m/sec over the 3.6 year segment considered was determined. The special nature of this trajectory resulted in less accurate predictions by the analytic technique with the total error amounting to 38.950 m/sec.

Chapter 8 summarizes the thesis and its contributions. Several applications of the techniques developed are suggested for further research.

Chapter 2

PATCHED CONIC ANALYSIS

2.0 Chapter Summary

The application of two patched conic models to multiple swingby trajectory analysis is described. The first of these, the simple patched conic model, consists of a sequence of heliocentric conic arcs matched in relative velocity magnitude at each planetary encounter. It is found to be most suitable for preliminary mission analysis. The second, the advanced patched conic model, considers the trajectory to be approximated by a series of alternating heliocentric and planetocentric conic arcs matched in position, velocity and time at the entry and exit points of the sphere of influence of each planet encountered. It is found to be a more useful model for reference trajectory calculations. The computational details of the advanced patched conic model are examined in depth and limitations on its accuracy considered.

2.1 The Simple Patched Conic Model

The simple patched conic model has been successfully employed for a number of preliminary trajectory and mission analysis studies. Examples of its use for multiple swingby missions may be found in [22, 7, 10, 16, 18, 6] and many others. The model consists of a sequence of heliocentric conic arcs matched in magnitude of velocity relative to the planet at each planetary encounter. An illustration of one such trajectory is given in Figure 2.1. The steps followed for a trajectory with N planetary encounters (launch, N-2 intermediate swingbys, and arrival) are:

1) Specify the launch date t_1, the arrival date t_N, and the N-2 intermediate encounter dates t_2, t_3,..., t_{N-1}.

2) At each date t_k, calculate the position $\underline{r}_{P,k}$ and the velocity $\underline{v}_{P,k}$ of the planet encountered.

3) For each date t_k (except for k=N) calculate a heliocentric conic arc running from $\underline{r}_{P,k}$ to $\underline{r}_{P,k+1}$ with a time of flight $T=t_{k+1}-t_k$ (See Appendix B for the method of calculating these arcs). Each arc will have associated with it a planetary departure velocity $\underline{v}_{D,k}$ and a planetary arrival velocity $\underline{v}_{A,k+1}$, both of which are measured relative to the sun.

4) For each intermediate date t_k (k=2,3,...N-1) calculate the incoming and outgoing velocities relative to the planet encountered.

$$\underline{v}_{I,k} = \underline{v}_{A,k} - \underline{v}_{P,k}$$
$$\underline{v}_{0,k} = \underline{v}_{D,k} - \underline{v}_{P,k} \qquad (2.1)$$

For a free-fall trajectory to be dynamically possible, the magnitudes of these velocities relative to the planet must be equal at each encounter. Using some convenient iteration scheme (see [22] for an example), the intermediate encounter dates are varied and steps 2 to 4 repeated until this condition is satisfied.

Note that while the incoming and outgoing velocities ($\underline{v}_{I,k}$ and $\underline{v}_{0,k}$) relative to the planet are equal in magnitude, the arrival and departure velocities ($\underline{v}_{A,k}$ and $\underline{v}_{D,k}$) relative to the sun usually differ in both magnitude and direction. The model considers the planetary swingby to be equivalent to an instantaneous velocity change of

$$\Delta \underline{v}_k = \underline{v}_{D,k} - \underline{v}_{A,k} \qquad (2.2)$$

relative to the sun applied at the time of encounter.

Once the simple patched conic trajectory has been determined, some information on the planetary encounter phases may be obtained. Using the incoming and outgoing velocities ($\underline{v}_{I,k}$ and $\underline{v}_{0,k}$) relative to the planet as approximations to the asymptotic velocity vectors, the constants for a planetocentric hyperbola may be determined and the relevant parameters for the swingby calculated. The accuracy of this approximation is studied in [27]. There it is shown that the approximate swingby parameters differ from their time values by terms of order ϵ, the planet-to-sun mass ratio.

The advantages of the simple patched conic model are its simplicity, ease of implementation, and speed of computation. A large number of trajectory alternatives may be explored with a relatively small investment in computer time. Thus this model is well suited for preliminary mission analysis. The basic limitations of the simple patched conic model are:

1) The heliocentric conic arcs and the planetocentric hyperbolas are matched only approximately. The model does not provide a continuous or highly accurate description of motion in the vicinity of a planetary encounter.

2) The effects of the planetary encounter are approximated as an impulse rather than considered to act over a region in space and time.

3) All trajectory segments are considered to be conic arcs. The effects of all perturbation other than the close planetary encounters are ignored completely.

2.2 Advanced Patched Conic Model

To eliminate some of the inaccuracies and assumptions of the

simple patched conic model and to lay the groundwork for a later perturbation analysis, a more advanced patched conic model is necessary. This model consists of a sequence of alternating heliocentric and planetocentric conic arcs constrained to match in position and time at the sphere of influence (SOI) entry and exit points of each planet encountered. An illustration is given in Figure 2.2. These entry and exit points are chosen initially from the solution for the simple patched conic model and usually result in velocity mis-matches between the conic arcs. An iterative procedure is necessary to drive this mismatch to zero. The SOI used is defined in Appendix C. It is somewhat larger than the Laplace SOI commonly used. The application of this model to a trajectory with N planetary encounters (launch, N-2 intermediate swingbys, and arrival) is as follows:

1) At each intermediate encounter, specify the entry and exit points on the planetary SOI. At the launch planet, specify the exit point and at the arrival point specify the entry point. An entry point on the SOI is given by its azimuth, elevation, and time of passage. An exit point on the SOI is given by the increments in azimuth, elevation and time from the corresponding entry point on the same SOI. The one exception to this is the exit point at the launch planet, which is specified in the same way as an entry point. The radius of the SOI is assumed to be a constant for each planet.

2) For each time t_k of entry or exit through the SOI calculate:

    a) the position $\underline{r}_{p,k}$ and velocity $\underline{v}_{p,k}$ of the planet (this is discussed in Appendix C).

b) the cartesian coordinates of the entry or exit point with respect to the planet encountered.

3) For each point k (except the last) calculate a conic arc from point k to point k+1. For even k (entry points), this will be planetocentric arc which will always be a hyperbola with a central angle greater than 180°. This arc will run from the entry point to the exit point of a single planet's SOI. For odd k (exit points), the arc will be heliocentric and may be either an ellipse or a hyperbola. It will run from the SOI exit point of one planet to the SOI entrance point of the next.

4) At each intermediate entry or exit point, calculate the difference in velocity between the heliocentric and planetocentric arcs. In Chapter 4, an iterative technique for varying the position and time of these points in order to eliminate the velocity mis-match is described.

After steps (1) - (4) have been repeated until convergence is achieved, the result is a series of conic arcs continuous in position, velocity and time at all points. Discontinuities in acceleration occur at the SOI entry and exit points since a planet's gravitational field is ignored outside of its SOI while the solar perturbing forces are neglected inside of an SOI. Several points to be noted about this model are:

1) For a trajectory with N planetary encounters, there are 2N-2 matching (entry or exit) points specified in position and time along the trajectory. Odd-numbered matching points are SOI exit points while even-numbered ones are SOI entry points.

2) The different means used to specify entry and exit points provides some separation in the effects of varying these points. The two heliocentric arcs touching the planet's SOI are affected primarily by changes in the entry point. The heliocentric arc leaving the planet is also affected by exit point changes but these effects are usually much smaller than those due to the entry point changes. The planetocentric arcs are affected primarily by exit point changes.

3) This model considers the effects of an planetary encounter to be distributed over a region in both time and space. This is a more accurate approximation to the actual interaction than is provided by the simple patched conic model.

4) A continuous description of the motion along every phase of the trajectory is given. This also provides a basis for the perturbation analysis to be described in Chapter 3.

A detailed discussion of the computations involved in several of the steps in the advanced patched conic model is given in the next section.

2.3 Computational Details

2.31 Entry and Exit Point Coordinates

The state vector for an entry or exit point is given by

$$\underline{x}_k = \begin{bmatrix} \theta_k \\ \phi_k \\ t_k \end{bmatrix} \qquad \begin{matrix} k=\text{even} \\ \text{or } k=1 \end{matrix} \qquad \begin{matrix} \text{(entry point)} \\ \text{(launch point)} \end{matrix} \qquad (2.3)$$

$$\underline{x}_k = \begin{bmatrix} \Delta\theta_k \\ \Delta\phi_k \\ \Delta t_k \end{bmatrix} \qquad k=\text{odd and} \neq 1 \qquad \text{(exit point)} \qquad (2.4)$$

where θ_k = azimuth of point k

ϕ_k = elevation of point k

t_k = time of passage through point k

$\Delta\theta_k$ = difference in azimuth between points k and k-1

$\Delta\phi_k$ = difference in elevation between points k and k-1

Δt_k = difference in passage time between points k and k-1

These coordinates are illustrated in Figure 2.3.

The planetocentric cartesian coordinates of an entry or exit point are calculated using

$$\underline{r}_{D,k} = \underline{r}_{s,i} \begin{bmatrix} \cos\alpha & \cos\beta \\ \sin\alpha & \cos\beta \\ & \sin\beta \end{bmatrix} = \begin{bmatrix} x_{D,k} \\ y_{D,k} \\ z_{D,k} \end{bmatrix} \qquad (2.5)$$

where $r_{s,i}$ = radius of SOI for planet i

$\alpha = \theta_k$ k=even or k=1

$= \theta_{k-1} + \Delta\theta_k$ k=odd and k≠1

$\beta = \phi_k$ k=even or k=1

$= \phi_{k-1} + \Delta\phi_k$ k=odd and k≠1

2.32 Calculation of Conic Arcs

In [3], it is shown that given their initial (r_1, t_1), and final (r_2, t_2) positions and times, it is possible using Lambert's theorem to calculate a two-body conic trajectory with initial velocity $\underline{v}_1$ and

final velocity $\underline{v}_2$ connecting any two points. This procedure is described in detail in Appendix B.

2.321 Planetocentric Arcs

These arcs run from the entry point on a planet's SOI to the corresponding exit point. They are always hyperbolic with respect to the planet and traverse a central angle greater than 180° but never make a complete revolution. The initial and final points are

$$\underline{r}_1 = \underline{r}_{D,k} \qquad t_1 = t_k$$

$$\underline{r}_2 = \underline{r}_{D,k+1} \qquad t_2 = t_k + \Delta t_{k+1} \qquad (k=\text{even}) \qquad (2.6)$$

The initial and final velocities are stored as

$$\underline{v}_{H,k} = \underline{v}_1$$

$$\underline{v}_{H,k+1} = \underline{v}_2 \qquad (2.7)$$

2.322 Heliocentric Arcs

The heliocentric arcs run from the SOI exit point on one planet's SOI to the entry point of the next. The initial and final points are

$$\underline{r}_1 = \underline{r}_{P,k} + \underline{r}_{D,k} \qquad t_1 = t_{k-1} + \Delta t_k \quad (=t_k \text{ for } k=1)$$

$$\underline{r}_2 = \underline{r}_{P,k+1} + \underline{r}_{D,k+1} \qquad t_2 = t_{k+1} \qquad (k=\text{odd}) \qquad (2.8)$$

In addition it is necessary to specify

1) The number of complete revolutions the arc traverses about the central body. This must be given a priori.

2) Whether that portion of the arc remaining after the complete revolutions have been finished traverses a central angle greater or less than 180°. Assuming that all heliocentric trajectories have inclinations less than 90°, this may be determined using

$$G_1 = \text{sgn}\,[\underline{i}_z \cdot (\underline{r}_1 \times \underline{r}_2)] \tag{2.9}$$

If $\underline{G}_1 > 0$, the central angle is less than 180° while if $\underline{G}_1 < 0$ it is greater than 180°.

3) Whether the arc is a hyperbola or an ellipse. This is determined by comparing the time of flight for the arc

$$T = t_2 - t_1 \tag{2.10}$$

with the parabolic time of flight (see [3])

$$\underline{T}_p = \frac{1}{2}\sqrt{\frac{2}{\mu}}\left[s^{3/2} - G_1(s-c)^{3/2}\right] \tag{2.11}$$

$$\underline{c} = \underline{r}_2 - \underline{r}_1 \qquad c = |\underline{c}|$$

$$s = \frac{1}{2}(r_1 + r_2 + c)$$

μ = gravitational parameter for the central body (in this case the sun)

G_1 = as defined above

between the same two points. Then, if $T > T_p$, the arc is an ellipse while if $T < T_p$, it is a hyperbola. If $T = T_p$, the arc is a parabola.

The initial and final velocities for the heliocentric arcs are stored as

$$\underline{v}_{E,k} = \underline{v}_1$$

$$\underline{v}_{E,k+1} = \underline{v}_2 \tag{2.12}$$

2.33 Calculation of Cost Function

At each entry or exit point along the trajectory (excluding the initial and final points) the velocity along both a heliocentric arc and a planetocentric arc have been calculated. In general, these velocities will not be consistent but instead will be mis-matched by an amount

$$\Delta\underline{v}_k = \underline{v}_{E,k} - \underline{v}_{H,k} - \underline{v}_{P,k} \tag{2.13}$$

where $\underline{v}_{E,k}$ = velocity relative to the sun along the heliocentric arc at point k

$\underline{v}_{H,k}$ = velocity relative to the planet along the planetocentric arc at point k

$\underline{v}_{P,k}$ = velocity of the planet relative to the sun at time t_k.

A scalar cost function J for the total velocity mis-match along the trajectory may then be calculated using

$$J = \sum_{k=2}^{2N-3} \Delta\underline{v}_k^T \, \Delta\underline{v}_k \tag{2.14}$$

This expression is positive definite and goes to zero only when velocities are matched along the entire trajectory.

2.4 Accuracy of the Model

The basic limitation on the accuracy of this model lies in the fact that it assumes each trajectory segment to be a pure two-body arc. The effects of direct planetary gravitational attractions are ignored outside of the planet's SOI while the effects of solar perturbing forces (due to the gradient of the sun's gravitational field) are neglected inside of a planet's SOI. Within these assumptions, the calculation of the trajectory segments is an exact solution to the non-linear two-body orbit determination problem. The accuracy of the solution is limited only by the computational round-off errors of the method used.

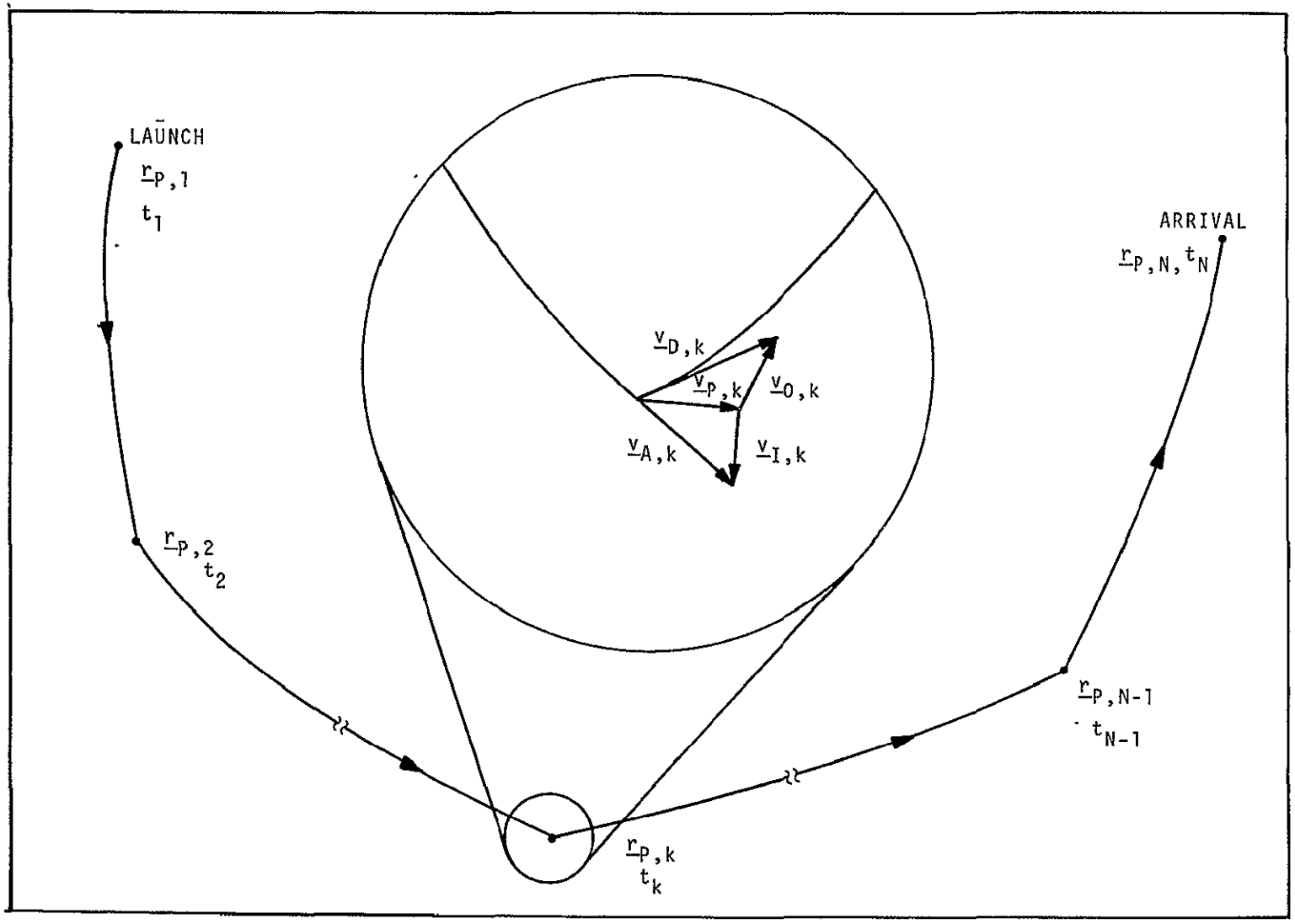

Figure 2.1 Simple Patched Conic Trajectory

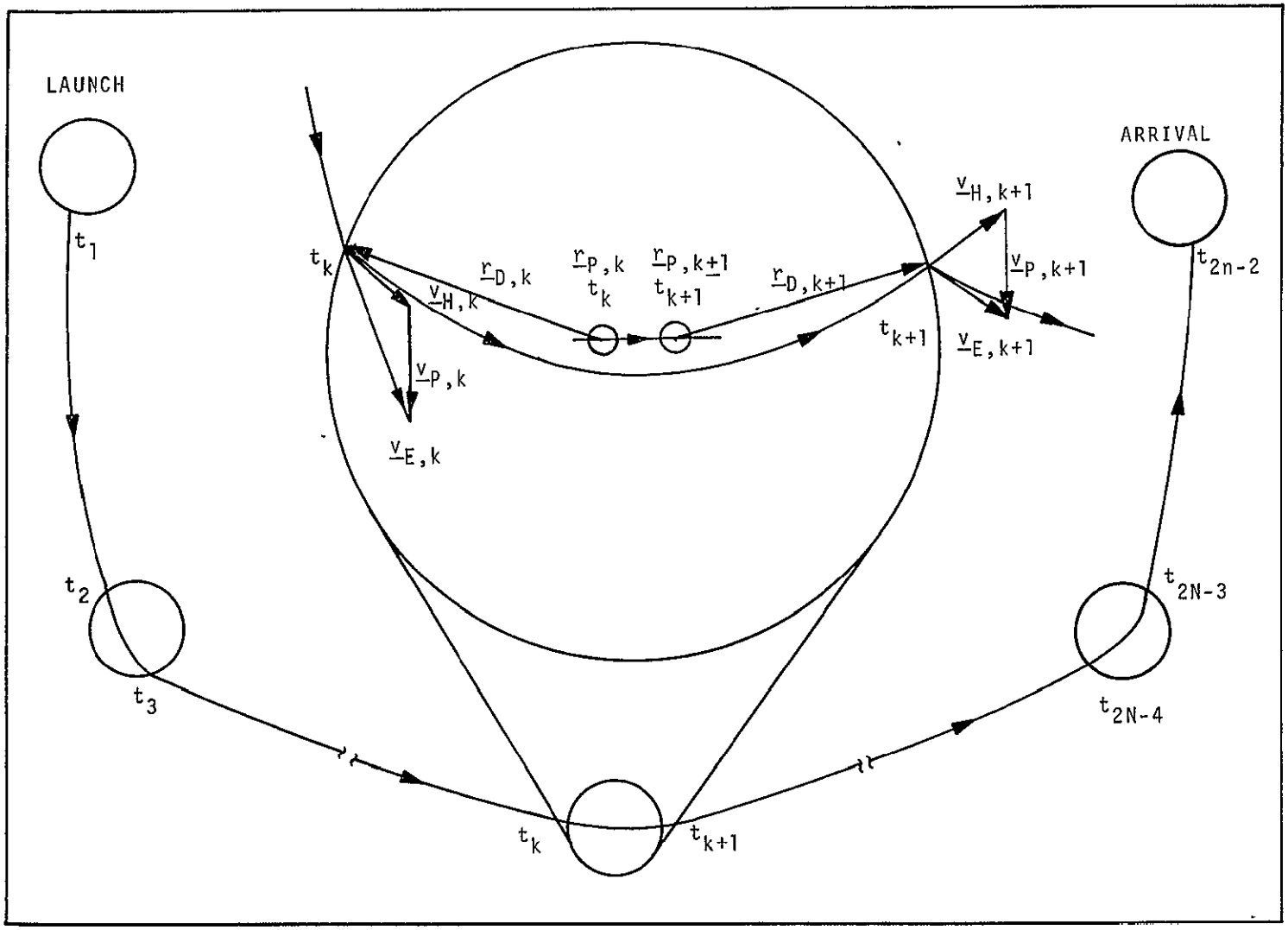

Figure 2.2 Advanced Patched Conic Model

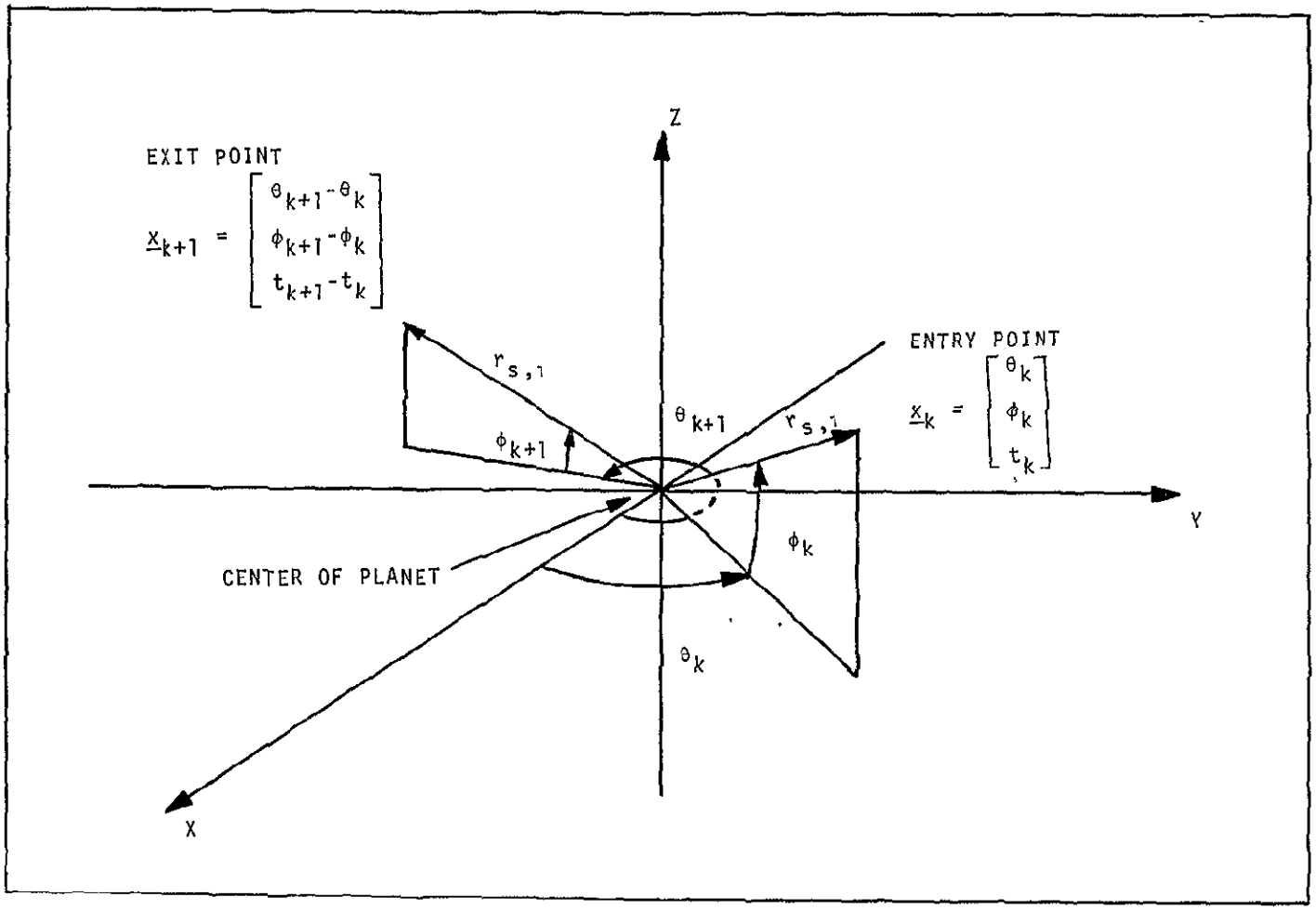

Figure 2.3 Entry and Exit Point Coordinates

Chapter 3

Perturbed Conic Analysis

3.0 Chapter Summary

Two approaches to computing the perturbed conic trajectory segments are considered. The first computes the perturbations for a trajectory running from the initial time to the final time. Perturbations due to disturbing accelerations near the initial time are found to grow to unacceptable levels near the final time. The second method starts at the trajectory mid-point and computes perturbations from there to both the initial and final times. The accuracy for this method is adequate. The details of evaluating the perturbations by quadrature are described. The method for determining the velocity offsets for a perturbed trajectory passing through the same initial and final position and time as the two-body trajectory is given. The source of error in the calculations are discussed.

3.1 Description of Approach

The object of this chapter is to take into account the fact that the segments of the true multi-swingby trajectory are only approximately two-body orbits. To do this, a set of perturbed conic trajectory segments (corresponding to the segments of the advanced patched conic model) are calculated. The heliocentric arcs take into account the disturbing effects of the attraction of the planets while the planetocentric arcs are affected by the disturbing forces due to the sun. The perturbed conic trajectory segments are constrained to match the same initial and final conditions in position and time as the corresponding segments in the advanced patched conic model but are offset in initial and final velocity. It is the calculation of these velocity offsets that is the main concern of this chapter.

Two approaches to the calculation of the velocity offsets were

tried. The first of these is similar to the implicit velocity offset technique used in space guidance [28]. This procedure is illustrated in Figure 3.1. Its steps for a single trajectory segment are described below.

1) Assume that the state

$$\underline{x}_0(t) = \begin{bmatrix} \underline{r}_0(t) \\ \underline{v}_0(t) \end{bmatrix} \tag{3.1}$$

along the advanced patched conic trajectory segment found in the preceding chapter may be expressed as a function of time. Starting with the same initial conditions as the two-body trajectory

$$\underline{x}(t_1) = \underline{x}_0(t_1) \tag{3.2}$$

calculate the perturbed trajectory $\underline{x}(t)$ using linear perturbation theory.

2) At the final time, calculate the position and velocity differences between the two-body and perturbed trajectories.

$$\delta\underline{x}(t_2) = \begin{bmatrix} \delta\underline{r}(t_2) \\ \delta\underline{v}(t_2) \end{bmatrix} = \underline{x}(t_2) - \underline{x}_0(t_2) \tag{3.3}$$

3) Using linear perturbation theory, calculate the velocity offset needed at the initial time to reduce the final time position offset value to zero.

$$
\begin{array}{lll}
\underline{\text{Before}} & & \underline{\text{After}} \\
\delta\underline{x}(t_1) = \begin{bmatrix} 0 \\ 0 \end{bmatrix} & \longrightarrow & \delta\hat{\underline{x}}(t_1) = \begin{bmatrix} 0 \\ \delta\hat{\underline{v}}(t_1) \end{bmatrix} \\
\delta\underline{x}(t_2) = \begin{bmatrix} \delta\underline{r}(t_2) \\ \delta\underline{v}(t_2) \end{bmatrix} & \longrightarrow & \delta\hat{\underline{x}}(t_2) = \begin{bmatrix} 0 \\ \delta\hat{\underline{v}}(t_2) \end{bmatrix}
\end{array}
\tag{3.4}
$$

This process also leads to a new velocity offset value $\delta\hat{\underline{v}}_2(t_2)$ at the final time. The above procedure proved to be highly inaccurate. All the trajectory segments have in common the characteristic of moving from a region of strong perturbing forces (near the sphere of influence boundary) into a region of weak perturbing forces (far from any planet for the heliocentric legs and deep inside the sphere of influence for the planetocentric legs) and then back into a region with strong perturbing forces. The effects of the initial strong perturbations grow rapidly along the trajectory and lead to very large deviations in position and velocity at the endpoint. These deviations are usually outside the linear range of the perturbation theory used in steps 1 and 3 above, thus leading to unacceptable errors in the calculation of the velocity offsets.

The reason for the failure of this first approach led to the use of the much more successful second approach. Referring to Figure 3.2, the steps for this method for a single trajectory segment are given below.

1) Assume that the state $\underline{x}_0(t)$ along the advanced patched conic trajectory segment is a known function of time. Starting at the mid-point

$$t_M = \frac{1}{2}(t_2 + t_1) \tag{3.5}$$

of the two-body segment with the same state as the

conic trajectory, calculate perturbed trajectories forward to the final time and backward to the initial time (See Figure 3.2a) from that point.

2) At the initial and final points, calculate the offsets in position and velocity between the two-body trajectory and the perturbed trajectory.

$$\delta\underline{x}(t_1) = \begin{bmatrix} \delta\underline{r}(t_1) \\ \delta\underline{v}(t_1) \end{bmatrix} = \underline{x}(t_1) - \underline{x}_0(t_1) \tag{3.6}$$

$$\delta\underline{x}(t_2) = \begin{bmatrix} \delta\underline{r}(t_2) \\ \delta\underline{v}(t_2) \end{bmatrix} = \underline{x}(t_2) - \underline{x}_0(t_2) \tag{3.7}$$

3) Using linear perturbation theory, calculate the offsets in both position and velocity at the mid-point time t_M needed to reduce the initial and final position offsets to zero.

$$\begin{array}{lll} & \underline{\text{Before}} & \underline{\text{After}} \\ \delta\underline{x}(t_1) = \begin{bmatrix} \delta\underline{r}(t_1) \\ \delta\underline{v}(t_1) \end{bmatrix} & \longrightarrow & \delta\hat{\underline{x}}(t_1) = \begin{bmatrix} 0 \\ \delta\hat{\underline{v}}(t_1) \end{bmatrix} \\ \delta\underline{x}(t_M) = \begin{bmatrix} 0 \\ 0 \end{bmatrix} & \longrightarrow & \delta\hat{\underline{x}}(t_M) = \begin{bmatrix} \delta\hat{\underline{r}}(t_M) \\ \delta\hat{\underline{v}}(t_M) \end{bmatrix} \\ \delta\underline{x}(t_2) = \begin{bmatrix} \delta\underline{r}(t_2) \\ \delta\underline{v}(t_2) \end{bmatrix} & \longrightarrow & \delta\hat{\underline{x}}(t_2) = \begin{bmatrix} 0 \\ \delta\hat{\underline{v}}(t_2) \end{bmatrix} \end{array} \tag{3.8}$$

This new trajectory is shown in Figure 3.2b.

This second approach provided the accuracy needed for the calculation of the initial and final velocity offsets ($\delta\hat{\underline{v}}(t_1)$ and $\delta\hat{\underline{v}}(t_2)$). Since the perturbed trajectories calculated in step 1 always run from regions of weak perturbations (the mid-section of the trajectory) to regions of strong perturbations (the end-points), large deviations (due to the accumulated effects of the strong perturbing forces) do not have the time to grow. Also, since the effects of the strong perturbing forces depend on the time spent in the vicinity of the sphere of influence boundaries at the end-points rather than on the time of flight of the trajectory, the size of the position and velocity offsets ($\delta\underline{x}(t_1)$ and $\delta\underline{x}(t_2)$) are not influenced heavily by the length of the trajectory. The computational details of the second approach are described in the next section.

Once the velocity offsets have been determined, a new cost function taking them into account is contructed. Then, the iterative procedure employed for the advanced patched conic model is used to match the perturbed conic segments in velocity as well as position and time at the entry and exit points.

3.2 Computational Details

3.21 Calculation of Perturbed Trajectory

It may be shown [3,29,30,31] that the solution (using linear perturbation theory) for the deviations between the perturbed and two-body trajectories is given by

$$\delta\underline{x}(t) = \Phi_0(t,t_i)\ \ \delta\underline{x}(t_i) + \int_{t_i}^{t} \Phi_0(t,\tau)\ \underline{f}_0(\tau)\ d\tau \qquad (3.9)$$

where

$$\delta\underline{x}(t) = \begin{bmatrix} \delta\underline{r}(t) \\ \\ \delta\underline{v}(t) \end{bmatrix}$$ = deviation from two-body orbit

$\Phi_0(t,t_i)$ = state transition matrix for the two-body orbit between t_i and t. (See Appendix D for a description of the properties of this matrix.)

$$\underline{f}_0(t) = \begin{bmatrix} \underline{0} \\ \\ \underline{a}_d(t) \end{bmatrix}$$ = disturbing vector

$\underline{a}_d(t)$ = disturbing acceleration evaluated as a function of time along the two-body trajectory.

All the quantities on the right-hand side of (3.9) are known functions of time evaluated along the two-body reference trajectory. Since the perturbed trajectory calculations start with

$$\underline{x}(t_M) = \underline{x}_0(t_M) \tag{3.10}$$

it can be seen that

$$\delta\underline{x}(t_M) = \begin{bmatrix} \underline{0} \\ \\ \underline{0} \end{bmatrix} \tag{3.11}$$

and that (3.9) becomes

$$\delta\underline{x}(t_1) = \int_{t_M}^{t_1} \Phi_0(t_1,\tau)\underline{f}_0(\tau)d\tau \tag{3.12}$$

for the integration to the initial point and

$$\delta\underline{x}(t_2) = \int_{t_M}^{t_2} \Phi_0\ (t_2,\tau)\underline{f}_0(\tau)d\tau \tag{3.13}$$

for the integration to the final point. Since the integrands in (3.12) and (3.13) are known functions of τ, the integrals may be evaluated by quadrature (See Appendix D for a discussion of the technique used).

3.22 Calculation of Disturbing Accelerations

The disturbing acceleration due to body P_j on the motion of P_2 with respect to P_1 (see Figure 3.3) is given by

$$\underline{a}_{d,j} = -\mu_j \left(\frac{1}{\ell_j^3}\ \underline{\ell}_j + \frac{1}{d_j^3}\ \underline{d}_j \right) \tag{3.14}$$

where

$\underline{\ell}_j$ = position vector from P_1 to P_j

$\underline{d}_j$ = position vector from P_j to P_2

μ_j = gravitational parameter for P_j

Numerical difficulties may arise in the use of (3.14) since $\underline{\ell}_j$ and $\underline{d}_j$ are often nearly equal and opposite vectors. These difficulties may be alleviated using a technique developed in [3]. Write

$$\frac{1}{\ell_j^3}\ \underline{\ell}_j + \frac{1}{d_j^3}\ \underline{d}_j = \frac{1}{d_j^3}\left[\underline{r} + \left(\frac{d_j^3}{\ell_j^3} - 1\right)\underline{\ell}_j\right] \tag{3.15}$$

where

$\underline{r}$ = position vector from P_1 to P_2

$= \underline{\ell}_j + \underline{d}_j$

Now, write

$$\left(\frac{d_j^3}{\ell_j^3} - 1\right) = W(q_j) \tag{3.16}$$

where

$$q_j = \frac{r}{\ell_j}\left(\frac{r}{\ell_j} - 2\cos\alpha_j\right) \tag{3.17}$$

$$W(q_j) = (1 + q_j)^{3/2} - 1 \tag{3.18}$$

α_j = angle between $\underline{r}$ and $\underline{\ell}_j$

To evaluate $W(q_j)$, re-write (3.18) as

$$W(q_j) = \frac{(1+q_j)^3-1}{(1+q_j)^{3/2}+1}$$

or

$$W(q_j) = q_j \frac{3+3q_j+q_j^2}{(1+q_j)^{3/2}+1} \tag{3.19}$$

Thus, substituting (3.19) and (3.16) into (3.15) yields

$$\underline{a}_{d,j} = -\frac{\mu_j}{d_j^3}\left[\underline{r} + W(q_j)\,\underline{\ell}_j\right] \tag{3.20}$$

The total disturbing acceleration is the sum of the individual contributions.

$$\underline{a}_d = \sum_{j=1}^{N} \underline{a}_{d,j} \tag{3.21}$$

For the heliocentric legs, all significant planetary disturbing accelerations are included in the calculation of (3.21). For the planetocentric legs, only the disturbing acceleration due to the sun is considered.

3.23 Calculation of Velocity Offsets

As shown in Appendix D, the state transition matrix may be partitioned into four sub-matrices.

$$\Phi_0(t,t_i) = \begin{bmatrix} A_0(t,t_i) & B_0(t,t_i) \\ C_0(t,t_i) & D_0(t,t_i) \end{bmatrix} \tag{3.22}$$

where

$$A_0(t,t_i) = \left[\frac{\partial \underline{r}(t)}{\partial \underline{r}(t_i)}\right]_0$$

$$B_0(t,t_1) = \left[\frac{\partial \underline{r}(t)}{\partial \underline{v}(t_i)}\right]_0$$

$$C_0(t,t_1) = \left[\frac{\partial \underline{v}(t)}{\partial \underline{r}(t_i)}\right]_0$$

$$D_0(t,t_1) = \left[\frac{\partial \underline{v}(t)}{\partial \underline{v}(t_i)}\right]_0$$

Having computed the initial and final perturbations ($\delta\underline{x}(t_1)$ and $\delta\underline{x}(t_2)$) corresponding to $\delta\underline{x}(t_M) = 0$, form the correction matrix

$$H_0(t_1,t_2,t_M) = \begin{bmatrix} A_0(t_1,t_M) & B_0(t_1,t_M) \\ A_0(t_2,t_M) & B_0(t_2,t_M) \end{bmatrix} \tag{3.23}$$

The new value for the deviation of the state at the mid-point $\delta\hat{\underline{x}}(t_M)$ is calculated to reduce the position deviations at the initial and final points to zero. From (3.9), (3.12), (3.13), (3.22), and (3.23), it can be seen that

$$\begin{bmatrix} \delta\hat{\underline{r}}(t_1) \\ \delta\hat{\underline{r}}(t_2) \end{bmatrix} = \begin{bmatrix} \underline{0} \\ \underline{0} \end{bmatrix} = H_0(t_1,t_2,t_M)\ \delta\hat{\underline{x}}(t_M) + \begin{bmatrix} \delta\underline{r}(t_1) \\ \delta\underline{r}(t_2) \end{bmatrix} \tag{3.24}$$

Thus,

$$\delta\hat{\underline{x}}(t_M) = -\ H_0^{-1}(t_1,t_2,\ t_M) \begin{bmatrix} \delta\underline{r}(t_1) \\ \delta\underline{r}(t_2) \end{bmatrix} \tag{3.25}$$

The new values for the state deviations at any point may be calculated using (3.9).

$$\delta\hat{\underline{x}}(t) = \Phi_0(t,t_M)\ \delta\hat{\underline{x}}(t_M) + \int_{t_M}^{t} \Phi_0(t,\tau)\underline{f}_0(\tau)d\tau \tag{3.26}$$

Specifically, the offsets at the initial and final points are given by

$$\delta\hat{\underline{x}}(t_1) = \begin{bmatrix} \underline{0} \\ \delta\hat{\underline{v}}(t_1) \end{bmatrix} = \Phi_0(t_1,t_M)\ \delta\hat{\underline{x}}(t_M) + \delta\underline{x}(t_1) \tag{3.27}$$

$$\delta\hat{\underline{x}}(t_2) = \begin{bmatrix} \underline{0} \\ \delta\hat{\underline{v}}(t_2) \end{bmatrix} = \Phi_0(t_2,t_M)\ \delta\hat{\underline{x}}(t_M) + \delta\underline{x}(t_2) \qquad (3.28)$$

3.24 Calculation of Cost Function

For a heliocentric arc running from $t_1 = t_k$ to $t_2 = t_{k+1}$, store the velocity offsets as

$$\delta\underline{v}_{E,k} = \delta\hat{\underline{v}}(t_1)$$

$$(k = \text{odd}) \qquad (3.29)$$

$$\delta\underline{v}_{E,k+1} = \delta\hat{\underline{v}}(t_2)$$

For a planetocentric arc running from $t_1 = t_k$ to $t_2 = t_{k+1}$, store the velocity offsets as

$$\delta\underline{v}_{H,k} = \delta\hat{\underline{v}}(t_1)$$

$$(k = \text{even}) \qquad (3.30)$$

$$\delta\underline{v}_{H,k+1} = \delta\hat{\underline{v}}(t_2)$$

Then, let

$$\Delta\underline{v}_k = \underline{v}_{E,k} + \delta\underline{v}_{E,k} - \underline{v}_{P,k} - \underline{v}_{H,k} - \delta\underline{v}_{H,k} \qquad (3.31)$$

and

$$J = \sum_{k=2}^{2N-3} \Delta\underline{v}_k{}^T\ \Delta\underline{v}_k \qquad (3.32)$$

3.3 Sources of Error

The errors associated with the calculation of the perturbed trajectories have as their source

1) Computational errors, in such areas as matrix inversion, calculation of the two body orbits and state transition matrices, evaluation of the perturbation integrals by quadrature, etc. These errors may be reduced to any level desired by increasing the precision of the calculations, reducing step-size for quadrature methods, and by increasing the accuracy level required for the termination of iterative solutions to transcendental equations. The ultimate level of accuracy due to errors of the above nature is limited only by the precision available on the computer used.

2) Errors associated with the approximations involved in the use of the trajectory model. Referring to (3.9), it can be seen that these errors occur because of the
   i) evaluation of the disturbing acceleration $\underline{a}_d$ on the two-body reference trajectory rather than on the perturbed trajectory.
   ii) use of the two-body state transition matrix $\Phi_0(t,t_i)$ calculated for the reference trajectory rather than the many-body state transition matrix $\Phi(t,t_i)$ evaluated along the perturbed trajectory.
   iii) use of linear perturbation theory.
   iv) neglect of smaller disturbing forces.

The error sources listed under 2) above are the dominant factors. Examining each of these sources in detail their importance can be estimated.

i) From (3.14), the disturbing acceleration is

$$\underline{a}_{d,j} = -\mu_j \left[\frac{1}{\ell_j^3} \underline{\ell}_j + \frac{1}{d_j^3} \underline{d}_j \right] \tag{3.14}$$

The gradient of this acceleration is given by

$$G(\underline{d}_j) = \frac{\partial \underline{a}_{d,j}}{\partial \underline{d}_j}$$

$$= -\mu_j \left[\frac{1}{d_j^3} \frac{\partial \underline{d}_j}{\partial \underline{d}_j} + \frac{\partial}{\partial \underline{d}_j} \left(\frac{1}{d_j^3}\right) \underline{d}_j \right]$$

$$G(\underline{d}_j) = \frac{\mu_j}{d_j^3} \left[3\, \underline{i}_{d_j} \underline{i}_{d_j}^T - I \right] \tag{3.33}$$

where $\underline{\ell}_j$ is considered a constant.

The change in $\underline{a}_{d,j}$ due to a small shift from the reference trajectory is given by

$$\delta \underline{a}_{d,j} = G(\underline{d}_j)\, \delta \underline{d}_j$$

$$= G(\underline{d}_j)\, \delta \underline{r} \tag{3.34}$$

since $\underline{r} = \underline{\ell}_j + \underline{d}_j$ implies $\delta \underline{r} = \delta \underline{d}_j$. From (3.33) and (3.34), it can be seen that the magnitude of $\delta \underline{a}_{d,j}$ is roughly

$$\delta a_{d,j} \cong \frac{\mu_j}{d_j^3} \delta r \tag{3.35}$$

The largest deviations from the reference trajectory for either planetocentric or heliocentric legs occurs at the sphere of influence (SOI) boundary. From the definition of the SOI (see Appendix C), the disturbing acceleration due to the sun equals the primary acceleration due

to the planet on this surface. On the heliocentric legs, the disturbing acceleration at the SOI boundary is largely due to the primary acceleration of the planet while on the planetocentric legs, the disturbing acceleration at the SOI boundary is due largely to the perturbing acceleration of the sun. From (C.9), the disturbing acceleration at the SOI boundary may be written approximately as

$$a_{d,j} = \left(\frac{\mu}{r^3}\right) r = \left(\frac{\mu_j}{\ell_j^3}\, r\right) \tag{3.36}$$

where

μ = gravitational parameter of the planet

μ_j = gravitational parameter of the sun

Since, at the SOI, $r \ll \ell$, (3.36) may be written as

$$a_{d,j} = \left(\frac{\mu_j}{d_j^3}\right) r \tag{3.37}$$

Then, from (3.35)

$$\frac{\delta a_{d,j}}{a_{d,j}} \simeq \frac{\delta r}{r} \tag{3.38}$$

at the SOI boundary. Typical maximum values for this ratio are 0.06 for inner planets and 0.01 for outer planets.

ii) Numerical studies comparing an analytic two-body state transition matrix with a many-body state transition determined by numerical integration showed that terms in both matrices remained equal to within a few percent for both heliocentric and planetocentric legs when the enlarged sphere of influence (see Appendix C) was used. When the Laplace SOI was used, large differences (often over 100%) occurred

in terms in the C and D matrices for the heliocentric legs.

iii) Numerical studies indicate that the perturbations ecountered in all the steps are small enough for the linear theory to remain valid. This is also shown by Slater and Stern in [28].

iv) The perturbing forces neglected in this model are those due to other planets during planetocentric legs, those due to oblateness and other higher-order terms in the gravitational field of the sun and planets and those due to non-gravitational effects such as drag, radiation pressure, etc. They are considered small compared to the forces included.

Numerical values for the accuracy of the perturbed trajectory calculations may be found in Chapters 5-7 and Appendix D. In general, the perturbed trajectory appears to eliminate about 98%-99% of the error between the conic and N-body trajectory segments. The largest error source is usually the difference between the two-body and N-body state transition matrices. This result is also indicated in [28].

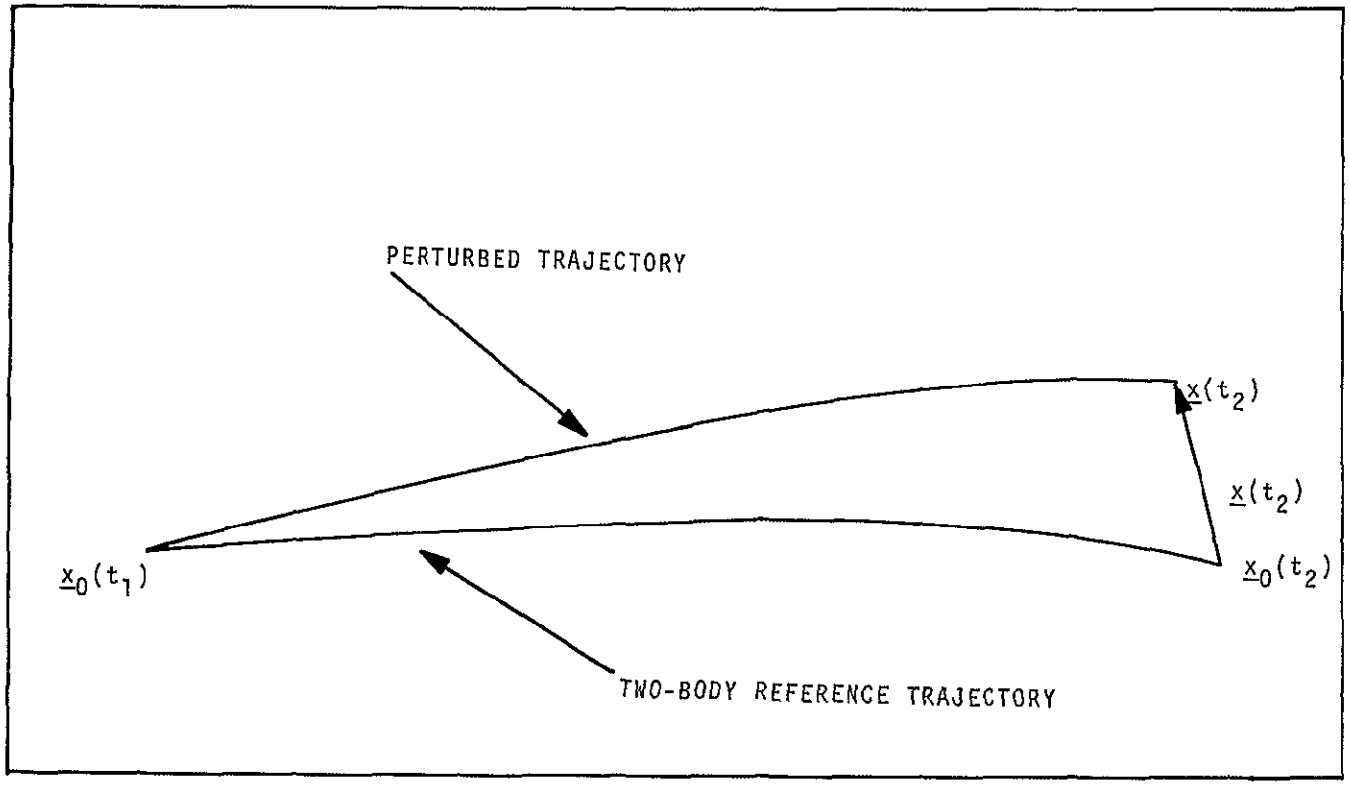

Figure 3.1 Offset Calculation [First Method]

Figure 3.2 Offset Calculation [second method]

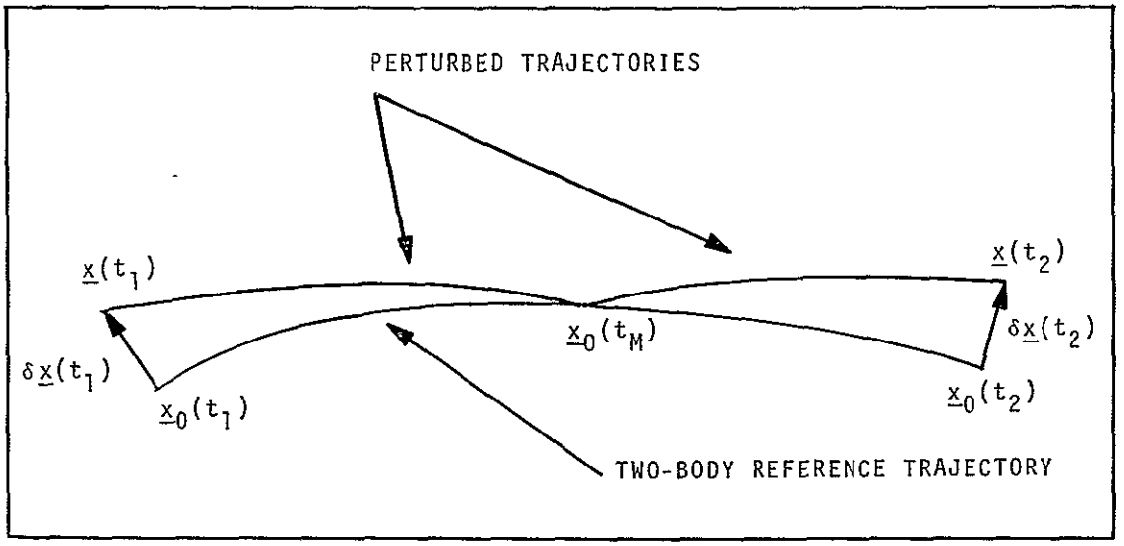

Figure 3.2(a) Offset Calculation, Step 1

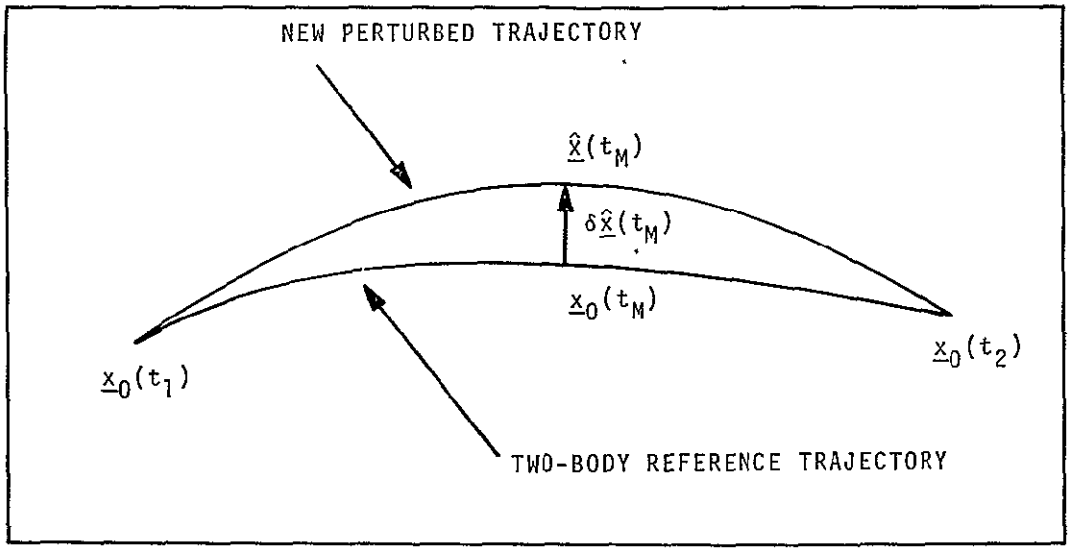

Figure 3.2(b) Offset Calculation, Step 2

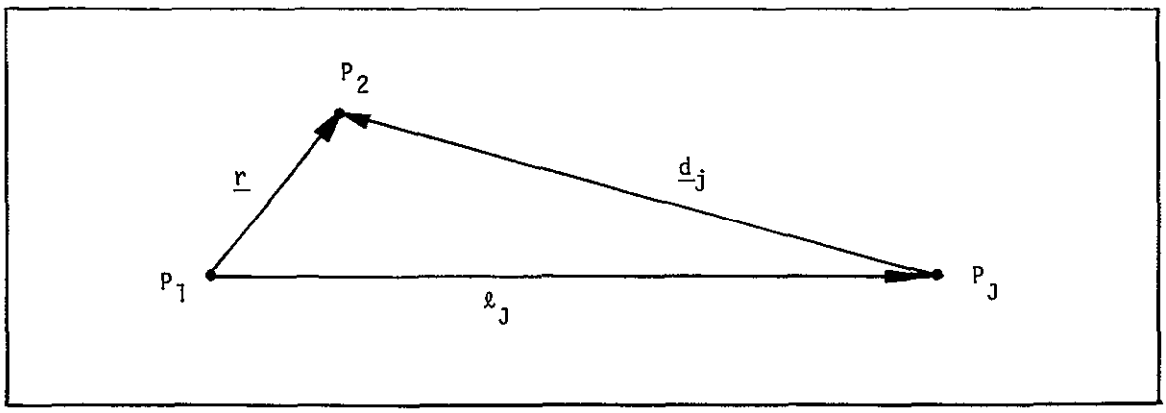

Figure 3.3 Disturbing Acceleration Geometry

Chapter 4

Trajectory Segment Matching Procedure

4.0 Chapter Summary

The problem of matching the trajectory segments in velocity as well as position and time is formulated as a parameter optimization exercise. The details of the calculation of the gradient of the cost function for the velocity mis-match are described. A number of first-order techniques (steepest decent, modified steepest descent, conjugate gradient, and acceleration steps) are applied to the problem. A second-order technique (generalized Newton-Rapheson) is also discussed and applied. The behavior of the different techniques is described and the best are selected. The application of inequality constraints on the distance of closest approach to each planet is detailed. The application of the trajectory segment matching procedure for the multiple swingby analysis is outlined.

4.1 Description of the Problem

The problem of minimizing the velocity mis-match at the trajectory entry and exit points may be formulated as a parameter optimization problem. For a trajectory with N planetary encounters (launch, N-2 intermediate swingbys, and arrival), define an expanded state vector and its variation as

$$\underline{s} = \begin{bmatrix} \underline{x}_2 \\ \underline{x}_3 \\ \cdot \\ \cdot \\ \cdot \\ \underline{x}_{2N-3} \end{bmatrix} \qquad \delta\underline{s} = \begin{bmatrix} \delta\underline{x}_2 \\ \delta\underline{x}_3 \\ \cdot \\ \cdot \\ \cdot \\ \delta\underline{x}_{2N-3} \end{bmatrix} \tag{4.1}$$

where $\underline{x}_k$ is defined as in (2.3) and (2.4). The launch point $\underline{x}_1$ and arrival point $\underline{x}_{2N-2}$ are considered fixed, so that

$$\delta \underline{x}_1 = \delta \underline{x}_{2N-2} \equiv \underline{0} \tag{4.2}$$

Similarly, for the 2N-4 trajectory matching points (the intermediate entry and exit points), define a velocity mis-match vector as

$$\underline{u} = \begin{bmatrix} \Delta \underline{v}_2 \\ \Delta \underline{v}_3 \\ \cdot \\ \cdot \\ \cdot \\ \Delta \underline{v}_{2N-3} \end{bmatrix} \tag{4.3}$$

and a cost function

$$J = \sum_{k=2}^{2N-3} \Delta \underline{v}_k{}^T \, \Delta \underline{v}_k \tag{4.4}$$

where $\Delta \underline{v}_k$ may be defined either as in (2.13) or in (3.31)

The object of the problem is to find the value of $\delta \underline{s}$ which minimizes J and if possible reduces J and $\underline{u}$ to zero. Both $\delta \underline{s}$ and $\underline{u}$ have 6(N-2) independent components, so that sufficient degrees of freedom exist for a solution to be possible.

To avoid unrealizable trajectories, it is necessary to apply the inequality constraint

$$r_{CA} \geq k_M \, r_e \tag{4.5}$$

where

r_{CA} = radius of closest approach of trajectory to the planet

r_e = equatorial radius of the planet

k_M = constant multiplier (nominal value = 1.1)

at each swingby. Changes in the value of $\delta\underline{s}$ which violate this inequality constraint are not allowed. The details of the constraint application are discussed in Section 4.5 of this chapter.

4.2 Calculation of Cost Function Gradient

4.21 Calculation of Lambert Problem Partials

During the calculation of the conic trajectory segments for the advanced patched conic model, it is also possible to calculate analytically the partial derivative matrices

$$\nabla_{1\underline{v}_1} = \frac{\partial \underline{v}_1}{\partial \underline{r}_1} \tag{4.6}$$

$$\nabla_{2\underline{v}_1} = \frac{\partial \underline{v}_1}{\partial \underline{r}_2} \tag{4.7}$$

$$\nabla_{1\underline{v}_2} = \frac{\partial \underline{v}_2}{\partial \underline{r}_1} \tag{4.8}$$

$$\nabla_{2\underline{v}_2} = \frac{\partial \underline{v}_2}{\partial \underline{r}_2} \tag{4.9}$$

and the partial derivative vectors

$$\frac{\partial \underline{v}_1}{\partial t_1}, \quad \frac{\partial \underline{v}_2}{\partial t_1}, \quad \frac{\partial \underline{v}_1}{\partial t_2}, \quad \frac{\partial \underline{v}_2}{\partial t_2} \tag{4.10}$$

where $\underline{r}_1, \underline{v}_1, t_1$ = initial position, velocity, and time for the conic arc

$\underline{r}_2, \underline{v}_2, t_2$ = final position, velocity, and time for the conic arc

The relations necessary for the calculation of these partial derivatives are given in Appendix B. They are in cartesian coordinates and must be converted to spherical coordinates for use in the cost function gradient. Recall from (2.6) that for a planetocentric conic segment

$$\begin{aligned} \underline{r}_1 &= \underline{r}_{D,k} & t_1 &= t_k \\ \underline{r}_2 &= \underline{r}_{D,k+1} & t_2 &= t_k + \Delta t_{k+1} \end{aligned} \tag{4.11}$$

and from (2.8) that for a heliocentric conic segment

$$\begin{aligned} \underline{r}_1 &= \underline{r}_{P,\,k} + \underline{r}_{D,\,k} & t_1 &= t_{k-1} + \Delta t_k \\ & & &\quad (= t_k \text{ for } k=1) \\ \underline{r}_2 &= \underline{r}_{P,\,k+1} + \underline{r}_{D,\,k+1} & t_2 &= t_{k+1} \end{aligned} \tag{4.12}$$

where, from (2.5), it may be written

$$\underline{r}_{D,\,k} = r_{s,1} \begin{bmatrix} \cos\theta_k \cos\phi_k \\ \sin\theta_k \cos\phi_k \\ \sin\phi_k \end{bmatrix} = \begin{bmatrix} x_k \\ y_k \\ z_k \end{bmatrix} \tag{4.13}$$

Since motion of the entry and exit points on the sphere of influence (SOI) does not affect the planetary position $\underline{r}_{P,k}$

$$\delta\underline{r}_1 = \delta\underline{r}_{D,k}$$

$$\delta\underline{r}_2 = \delta\underline{r}_{D,k+1} \tag{4.14}$$

for both planetocentric and heliocentric arcs. The relation between variations in cartesian and spherical coordinates is given by

$$\delta\underline{r}_j = \begin{bmatrix} \delta x_j \\ \delta y_j \\ \delta z_j \end{bmatrix}$$

$$= \begin{bmatrix} -r_{s,1}\cos\phi_j \sin\theta_j & -r_{s,i}\sin\phi_j \cos\theta_j & \cos\phi_j \cos\theta_j \\ r_{s,1}\cos\phi_j \cos\theta_j & -r_{s,1}\sin\phi_j \sin\theta_j & \cos\phi_j \sin\theta_j \\ 0 & r_{s,1}\cos\phi_j & \sin\phi_j \end{bmatrix} \begin{bmatrix} \delta\theta_j \\ \delta\phi_j \\ \delta r_{s,i} \end{bmatrix} \tag{4.15}$$

Since the entry and exit points may vary only on the SOI, it is necessary that

$$\delta r_{s,1} \equiv 0 \tag{4.16}$$

so that (4.15) may be written as

$$\delta \underline{r}_j = \begin{bmatrix} -r_{s,1} \cos\phi_j \sin\theta_j & -r_{s,1} \sin\phi_j \cos\theta_j & 0 \\ r_{s,1} \cos\phi_j \cos\theta_j & -r_{s,i} \sin\phi_j \sin\theta_j & 0 \\ 0 & r_{s,1} \cos\phi_j & 0 \end{bmatrix} \begin{bmatrix} \delta\theta_j \\ \delta\phi_j \\ 0 \end{bmatrix} \tag{4.17}$$

$$= R_j \begin{bmatrix} \delta\theta_j \\ \delta\phi_j \\ 0 \end{bmatrix}$$

Referring to (4.11) and (4.12), it can be seen that the partial derivative vectors (4.10) are affected by planetary motion for the heliocentric legs but not for planetocentric legs. This effect is given by

$$\frac{d\underline{v}_1}{dt_1} = \frac{\partial \underline{v}_1}{\partial t_1} + \frac{\partial \underline{v}_1}{\partial \underline{r}_{p,k}} \frac{\partial \underline{r}_{p,k}}{\partial t_1}$$

$$= \frac{\partial \underline{v}_1}{\partial t_1} + (\nabla_1 \underline{v}_1)\, \underline{v}_{p,k} \tag{4.18}$$

since $\dfrac{\partial \underline{v}_1}{\partial \underline{r}_{p,k}} = \dfrac{\partial \underline{v}_1}{\partial r_1} = \nabla_1 \underline{v}_1$

when $\underline{r}_{D,k}$ = fixed.

Similarly,

$$\frac{d\underline{v}_1}{dt_2} \quad \frac{\partial \underline{v}_1}{\partial t_2} + (\nabla_2 \underline{v}_1)\, \underline{v}_{p,k+1} \tag{4.19}$$

$$\frac{d\underline{v}_2}{dt_1} = \frac{\partial \underline{v}_2}{\partial t_1} + (\nabla_1 \underline{v}_2)\ \underline{v}_{P,k} \tag{4.20}$$

$$\frac{d\underline{v}_2}{dt_2} = \frac{\partial \underline{v}_2}{\partial t_2} + (\nabla_2 \underline{v}_2)\ \underline{v}_{P,k+1} \tag{4.21}$$

Note that the relations (4.18)-(4.21) are used only for the heliocentric legs. For the planetocentric legs

$$\frac{d\underline{v}_i}{dt_j} = \frac{\partial \underline{v}_i}{\partial t_j} \qquad (i,\ j = 1,\ 2) \tag{4.22}$$

If a new state vector $\underline{y}$ (differing from the state vector $\underline{x}$) is defined as

$$\underline{y}_j = \begin{bmatrix} \theta_j \\ \phi_j \\ t_j \end{bmatrix} \tag{4.23}$$

for all j, it is then possible to define the partial derivative matrices

$$\frac{\partial \underline{v}_1}{\partial \underline{y}_1} = Q_{11} = (\nabla_1 \underline{v}_1)\ R_1 + \begin{bmatrix} 0 & 0 & | \\ 0 & 0 & \dfrac{d\underline{v}_1}{dt_1} \\ 0 & 0 & | \end{bmatrix} \tag{4.24}$$

$$\frac{\partial \underline{v}_1}{\partial \underline{y}_2} = Q_{21} = (\nabla_2 \underline{v}_1)\ R_2 + \begin{bmatrix} 0 & 0 & | \\ 0 & 0 & \dfrac{d\underline{v}_1}{dt_2} \\ 0 & 0 & | \end{bmatrix} \tag{4.25}$$

$$\frac{\partial \underline{v}_2}{\partial \underline{y}_1} = Q_{12} = (\nabla_1 \underline{v}_2)\, R_1 + \begin{bmatrix} 0 & 0 & | \\ 0 & 0 & \frac{d\underline{v}_2}{dt_1} \\ 0 & 0 & | \end{bmatrix} \tag{4.26}$$

$$\frac{\partial \underline{v}_2}{\partial \underline{y}_2} = Q_{22} = (\nabla_2 \underline{v}_2)\, R_2 + \begin{bmatrix} 0 & 0 & | \\ 0 & 0 & \frac{d\underline{v}_2}{dt_2} \\ 0 & 0 & | \end{bmatrix} \tag{4.27}$$

For each conic arc (either heliocentric or planetocentric) from point k to point k+1, the partial derivatives (4.24)-(4.27) are stored as

$$A_k = Q_{12} \tag{4.28}$$

$$B_{k+1} = Q_{22} \tag{4.29}$$

$$C_k = Q_{11} \tag{4.30}$$

$$D_{k+1} = Q_{21} \tag{4.31}$$

4.22 Calculation of Gradient

From (2.14), the cost function was given by

$$J = \sum_{k=2}^{2N-3} \Delta \underline{v}_k{}^T \, \Delta \underline{v}_k \tag{4.32}$$

Its gradient with respect to $\underline{x}_\ell$ is given by

$$\underline{g}_\ell = \frac{\partial J}{\partial \underline{x}_\ell} = 2 \sum_{k=2}^{2N-3} \Delta \underline{v}_k{}^T \, \frac{\partial \Delta \underline{v}_k}{\partial \underline{x}_\ell} \tag{4.33}$$

where

$$\ell = 2,3,4, \ldots, 2\ell-3$$

and, from (2.13)

$$\Delta \underline{v}_k = \underline{v}_{E,k} - \underline{v}_{P,k} - \underline{v}_{H,k} \tag{4.34}$$

From the definition of the state vector $\underline{x}_k$ given in (2.3) and (2.4), the effects on the state vector $\underline{y}_k$ defined in (4.23) and hence on the terms in (4.34) due to a change in $\underline{x}_k$ occur at

Point affected	$\underline{y}_k$	$\underline{v}_{E,k}$	$\underline{v}_{P,k}$	$\underline{v}_{H,k}$
k-1		x		
k	x	x	x	x
k+1	x	x	x	x
k+2		x		

for an entry point and at

Point affected	$\underline{y}_k$	$\underline{v}_{E,k}$	$\underline{v}_{P,k}$	$\underline{v}_{H,k}$
k-1				x
k	x	x	x	x
k+1		x		

for an exit point. The effect on $\underline{v}_{P,k}$ is due solely to the change in the time t_k associated with point k. This is given by

$$P_k = \frac{\partial \underline{v}_{P,k}}{\partial \underline{Y}_k}$$

$$= \begin{bmatrix} 0 & 0 & | \\ 0 & 0 & \frac{\partial \underline{v}_{P,k}}{\partial t_k} \\ 0 & 0 & | \end{bmatrix} = \begin{bmatrix} 0 & 0 & | \\ 0 & 0 & \underline{a}_{P,k} \\ 0 & 0 & | \end{bmatrix} \qquad (4.35)$$

where

$$\underline{a}_{P,k} = - \frac{\mu_s}{r_{P,k}^3} \underline{r}_{P,k} \qquad (4.36)$$

μ_s = gravitational parameter of the sun

$\underline{Y}_k$ = as defined in (4.23)

Thus, using (4.33) the gradient at an entry point may be written as

$$\begin{aligned} \underline{g}_k = 2 \Bigg\{ & \Delta \underline{v}_{k-1}^T \left[\frac{\partial \underline{v}_{E,k-1}}{\partial \underline{x}_k} \right] \\ & + \Delta \underline{v}_k^T \left[\frac{\partial \underline{v}_{E,k}}{\partial \underline{x}_k} - \frac{\partial \underline{v}_{P,k}}{\partial \underline{x}_k} - \frac{\partial \underline{v}_{H,k}}{\partial \underline{x}_k} \right] \\ & + \Delta \underline{v}_{k+1}^T \left[\frac{\partial \underline{v}_{E,k+1}}{\partial \underline{x}_k} - \frac{\partial \underline{v}_{P,k+1}}{\partial \underline{x}_k} - \frac{\partial \underline{v}_{H,k+1}}{\partial \underline{x}_k} \right] \\ & + \Delta \underline{v}_{k+2}^T \left[\frac{\partial \underline{v}_{E,k+2}}{\partial \underline{x}_k} \right] \Bigg\} \end{aligned} \qquad (4.37)$$

Using the relations (4.28)-(4.31), this becomes

$$\underline{g}_k = 2 \left\{ \Delta\underline{v}_{k-1}^T \left[D_k\right] + \Delta\underline{v}_k^T \left[B_k - P_k - C_k - D_{k+1}\right] \right.$$

$$+ \Delta\underline{v}_{k+1}^T \left[- A_k - B_{k+1} - P_{k+1} + C_{k+1}\right] \qquad (4.38)$$

$$\left. + \Delta\underline{v}_{k+2}^T \left[A_{k+1}\right] \right\}$$

since $$\frac{\partial \underline{\alpha}_\ell}{\partial \underline{x}_k} = \frac{\partial \underline{\alpha}_\ell}{\partial \underline{y}_k} + \frac{\partial \underline{\alpha}_\ell}{\partial \underline{y}_{k+1}}$$

where $$\underline{\alpha}_\ell = \underline{v}_{E,\ell} \text{ , } \underline{v}_{P,\ell} \text{ , or } \underline{v}_{H,\ell}$$

for an entry point.

For an exit point, the gradient is given by

$$\underline{g}_k = 2 \left\{ \Delta\underline{v}_{k-1}^T \left[- \frac{\partial \underline{v}_{H,k-1}}{\partial \underline{x}_k} \right] \right.$$

$$+ \Delta\underline{v}_k^T \left[\frac{\partial \underline{v}_{E,k}}{\partial \underline{x}_k} - \frac{\partial \underline{v}_{P,k}}{\partial \underline{x}_k} - \frac{\partial \underline{v}_{H,k}}{\partial \underline{x}_k} \right]$$

$$\left. + \Delta\underline{v}_{k+1}^T \left[\frac{\partial \underline{v}_{E,k+1}}{\partial \underline{x}_k} \right] \right\} \qquad (4.39)$$

Using (4.28)-(4.31), this becomes

$$g_k = 2 \left\{ \Delta\underline{v}_{k-1}^T \left[-D_k\right] + \Delta\underline{v}_k^T \left[C_k - P_k - B_k\right] \right. \qquad (4.40)$$

$$\left. + \Delta\underline{v}_{k+1}^T \left[A_k\right] \right\}$$

since $\frac{\partial \underline{\alpha}_\ell}{\partial \underline{x}_k} = \frac{\partial \underline{\alpha}_\ell}{\partial \underline{Y}_k}$ for an exit point

The gradient vectors are calculated for all entry and exit points except the launch and arrival points (these are considered fixed boundary conditions) and then formed into an enlarged gradient vector

$$\underline{g} = \begin{bmatrix} \underline{g}_2 \\ \underline{g}_3 \\ \cdot \\ \cdot \\ \cdot \\ \underline{g}_{2N-3} \end{bmatrix} \tag{4.41}$$

4.3 First-Order Techniques

In finding a solution $z=\alpha$ of an equation $f(z)=a$, an iterative technique which functions such that

$$z_{k+1} - \alpha = q_k (z_k - \alpha) \qquad |q_k| < 1 \tag{4.42}$$

is known as a first-order technique. Several first-order techniques were employed to minimize the cost function J.

4.31 Steepest Descent

Referring to the notation of (4.1), the method of steepest descent prescribes a change

$$\underline{s}_{k+1} = \underline{s}_k + \delta \underline{s}_k \tag{4.43}$$

$$\delta \underline{s}_k = - h_k \, \underline{g}(\underline{s}_k) \tag{4.44}$$

The multiplier h_k is used to set the step size. One method of determining it is on the basis of desired change in the cost J. Since

$$\delta J = \underline{g}^T (\underline{s}_k)\ \delta \underline{s}_k$$

$$= - h_k\ \underline{g}^T (\underline{s}_k)\, \underline{g}(\underline{s}_k) \tag{4.45}$$

the value of h_k is given by

$$h_k = - \frac{\delta J}{\underline{g}^T(\underline{s}_k)\underline{g}(\underline{s}_k)} \tag{4.46}$$

The value of δJ is chosen to be some fraction of the cost J at the state $\underline{s}_k$. Thus

$$\delta J = - \gamma_k\ J(\underline{s}_k) \tag{4.47}$$

Thus

$$h_k = \frac{\gamma_k J(\underline{s}_k)}{\underline{g}^T(\underline{s}_k)\underline{g}(\underline{s}_k)} \tag{4.48}$$

The initial value of γ_k is $\gamma_1 = 1$.

The procedure for a single steepest descent step is as follows

1) At the present state $\underline{s}_k$, evaluate the gradient $\underline{g}(\underline{s}_k)$ and the multiplier h_k.
2) Take the step given by (4.44). At the new state $\underline{s}_{k+1}$, evaluate the cost $J(\underline{s}_{k+1})$.
3) If the new cost $J(\underline{s}_{k+1})$ is less than the old cost $J(\underline{s}_k)$, accept the step and set

$$\gamma_{k+1} = 1.1\ \gamma_k \tag{4.49}$$

4) If the new cost is greater than the old cost, reject the step. Set

$$\gamma_{k+1} = 0.5\ \gamma_k \tag{4.50}$$

and repeat the step.

This form of the steepest descent technique suffers from two shortcomings. The first of these is the method of step-size control. While it does insure that each accepted step will reduce the cost function, it does not usually take the best possible step. The second, and more serious, concerns the nature of the cost function, which is much steeper in directions corresponding to changes in the angle components of $\underline{s}$ than in directions corresponding to changes in the time components. This is the common "ravine" problem encountered in many parameter optimization situations. As depicted in Figure 4.1, it results in a zig-zag path yielding little cost reduction for each step. The means of alleviating both these shortcomings are dealt with in the next section.

4.32 Modified Steepest Descent

4.321 Optimum Step-Size Selection

To insure an optimum step in the direction specified by (4.44), a parabola is fitted to the cost function in that direction and the step taken to its minimum. For a parabola given by

$$(y-c_0) = c_1(x-c_2)^2 \tag{4.51}$$

the constants c_0, c_1, c_2 may be determined from the values of the ordinate y at x=0 and x=1 and the slope at x=0.

$$y_0 = y(0) \qquad y_0' = \frac{dy}{dx}\Big|_{x=0} \tag{4.52}$$

$$y_1 = y(1)$$

Substituting (4.52) into (4.51) yields three equations

$$y_0 - c_0 = c_1 c_2^2 \tag{4.53}$$

$$y_1 - c_0 = c_1 (1-c_2)^2 \tag{4.54}$$

$$y_0' = -2c_1 c_2 \tag{4.55}$$

Solving (4.53)-(4.55) for c_0, c_1, c_2 yields

$$c_1 = y_1 - y_0 - y_0' \tag{4.56}$$

$$c_2 = -\frac{y_0'}{2c_1} \tag{4.57}$$

$$c_0 = y_0 - c_1 c_2^2 \tag{4.58}$$

This technique searches for the minimum of the cost function along the line $\underline{s} = \underline{s}_k + x\delta\underline{s}_k$. The units are such that x=1 corresponds to the step taken in the preceding section.

The procedure for taking an optimum step is as follows:

1) At the present state $\underline{s}_k$, evaluate the cost $J(\underline{s}_k)$, the gradient $\underline{g}(\underline{s}_k)$, and the multiplier h_k.

2) Take the step $\delta\underline{s}_k$ given by (4.44). At the new state $\hat{\underline{s}}_k$ evaluate the cost $J(\hat{\underline{s}}_k)$.

3) For the parabolic fit, set

$$y_0 = J(\underline{s}_k) \qquad (x=0) \tag{4.59}$$

$$y_1 = J(\hat{\underline{s}}_k) \qquad (x=1) \tag{4.60}$$

$$y_0' = \delta J = -\gamma_k J(\underline{s}_k) \qquad (x=0) \tag{4.61}$$

Solve for the values of c_0, c_1, c_2 using (4.56)-(4.58).

4) Take the optimum step

$$\underline{s}_{k+1} = \underline{s}_k + c_2\, \delta\underline{s}_k \tag{4.62}$$

and set

$$\gamma_{k+1} = c_2\, \gamma_k \tag{4.63}$$

This technique requires one additional evaluation of the cost function (in step 2)

4.322 Gradient Weighting Matrix Selection

From Figure 4.1, it can be seen that the gradient components directed across the "ravine" will experience a sign change at each step while those components along the axis of the "ravine" will remain unchanged in sign. Thus, the ravine problem may be alleviated by adding a weighting matrix W_k which turns the step direction along those gradient components which do not change sign. This modification of (4.44) results in the new step

$$\delta\underline{s}_k = -h_k\, W_k\, \underline{g}(\underline{s}_k) \tag{4.64}$$

The weighting matrix is a diagonal matrix of weighting coefficients

$$W_k = \begin{bmatrix} w_{1,k} & & & & \\ & w_{2,k} & & & \\ & & w_{3,k} & & \\ & & & \ddots & \\ & & & & w_{6N-12,k} \end{bmatrix} \tag{4.65}$$

each of which corresponds to one component of the gradient vector. The initial value of the weighting matrix is an identity matrix.

$$W_1 = I \tag{4.66}$$

After each step, each component of the gradient is tested to see if it has changed sign. The weighting coefficients corresponding to those components which have not changed sign are increased by an amount w_g.

$$w_{i,k+1} = w_{i,k} + w_g \tag{4.67}$$

while the coefficients corresponding to components which have changed sign are decreased by a like amount.

$$w_{i,k+1} = w_{i,k} - w_g \tag{4.68}$$

All weighting coefficients are constrained to lie in the range

$$1 \leq w_{i,k} \leq w_M \tag{4.69}$$

Different values of gain w_g and maximum value w_M are assigned to coefficients corresponding to the θ, ϕ, and t components.

The net result of this procedure is to bias the direction of the step in favor of those components of the gradient whose sign remains unchanged. This is exactly what is needed to proceed down the length of the "ravine". The technique which incorporates both the optimum step-size control and the weighted gradient step will be termed the optimum gradient step (OGS).

4.33 Conjugate Gradient Method

The method of conjugate gradients uses the information gained from previous steps taken to gradually construct a set of mutually conjugate directions. If the cost function J were an N-dimensional quadratic form, a sequence of N one-dimensional minimizations along these conjugate directions would locate the minimum of the cost function. For general functions, the process is iterative rather than convergent in a finite number of steps. The method is detailed in [32]. The computer subroutine used is DFMCG taken from [33].

4.34 Use of Acceleration Steps

This method is a modification of steepest descent used to avoid the ravine problem. It uses steepest descent steps with occasional acceleration steps given by

$$\delta \underline{s}_k = p_k(\underline{s}_k - \underline{s}_{k-2})$$

where p_k = multiplier chosen for step-size control.
These acceleration steps have the effect of moving along the axis of the zig-zag pattern shown in Figure 4.1 when the ravine problem is encountered. A modification of this procedure using alternating steepest descent and acceleration steps is given [34].

4.4 Second-Order Techniques

In finding a solution $z=\alpha$ to an equation $f(z)=a$, an iterative technique which acts such that

$$z_{k+1} - \alpha = q_k(z_k-\alpha)^2 \qquad |q_k|<1 \tag{4.70}$$

is known as a second-order technique. The technique used in this thesis is a generalized Newton-Rapheson iteration. It may be used only if the minimum value of the cost function J is zero since it searches for a zero of the $\underline{u}$ vector.

Using the notation of (4.1) and (4.3), it is possible to construct the matrix equation

$$-\underline{u} = H\ \delta\underline{s} \tag{4.71}$$

where H is a matrix built up of the (3x3) sub-matrices $H_{i,j}$ according to the rules

1) For i = odd,

$$H_{i-1,i} = D_{i+1} \qquad (=0 \text{ for } i=1) \tag{4.72}$$

$$H_{i,i} = B_{i+1} - P_{i+1} - C_{i+1} - D_{i+2} \tag{4.73}$$

$$H_{i+1,i} = - A_{i+1} - B_{i+2} - P_{i+2} + C_{i+2} \tag{4.74}$$

$$H_{i+2,i} = A_{i+2} \qquad (=0 \text{ for } i=2N-3) \tag{4.75}$$

2) For i = even

$$H_{i-1,i} = - D_{i+1} \tag{4.76}$$

$$H_{i,i} = C_{i+1} - P_{i+1} - B_{i+1} \tag{4.77}$$

$$H_{i+1,i} = A_{i+1} \qquad (=0 \text{ for } i=2N-4) \tag{4.78}$$

3) For all $H_{i,j}$ not covered by (4.72)-(4.78)

$$H_{i,j} = \begin{bmatrix} 0 & 0 & 0 \\ 0 & 0 & 0 \\ 0 & 0 & 0 \end{bmatrix} \tag{4.79}$$

These matrices are identical to the bracketed terms in (4.38) and (4.40). The subscripts are offset by 1 since the terms in $\underline{u}$ and $\delta\underline{s}$ run from 2 to 2N-3 while the subscripts of $H_{1,J}$ run from 1 to 2N-4.

Solving (4.71) yields the variation which would cancel the velocity mis-match vector if the linearization were an exact process

$$\delta\underline{s} = - H^{-1} \underline{u} \tag{4.80}$$

Since the linearization yields only a local approximation to the cost function surface, this process is iterative. However, second-order convergence is achieved.

The matrix H to be inverted in (4.80) is of dimension 6(N-2) where N may be quite large. The inversion may be considerably simplified by noting that H is a banded matrix (i.e. has non-zero terms only on or near its main diagonal). Using this property solution (4.80) may be obtained by solving the set of linear equations (4.71) using a Gauss-Jordan method which stores and manipulates only the non-zero elements. This allows the storage and computational time to be reduced considerably. The computer subroutine used is DGELB from [33].

4.5 Application of Inequality Constraints

At a planet, the coordinates of the entry and exit points are given by

$$\text{entry point} = \underline{x}_k = \begin{bmatrix} \theta_k \\ \phi_k \\ t_k \end{bmatrix} \tag{4.81}$$

$$\text{exit point} = \underline{x}_{k+1} = \begin{bmatrix} \Delta\theta_{k+1} \\ \Delta\phi_{k+1} \\ \Delta t_{k+1} \end{bmatrix} \tag{4.82}$$

Unit vectors centered in the planet in the direction of the entry and exit points are given by

$$\underline{i}_k = \begin{bmatrix} \cos\theta_k & \cos\phi_k \\ \sin\theta_k & \cos\phi_k \\ \sin\phi_k & \end{bmatrix} \tag{4.83}$$

$$\underline{i}_{k+1} = \begin{bmatrix} \cos(\theta_k + \Delta\theta_{k+1})\cos(\phi_k + \Delta\phi_{k+1}) \\ \sin(\theta_k + \Delta\theta_{k+1})\cos(\phi_k + \Delta\phi_{k+1}) \\ \sin(\phi_k + \Delta\phi_{k+1}) \end{bmatrix} \tag{4.84}$$

Assuming that these unit vectors approximate the asymptotes of the swingby hyperbola, the turn angle ν of the hyperbola is given by

$$\nu = \pi - \cos^{-1}\left[\underline{i}_k \cdot \underline{i}_{k+1}\right] \tag{4.85}$$

$$= \pi - \cos^{-1}\left[\cos(\Delta\theta_{k+1})\cos\phi_k\cos(\phi_k+\Delta\phi_{k+1})\right.$$

$$\left. + \sin\phi_k\sin(\phi_k+\Delta\phi_{k+1})\right] \tag{4.86}$$

See Figure (4.2) for an illustration of this angle. The maximum turn angle possible for a minimum periapse radius of r_{PA} is given by

$$\nu_M = 2 \sin^{-1} \left[\frac{1}{1 + \frac{r_{PA} v_I^2}{\mu_i}} \right] \tag{4.87}$$

where

μ_i = gravitational parameter of the planet

v_I = hyperbolic excess velocity

$$= \left[\underline{v}_{H,k}^T \underline{v}_{H,k} - 2 \frac{\mu_i}{r_{s,i}} \right]^{\frac{1}{2}} \tag{4.88}$$

$r_{s,i}$ = radius of planetary sphere of influence

Before the acceptance of a step $\delta\underline{x}_k$ and $\delta\underline{x}_{k+1}$ for a planet's entry and exit points, the values of ν and ν_M are calculated for the projected new values

$$\begin{aligned} \hat{\underline{x}}_k &= \underline{x}_k + \delta\underline{x}_k \\ \hat{\underline{x}}_{k+1} &= \underline{x}_{k+1} + \delta\underline{x}_{k+1} \end{aligned} \tag{4.89}$$

If $\nu > \nu_M$, the components of $\delta\underline{x}_{k+1}$ are set equal to zero and the components of $\delta\underline{x}_k$ are left unchanged. This procedure is repeated for each swingby on every iteration. The criterion for the minimum periapse distance is

$$r_{P,A} = k_M r_e \tag{4.90}$$

where

r_e = equatorial radius of the planet

k_M = constant multiplier (usually 1.1)

4.6 Behavior of Minimization Techniques

In general, the techniques discussed in sections 4.3 and 4.4 behaved as follows;

1) The steepest descent technique suffered badly from the ravine problem. It was not used extensively.

2) The optimum gradient step (OGS) dealt with the ravine problem fairly well and also solved the step-size control difficulties. It was adapted easily to the constrained case. The OGS was the most useful first-order technique employed.

3) The conjugate gradient method proved to be slightly faster than the OGS. It was not adaptable to the constrained problem. Thus it was employed mainly as a check on the performance of the OGS.

4) The acceleration steps showed no noticeable improvement over the OGS. They were not used extensively.

5) The generalized Newton-Rapheson technique showed second-order convergence near the solution. However, it sometimes diverged when started too far from the solution point. Also, it was applicable only when the minimum of the cost function was zero.

In general, the first-order techniques showed a diminishing speed of convergence as they approach the solution point. They were useful

mainly to reach the neighborhood of the minimum. If applicable (i.e. if an admissible minimum equal to zero exists) the second-order technique was used to converge to the solution. Otherwise the OGS technique was used for the whole process.

4.7 Application of the Trajectory Segment Matching Technique

The procedure for application of the trajectory segment matching procedure is as follows.

1) Using the cost function given in (2.13) and (2.14) converge to a minimum of the cost for the advanced patched conic model.

2) For this solution, compute the velocity offsets as described in Chapter 3.

3) Using the cost function given in (3.31) and (3.32) converge to a minimum of the cost for the perturbed conic model. During this iteration, the offsets $\delta \underline{v}_{E,k}$ and $\delta \underline{v}_{H,k}$ are considered to be constants and thus remain unchanged.

4) For this new solution, re-compute the velocity offsets. If they have changed measurably, return to step 3. Otherwise, terminate the process.

The result is a sequence of perturbed conic legs matched in position, velocity, and time at the sphere of influence entry and exit points. The accuracy of this sequence may be checked by determining a set of exact trajectory legs (corresponding to the same initial and final conditions on position and time) by numerical integration. In all cases examined, the perturbed conic legs have been close enough that the numerical trajectory integration has converged to the desired boundary conditions within two or three iterations.

Examples of the use of this technique are given in the next three chapters.

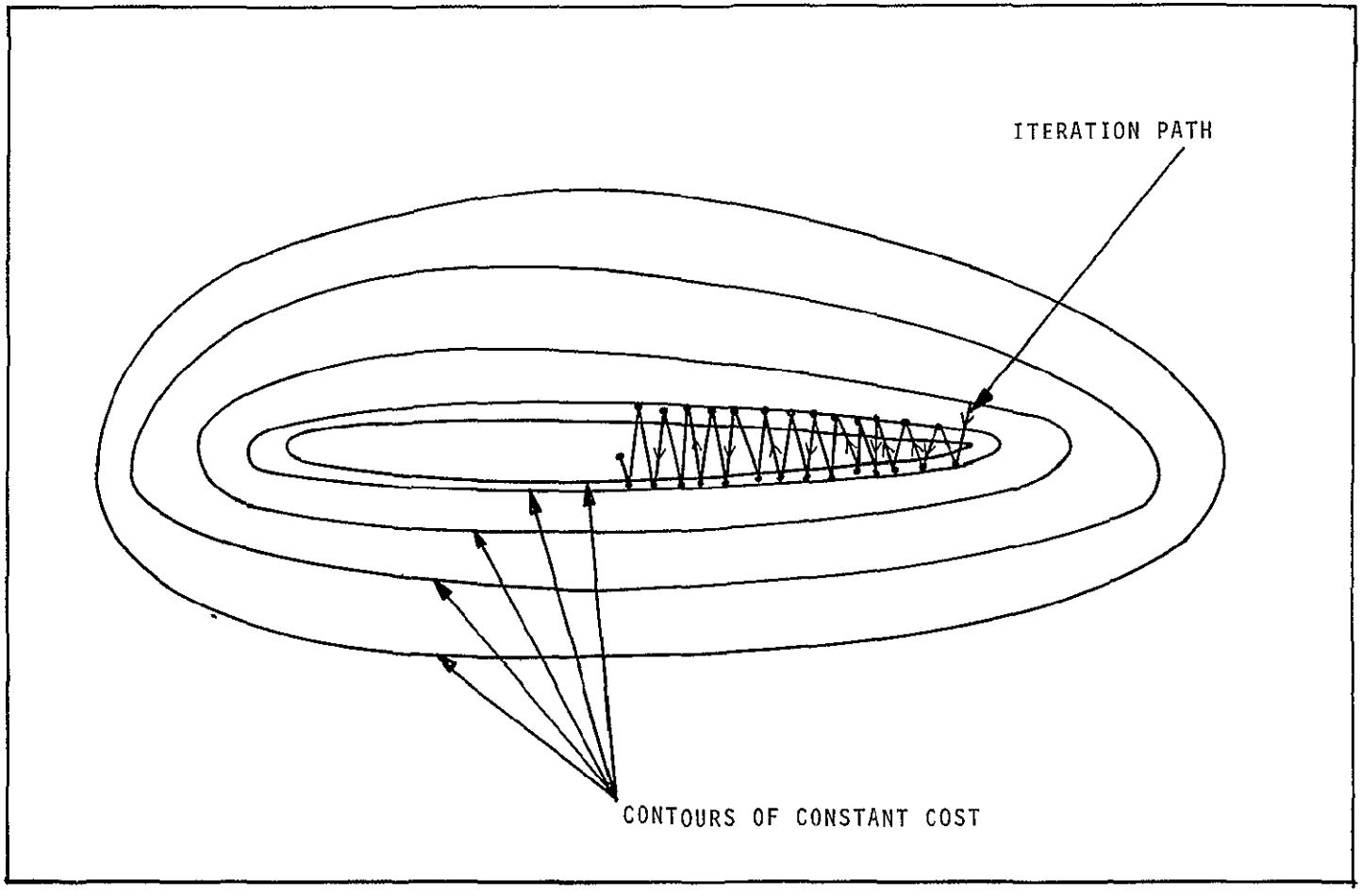

Figure 4.1 Behavior of Steepest Descent Technique in a "Ravine"

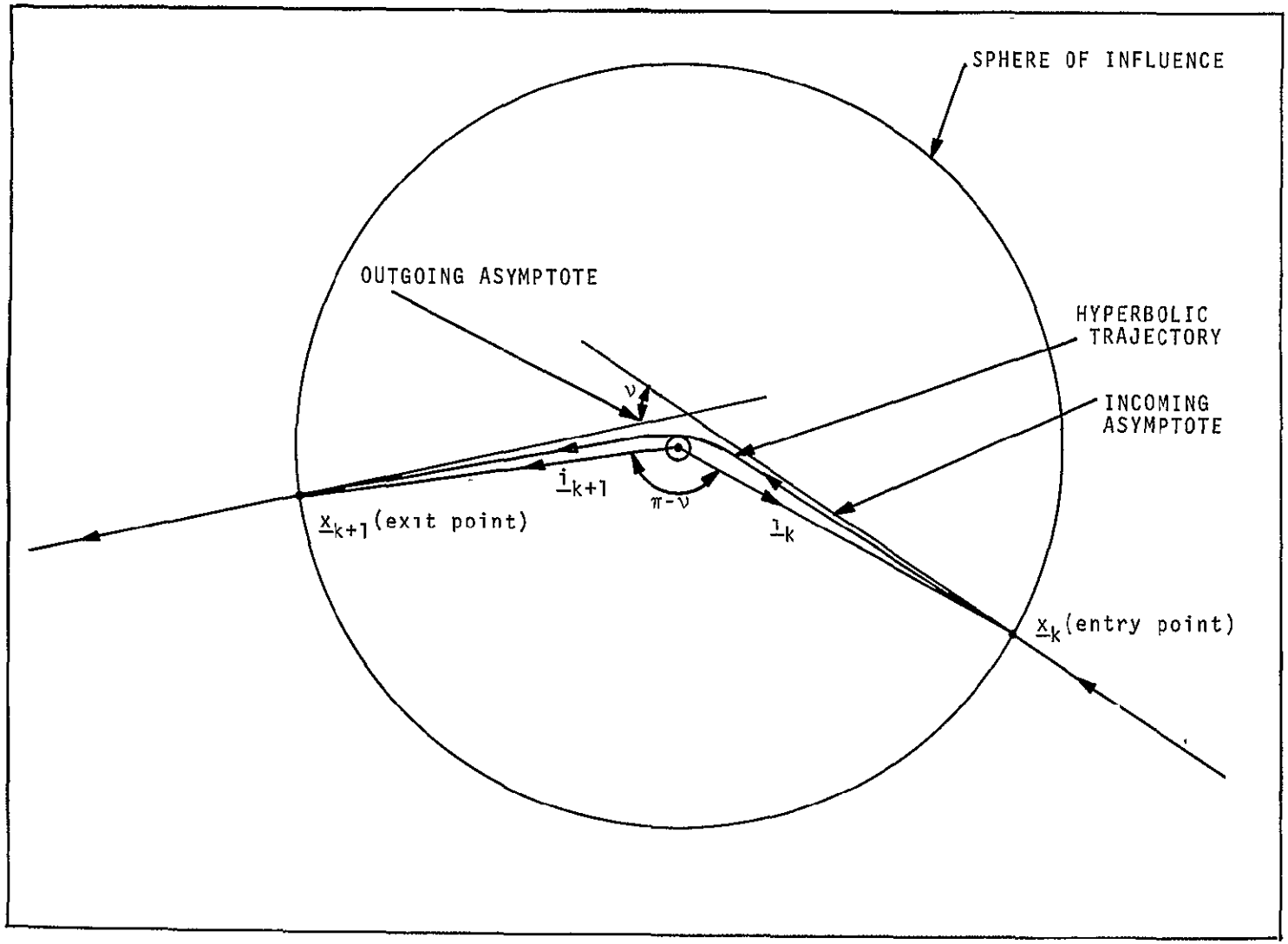

Figure 4.2 Calculation of Turn Angle

Chapter 5

Dual Planet Reconnaissance Trajectory Example

5.0 Chapter Summary

The dual planet reconnaissance trajectory is described. The coordinates of the sphere of influence entry and exit points and the orbital elements of the individual trajectory legs are given. The performance of the trajectory segment matching technique is discussed. The results of the perturbed conic analysis are tabulated and the analytic predictions are compared with numerically integrated trajectory legs. The resulting comparison shows that the trajectory may be predicted to within a total correction of 0.2263 m/sec.

5.1 Description of the Mission

This mission employs a free-fall trajectory (see Figure 5.1) which leaves Earth, makes a close pass first to Venus and then to Mars, and then returns to Earth. It would be possible for a reconnaissance mission of both Mars and Venus by manned or unmanned spacecraft. In the unmanned case the return to earth would allow recovery of high resolution photographs taken during the swingbys. This mission is described in [3]. A method for finding these dual planet swingbys using the simple patched conic model is given in [10].

The final trajectory is specified by the following set of planetary sphere of influence (SOI) entry and exit points. The SOI radii are given in Appendix C.

Point	Julian Date	Location
1	2441478.80000	Earth SOI exit point (launch)
2	2441634.11977	Venus SOI entry point
3	2441637.99955	Venus SOI exit point
4	2441787.28715	Mars SOI entry point
5	2441792.32920	Mars SOI exit point
6	2441949.20000	Earth SOI entry point (arrival)

The spherical coordinates of the SOI entry and exit points given in a planetocentric ecliptic coordinate system (see Appendix A) are

Point	Azimuth	Elevation
1	142.800°	-19.600°
2	332.249°	-2.637°
3	177.796°	1.716°
4	43.066°	4.118°
5	222.458°	3.885°
6	8.300°	5.700°

The complete set of cartesian coordinates of the SOI entry and exit points in the heliocentric and planetocentric coordinate frames plus the heliocentric coordinates of the planet are given in Appendix E.

The total time of flight is relatively short (about 1.3 years) and divided approximately evenly among the heliocentric legs.

Leg	Time of Flight (days)	Central Angle Traversed
1-2	155.31977	244.268°
2-3	3.87978	193.491°
3-4	149.28760	122.855°
4-5	5.04205	184.410°
5-6	156.87080	85.562°

The legs (2-3) and (4-5) are planetocentric hyperbolas, while legs (1-2),(3-4) and (5-6) are heliocentric ellipses. The orbital elements of these legs are

Leg	Semi-Major Axis		Eccentricity	Inclination
1-2	0.80837	a.u.	0.25644	3.348°
2-3	0.72733	r_p	4.28637	3.053°
3-4	1.07057	a.u.	0.37045	3.290°
4-5	0.24513	r_p	13.00436	94.337°
5-6	1.06599	a.u.	0.37479	1.310°

The semi-major axis is given in astronomical units (a.u.) for the heliocentric legs and in planetary radii for the planetocentric legs.

The vis-viva energy at earth needed to launch on this trajectory is

$$C_3 = 18\ 378\ \ km^2/sec^2$$

while the re-entry velocity on return to earth is

$$V_R = 15{,}639.128\ m/sec$$

The periapse radius (in kilometers and planetary radii), the periapse velocity (in km/sec), and the turn angle (as defined in Section 4.5) for the planetocentric legs are

Leg	Periapse Radius	Periapse Velocity	Turn Angle
2-3	14,461.578 (2.3903)	10.904491	13.491°
4-5	10,034.548 (2.9427)	7.737818	4.410°

The time of periapse is the mid-point between the entry and exit times on the sphere of influence.

All of the parameters listed in this section are for the two-body trajectory legs used as reference orbits for the final perturbed conic analysis.

5.2 Performance of Trajectory Segment Matching Techniques

The trajectory segment matching technique is repeated through several cycles. The first of these uses only the advanced conic model. The initial conditions are obtained from [10] where the trajectory was determined using the simple patched conic model. All successive cycles employ the perturbed conic model with the velocity offsets re-calculated

for each cycle. The column labeled method indicates whether the optimum gradient step (OGS) or the generalized Newton-Rapheson (GNR) procedure is used for that step. The cost function is defined by (2.13-.14) for the first cycle and by (3.31-.32) for successive cycles.

First Cycle: Iteration	Method	Cost Function (km/sec)
Initial Conditions	-	3.87296
1	OGS	2.81187
2	OGS	0.35187
3	GNR	0.29405 (10^{-3})
4	GNR	0.34828 (10^{-9})
5	GNR	0.36653 (10^{-17})

Second Cycle: Iteration	Method	Cost Function
Initial Conditions	-	0.35299 (10^{-3})
1	GNR	0.14899 (10^{-9})
2	GNR	0.17063 (10^{-17})

Third Cycle: Iteration	Method	Cost Function
Initial Conditions	-	0.65610 (10^{-8})
1	GNR	0.10061 (10^{-16})

Fourth Cycle: Iteration	Method	Cost Function
Initial Conditions	-	0.31691 (10^{-12})

The change from OGS to GNR occurred when the cost function fell below 0.5. A cycle was terminated when the cost went below 1.0 (10^{-14}) and the whole procedure was ended when the cost at the initial point of a new cycle was less than 1.0 (10^{-10}). The total running time of this process on the IBM 360/65 was 48 sec.

5.3 Perturbed Conic Results

The first step in the perturbed conic model was the calculation of the perturbations in the initial and final position and velocity

for each leg due to the disturbing accelerations. The magnitudes of these perturbations (in km and m/sec) for the last cycle are

Leg	$\delta r(t_1)$	$\delta v(t_1)$	$\delta r(t_2)$	$\delta v(t_2)$
1-2	35,161.42	39.727	9331.04	25.252
2-3	1,482.11	26.470	1335.23	23.669
3-4	11,780.23	26.099	2069.76	3.544
4-5	242.58	3.347	236.88	3.248
5-6	4,769.78	3.698	6545.68	15.886

The next step is the calculation of the position and velocity perturbations at the mid-point that eliminate the position perturbations at the initial and final points. These mid-point perturbation magnitudes (in km and m/sec) for the last cycle are

Leg	$\delta\hat{r}(t_M)$	$\delta\hat{v}(t_M)$
1-2	9197.48	4.882
2-3	324.23	50.435
3-4	6059.22	0.448
4-5	9.31	1.330
5-6	3618.21	0.723

The last step is the calculation of the offsets of the initial and final velocities. These offset magnitudes (in m/sec) for the last cycle are

Leg	$\delta\hat{v}(t_1)$	$\delta\hat{v}(t_2)$
1-2	34.286	24.139
2-3	19.034	14.558
3-4	22.322	3.211
4-5	2.221	2.183
5-6	2.997	14.982

5.4 Comparison with Numerically Integrated Results

The accuracy of the analytic procedure is evaluated by comparison with numerically integrated trajectory legs determined using the following procedure:

1) The initial conditions for the numerical integration are set equal to the conic position and the perturbed conic velocity at the initial time t_1.

$$\tilde{\underline{r}}(t_1) = \underline{r}_0(t_1)$$

$$\tilde{\underline{v}}(t_1) = \underline{v}_0(t_1) + \delta\hat{\underline{v}}(t_1) \tag{5.1}$$

[~ denotes values on the numerically integrated trajectory]

2) The N-body equations of motion and the differential equations for the N-body state transition matrix are integrated forward to the final time t_2. The errors in position and velocity at the final time are given by

$$\Delta\underline{r}(t_2) = \tilde{\underline{r}}(t_2) - \underline{r}_0(t_2) \tag{5.2}$$

$$\Delta\underline{v}(t_2) = \tilde{\underline{v}}(t_2) - [\underline{v}_0(t_2) + \delta\hat{\underline{v}}(t_2)] \tag{5.3}$$

The numerical integration routine is described in [26].

3) Using the N-body state transition matrix between t_1 and t_2, the change in $\tilde{\underline{v}}(t_1)$ needed to eliminate $\Delta\underline{r}(t_2)$ is calculated.

Steps 2) and 3) are repeated until $\Delta\underline{r}(t_2)$ is driven to zero. If the initial guess is close this happens quite rapidly. For this example, $\Delta\underline{r}(t_2)$ was reduced to under 10^{-5} km in two iterations.

The quantities chosen to indicate the accuracy of the analytic techniques are the magnitude of the velocity error at t_1

$$\Delta\underline{v}(t_1) = \tilde{\underline{v}}(t_1) - [\underline{v}_0(t_1) + \delta\hat{\underline{v}}(t_1)], \tag{5.4}$$

the magnitude of the velocity error at t_2

$$\Delta\underline{v}(t_2) = \tilde{\underline{v}}(t_2) - [\underline{v}_0(t_2) + \delta\hat{\underline{v}}(t_2)], \tag{5.5}$$

and the position error at t_2 due to the use of the analytically determined velocity at t_1 for the numerical integration

$$\Delta\underline{r}(t_2) = \tilde{\underline{r}}(t_2) - \underline{r}_0(t_2) \tag{5.6}$$

for

$$\tilde{\underline{v}}(t_1) = \underline{v}_0(t_1) + \delta\hat{\underline{v}}(t_1) \quad .$$

These values (in km and m/sec) are

Leg	$\Delta v(t_1)$	$\Delta v(t_2)$	$\Delta r(t_2)$
1-2	.1250	.0450	5327.23
2-3	.0030	.0091	9.71
3-4	.0430	.0041	1306.60
4-5	.0028	.0030	1.62
5-6	.0017	.0173	15.39

In order to fly the trajectory, it would be necessary to apply velocity corrections at each of the SOI entry and exit points to

eliminate these errors. The magnitudes of these corrections (in m/sec) are

Point	Correction
1	0.1250
2	0.0448
3	0.0340
4	0.0022
5	0.0030
6	0.0173

The total correction needed is

$$\Delta v = 0.2263 \text{ m/sec.}$$

It is also possible to compare the periapse conditions of the numerically integrated trajectory with those of the two-body reference trajectory used in the perturbed conic analysis. The differences are

Leg	Δr_π	Δv_π	Δt_π
2-3	8.3576 km	8.0255 m/sec	-29.142 sec
4-5	0.6106 km	1.1715 m/sec	-1.223 sec

where

t_{π_0} = time of periapse for two-body reference orbit

$\tilde{t}_\pi$ = time of periapse for numerically integrated trajectory

$$\Delta \underline{r}_\pi = \tilde{\underline{r}}_\pi(\tilde{t}_\pi) - \underline{r}_0(t_{\pi_0})$$

$$\Delta \underline{v}_\pi = \tilde{\underline{v}}_\pi(\tilde{t}_\pi) - \underline{v}_{\pi_0}(t_{\pi_0})$$

$$\Delta t_\pi = \tilde{t}_\pi - t_{\pi_0}$$

5.5 Discussion of Results

The analytic technique has provided an accurate description of the legs of the dual planet reconnaissance trajectory. The velocity errors described in the last section could be eliminated by running the trajectory segment matching procedure for a few more cycles using offsets calculated by numerical integration rather than by the analytic techniques of Chapter 3. Instead, it is probably easier to absorb these errors in the mid-course corrections made on approach and departure from each planet.

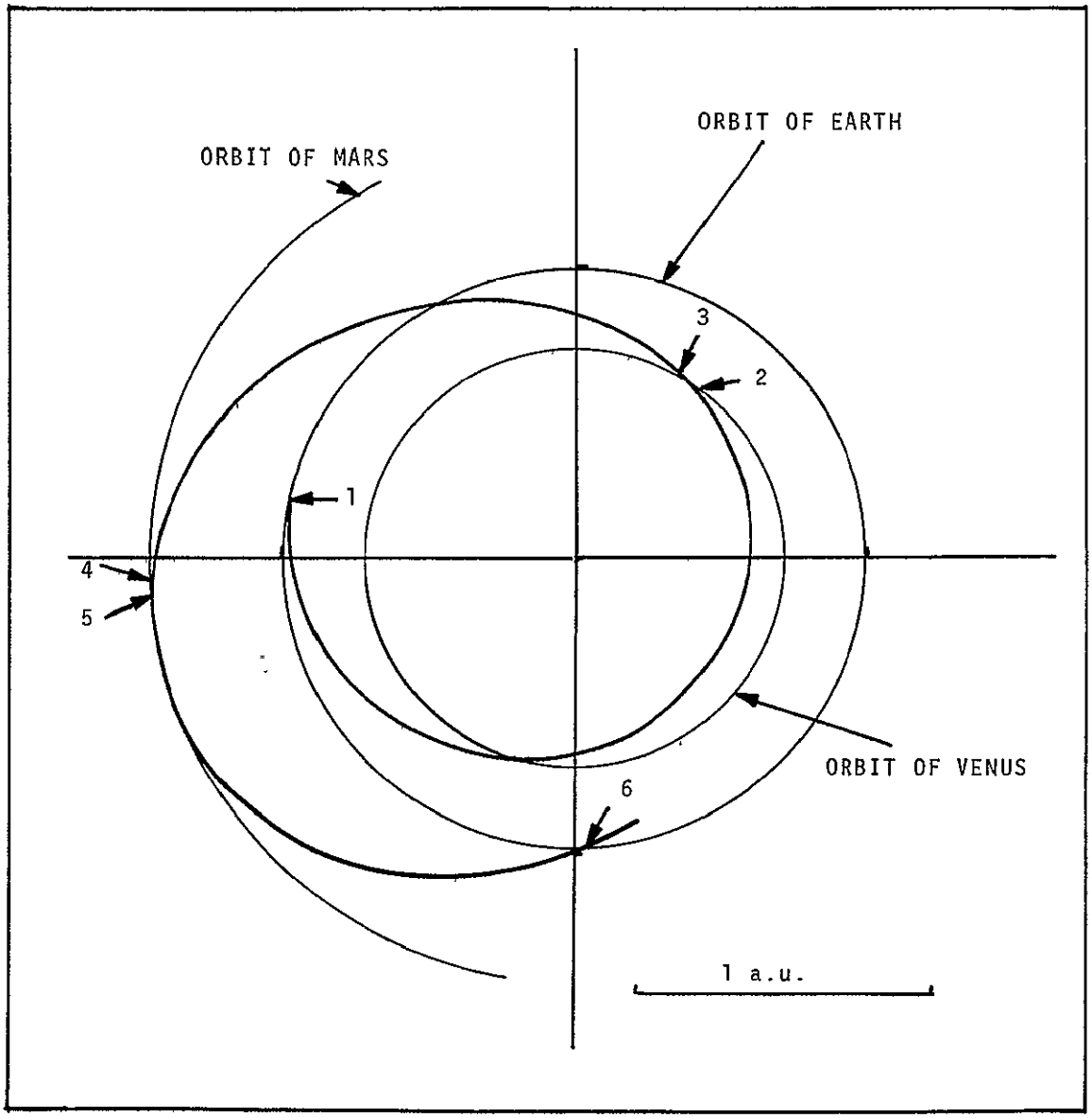

Figure 5.1 Dual Planet Reconnaisance Trajectory

Chapter 6

Grand Tour Trajectory Example

6.0 Chapter Summary

The Grand Tour mission is described. The coordinates of the sphere of influence entry and exit points and the orbital elements of the individual trajectory legs are given. The performance of the trajectory segment matching procedure is discussed. The results of the perturbed conic analysis are tabulated and the analytic predictions are compared with numerically integrated trajectory legs. This comparison shows that the trajectory may be predicted to within a total correction of 2.652 m/sec. The accuracy of the model for the disturbing acceleration during the planetocentric phase is considered.

6.1 Description of the Mission

This mission employs a free-fall trajectory (see Figures 6.1 and 6.2) which leaves Earth and makes successive close passes to Jupiter, Saturn, Uranus, and Neptune. The configuration of the planets necessary for the Grand Tour occur only once every 179 years with the next opportunity occurring in the period 1975-1981. Descriptions of this type of mission may be found in [16],[17], and [20] where the simple patched conic model is used to determine launch windows and approximate trajectory parameters. The specific trajectory chosen for this chapter leaves Earth in October, 1978.

The final trajectory is specified by the following set of planetary sphere of influence (SOI) entry and exit points. The SOI radii are listed in Appendix C.

Point	Julian Date	Location
1	2443787.00000	Earth SOI exit point (launch)
2	2444291.61927	Jupiter SOI entry point

Point	Julian Date	Location
3	2444457.85596	Jupiter SOI exit point
4	2444930.62043	Saturn SOI entry point
5	2445126.30248	Saturn SOI exit point
6	2446481.99628	Uranus SOI entry point
7	2446638.44605	Uranus SOI exit point
8	2447720.00000	Neptune SOI entry point (arrival)

The launch date is October 6, 1978 while the arrival date is July 13, 1989 (which luckily occurs on a Thursday in that year).

The spherical coordinates of the SOI entry and exit points given in a planetocentric ecliptic coordinate system (see Appendix A) are

Point	Azimuth	Elevation
1	101.424°	8.720°
2	312.920°	1.093°
3	180.066°	4.253°
4	16.039°	-3.433°
5	281.565°	-2.502°
6	94.166°	1.665°
7	291.444°	2.975°
8	114.270°	-2.812°

The complete set of cartesian coordinates of the SOI entry and exit points in the heliocentric and planetocentric coordinate frames plus the heliocentric coordinates of the planets at encounter are given in Appendix E.

The total flight time for the trajectory is short (about 10.77 years) considering the distance covered. The time of flight and central angle traversed for the individual legs are

Leg	Time of Flight (days)	Central Angle Traversed
1-2	504.61927	144.498°
2-3	166.23669	205.609°
3-4	472.76447	25.902°
4-5	195.68205	223.050°
5-6	1355.69380	54.438°
6-7	156.44977	189.035°
7-8	1081.55395	17.392°

The legs (2-3), (4-5), and (6-7) are planetocentric hyperbolas about Jupiter, Saturn, and Uranus respectively. The leg (1-2) is a heliocentric ellipse while legs (3-4), (5-6) and (7-8) are heliocentric hyperbolas. Each swingby adds energy to the trajectory, keeping it above solar escape energy after the Jupiter swingby. The orbital elements for the trajectory legs are

Leg	Semi-Major Axis	Eccentricity	Inclination
1-2	4.61480 a.u.	0.78328	2.383°
2-3	17.22512 r_p	2.31355	6.881°
3-4	28.43593 a.u.	1.14287	2.857°
4-5	5.23592 r_p	1.46490	4.412°
5-6	3.77866 a.u.	3.54820	2.836°
6-7	1.10298 r_p	6.36816	15.110°
7-8	3.06068 a.u.	5.41387	2.821°

The semi-major axis is given in astronomical units (a.u.) for the heliocentric legs and in planetary radii for the planetocentric legs.

The vis-viva energy at earth needed to launch on this trajectory is

$$C_3 = 101.520 \text{ km}^2/\text{sec}^2$$

The periapse radius (in kilometers and planetary radii), the periapse velocity (in km/sec) and the turn angle (as defined in Section 4.5) for the planetocentric legs are

Leg	Periapse Radius	Periapse Velocity	Turn Angle
2-3	1,615,506.286 (22.62614)	16.121540	25.609°
4-5	147,025.929 (2.4342)	25.207545	43.050°
6-7	139,143.535 (5.9210)	17.530135	9.035°

The time of periapse is the mid-point between the entry and exit times on the SOI.

All the parameters listed in this section are for the two-body trajectory legs used as reference orbits for the final perturbed conic analysis.

6.2 Performance of Trajectory Segment Matching Technique

The trajectory segment matching procedure is repeated through several cycles. The first of these uses the advanced patched conic model. The initial conditions are obtained from [16] where the trajectory was determined using the simple patched conic model. All successive cycles employ the perturbed conic model with offsets re-calculated for each cycle. The column labelled method indicates whether the optimum gradient step (OGS) or the generalized Newton-Rapheson (GNR) procedure is used for that step. The cost function is defined by (2.13-.14) for the first cycle and by (3.31-.32) for successive cycles.

First Cycle: Iteration	Method	Cost Function (km^2/sec^2)
Initial Conditions	-	4.04945
1	OGS	3.96201
2	OGS	3.89372
3	OGS	3.79476
4	OGS	3.76557

First Cycle: Iteration	Method	Cost Function (km^2/sec^2)
5	OGS	3.72571
	:	:
:	:	
92	OGS	1.47623
93	OGS	1.47268
94	OGS	1.46821
95	GNR	0.47856 (10^{-2})
96	GNR	0.23789 (10^{-7})
97	GNR	0.80956 (10^{-13})
98	GNR	0.10929 (10^{-18})

Second Cycle· Iteration	Method	Cost Function
Initial Conditions	-	0.10898 (10^{-1})
1	GNR	0.10408 (10^{-5})
2	GNR	0.13908 (10^{-11})
3	GNR	0.32573 (10^{-17})

Third Cycle: Iteration	Method	Cost Function
Initial Conditions	-	0.10560 (10^{-5})
1	GNR	0.10959 (10^{-11})
2	GNR	0.19818 (10^{-17})

Fourth Cycle. Iteration	Method	Cost Function
Initial Conditions	-	0.15182 (10^{-9})
1	GNR	0.24154 (10^{-15})

Fifth Cycle: Iteration	Method	Cost Function
Initial Conditions	-	0.15638 (10^{-11})

The change from OGS to GNR occurred when the cost function fell below 1.47. A cycle was terminated when the cost fell below 1.0 (10^{-14}) and the whole procedure was ended when the cost at the beginning of

a new cycle was less than 1.0 (10^{-10}). The total running time on the IBM 360/65 was about 172 seconds.

6.3 Perturbed Conic Results

The first step in the perturbed conic model was the calculation of the perturbations in the initial and final position and velocity for each leg due to the disturbing accelerations. The magnitudes of these perturbations (in km. and m/sec) for the last cycle are

Leg	$\delta r(t_1)$	$\delta v(t_1)$	$\delta r(t_2)$	$\delta v(t_2)$
1-2	144,135.26	20.974	680,081.06	115.831
2-3	350,124.98	146.486	317,175.98	126.799
3-4	681,236.05	117.365	90,828.50	7.226
4-5	106,229.23	38.040	51,438.66	18.086
5-6	847,681.45	46.614	464,247.07	12.626
6-7	8,764.69	3.921	7,684.89	3.384
7-8	246,233.21	11.917	222,593.00	10.058

The next step is the calculation of the position and velocity perturbations at the mid-point that eliminate the position perturbations at the initial and final points. The magnitudes of these mid-point perturbations (in km and m/sec) for the last cycle are

Leg	$\delta\hat{r}(t_M)$	$\delta\hat{v}(t_M)$
1-2	276,302.85	13.418
2-3	14,105.26	56.324
3-4	367,398.01	14.229
4-5	174,611.87	12,147.092
5-6	616,749.98	3.755
6-7	1,673.59	29.264
7-8	215,439.75	2.071

The last step is the calculation of the offsets of the initial

and final velocities. These offset magnitudes (in m/sec) for the last cycle are

Leg	$\delta\hat{v}(t_1)$	$\delta\hat{v}(t_2)$
1-2	16.800	92.557
2-3	94.702	81.347
3-4	100.210	10.165
4-5	34.432	20.439
5-6	42.388	14.480
6-7	2.820	2.104
7-8	10.560	9.195

6.4 Comparison with Numerically Integrated Results

The accuracy of the analytic procedure is evaluated by comparison with numerically integrated trajectory legs using the procedure described in Section 5.4. The quantities used to evaluate the accuracy of the analytic technique are the errors in the velocity offsets at the initial and final times and the position error at the final time due to the use of the analytically determined initial velocity. The magnitudes of these quantities (in km and m/sec) are

Leg	$\Delta v(t_1)$	$\Delta v(t_2)$	$\Delta r(t_2)$
1-2	0.305	0.139	8185.05
2-3	0.622	0.438	8955.75
3-4	0.353	0.089	15,348.52
4-5	0.335	0.184	239,662.60
5-6	0.052	0.095	6444.35
6-7	0.0081	0.0071	1904.25
7-8	0.095	0.095	8833.50

In order to fly the trajectory, it would be necessary to apply velocity corrections at each SOI entry and exit point to eliminate the

above errors. The magnitudes of these corrections (in m/sec) are

Point	Correction
1	0.305
2	0.667
3	0.787
4	0.424
5	0.179
6	0.103
7	0.092
8	0.095

The total correction needed is

$$\Delta v = 2.652 \text{ m/sec.}$$

The differences in the periapse conditions between the numerically integrated trajectory legs and the two-body reference values for the planetocentric legs are

Leg	Δr_π	Δv_π	Δt_π
2-3	1025.172 km	29.075 m/sec	18.5368 minutes
4-5	40.068 km	5.083 m/sec	-116.5053 minutes
6-7	8.162 km	1.216 m/sec	-1.5907 minutes

6.5 Discussion of Results

The assumption that the disturbing acceleration due to other planets has negligible effect during the planetocentric legs of the trajectory does not prove to be as good for this example as it did for the dual planet reconnaissance trajectory. This shows up most strongly for the planetocentric leg about Saturn due to the long time inside the sphere of influence (196 days) and the proximity of Jupiter (about

5 a.u. away). To evaluate the effects of the other planets, the numerical integration of the Saturn planetocentric leg was repeated using the sun as the only disturbing body. The results are

$\Delta v(t_1)$ = 0.026 m/sec (0.335 m/sec)

$\Delta v(t_2)$ = 0.004 m/sec (0.184 m/sec)

$\Delta r(t_2)$ = 1704.871 km (239,662.60 km)

Δr_π = 37.827 km (40.068 km)

Δv_π = 4.918 m/sec (5.083 m/sec)

Δt_π = -115.4210 minutes (-116.5053 minutes)

The corresponding figures for the numerical integration of the same leg using all the other planets as well as the sun as disturbing bodies are shown in parenthesis.

The large shift in periapse time at Saturn shows up in large values of $\delta\hat{r}(t_M)$ and $\delta\hat{v}(t_M)$ given in Section 6.3. Position and velocity change quite rapidly near periapse for a hyperbola.

The general accuracy of the analytic procedure as applied to this trajectory is quite adequate. The total correction needed (2.652 m/sec) may be quite easily absorbed into the mid-course correction allowance. Based on the results described above, about 40% of the total correction magnitude could be eliminated by using a perturbed conic model which includes the disturbing accelerations of the other planets during the planetocentric phases.

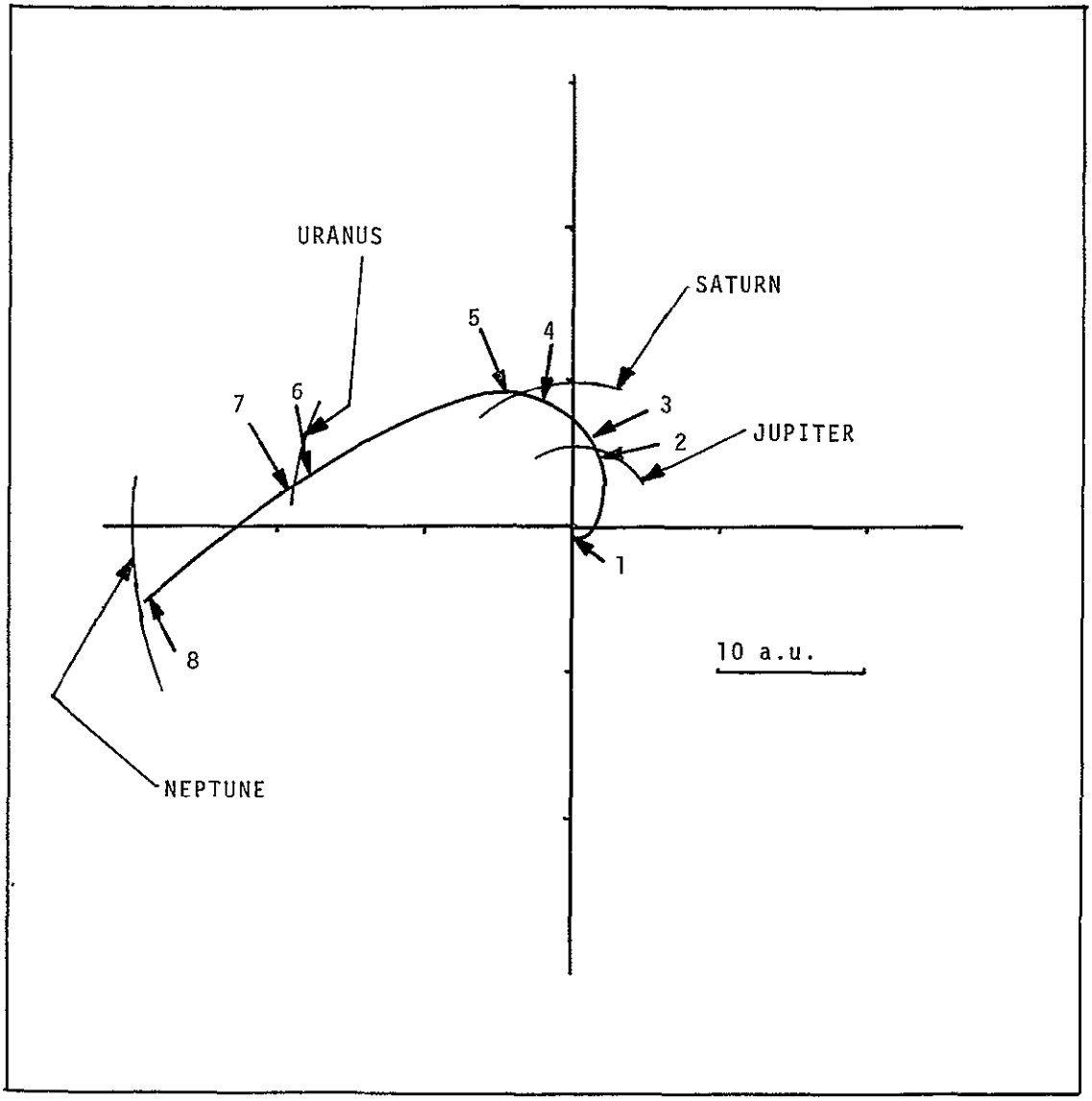

Figure 6.1 Grand Tour Trajectory

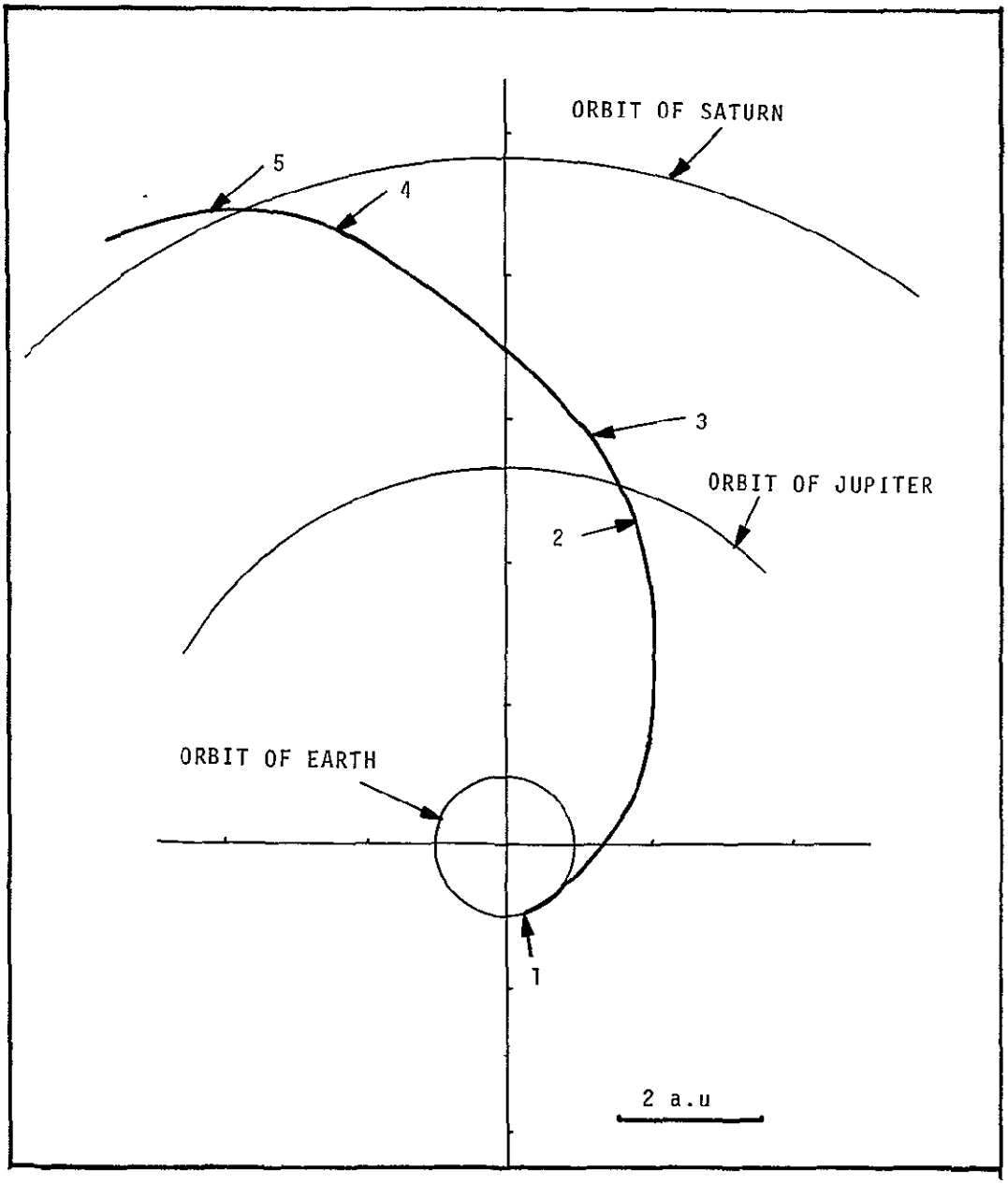

Figure 6.2 Grand Tour Trajectory Segment

Chapter 7

Periodic Trajectory Example

7.0 Chapter Summary

The periodic trajectory example is described. The coordinates of the sphere of influence entry and exit points and the orbital elements of the individual trajectory legs are given. The performance of the trajectory segment matching procedure is discussed. The results of the perturbed conic analysis are tabulated and the analytic predictions are compared with numerically integrated trajectory legs. The solution found is not a free-fall trajectory but requires a total impulse of 220.534 m/sec applied at the various sphere of influence (SOI) entry and exit points. The total error in the calculation of the trajectory legs amounted to 38.950 m/sec which would also be applied at the SOI entry and exit points. The sources of these errors are discussed.

7.1 Description of Mission

The term periodic orbit is used here to mean an interplanetary free-fall trajectory which shuttles back and forth between two planets. Once this orbit is established, it continues indefinitely with only minor guidance corrections. The existence of such trajectories was first explored by Hollister in [22]. Using the simple patched conic model, a general search procedure for periodic trajectories was developed and three types of trajectories connecting Earth and Venus were discovered. This work was extended by Menning [23] who found additional Earth-Venus trajectories and by Rall [25] who examined Earth-Mars periodic trajectories. The guidance requirements for the Earth-Venus trajectories were examined by Hickman in [24].

The trajectory chosen for closer examination using the technique developed in this thesis is a segment of Periodic Orbit I given in

[22]. It consists of the sequence

1) Earth to Venus transfer
2) Direct Return to Venus
3) Direct Return to Venus
4) Venus to Earth transfer
5) Direct Return to Earth
6) Earth to Venus transfer

The direct return legs are trajectories which return to the launch planet one planetary year later. This sequence (illustrated in Figures 7.1 to 7.3) forms a part of a larger (16 year) orbit which repeats indefinitely between Earth and Venus.

The final trajectory is specified by the following set of planetary sphere of influence (SOI) entry and exit points. The SOI radii are given in Appendix C.

Point	Julian Date	Location
1	2440811.29805	Earth SOI exit point (launch)
2	2440968.17351	Venus SOI entry point
3	2440974.71063	Venus SOI exit point
4	2441192.53554	Venus SOI entry point
5	2441199.05152	Venus SOI exit point
6	2441416.81361	Venus SOI entry point
7	2441423.35856	Venus SOI exit point
8	2441587.41963	Earth SOI entry point
9	2441598.42073	Earth SOI exit point
10	2441951.97897	Earth SOI entry point
11	2441962.96593	Earth SOI exit point
12	2442123.36905	Venus SOI entry point (arrival)

The launch date is on August 11, 1970 with the arrival date on March

13, 1974 (which is a Wednesday).

The spherical coordinates of the SOI entry and exit points in a planetocentric ecliptic coordinate system (see Appendix A) are

Point	Azimuth	Elevation
1	-68.845°	-71.474°
2	35.165°	-52.462°
3	157.616°	18.414°
4	336.896°	-16.982°
5	154.209°	-54.071°
6	334.844°	55.489°
7	90.723°	-121.732°
8	76.408°	-48.250°
9	3.803°	41.428°
10	183.950°	-40.474°
11	314.174°	-42.542°
12	151.149°	-65.069°

The complete set of cartesian coordinates of the SOI entry and exit points in the heliocentric and planetocentric coordinate frames plus the heliocentric coordinates of the planets at encounter are given in Appendix E.

The total flight time for the trajectory is 3.59 years which is about one-fifth of the basic periodic orbit period. The time of flight and central angle traversed for the individual legs are

Leg	Time of Flight (days)	Central Angle Traversed
1-2	156.87546	196.498°
2-3	6.53712	208.873°
3-4	217.82491	348.950°
4-5	6.51598	216.238°

Leg	Time of Flight (days)	Central Angle Traversed
5-6	217.76209	348.831°
6-7	6.54495	208.537°
7-8	164.06107	198.183°
8-9	11.00109	215.694°
9-10	353.55824	348.607°
10-11	10.98699	227.708°
11-12	159.40312	192.359°

The legs (2-3), (4-5), (6-7), (8-9) and (10-11) are planetocentric hyperbolas while the legs (1-2), (3-4), (5-6), (7-8), (9-10), and (11-12) are heliocentric ellipses. The orbital elements of these legs are

Leg	Semi-Major Axis	Eccentricity	Inclination
1-2	0.86448	0.17688	7.058°
2-3	2.15499	2.07092	126.095°
3-4	0.72333	0.13795	4.093°
4-5	2.14851	1.69163	91.594°
5-6	0.72333	0.07569	7.270°
6-7	2.16000	2.09324	70.943°
7-8	0.86362	0.16973	6.908°
8-9	3.26454	1.71393	59.504°
9-10	0.99995	0.09105	5.438°
10-11	3.27180	1.35186	115.417°
11-12	0.86564	0.16374	6.373°

The semi-major axis is given in astronomical units for the heliocentric legs and in planetary radii for the planetocentric legs.

The vis-viva energy at earth needed to launch on this trajectory is

$$C_3 = 18.427 \text{ km}^2/\text{sec}^2$$

The periapse radius (in kilometers and planetary radii), the periapse velocity (in km/sec) and the turn angle (as defined in Section 4.5) for the planetocentric legs are

Leg	Periapse Radius	Periapse Velocity	Turn Angle
2-3	13,962.344 (2.30783)	8.45835	28.873°
4-5	8,990.130 (1.48597)	9.86860	36.238°
6-7	14,286.449 (2.36140)	8.39219	28.537°
8-9	14,865.250 (2.33065)	8.52453	35.694°
10-11	7,342.533 (1.15120)	11.29118	47.708°

The time of periapse is the mid-point between the entry and exit points on the sphere of influence.

All of the parameters listed in this section are for the two-body trajectory legs used as reference orbits for the final perturbed conic analysis.

7.2 Performance of Trajectory Segment Matching Technique

No free-fall solution was found for the trajectory sequence chosen for detailed examination. Since no zero of the cost function existed, the generalized Newton-Rapheson (GNR) technique could not be used. All attempts at application of GNR resulted in a rapid divergence from the minimum. Thus, the trajectory segment matching procedure was restricted to the first-order optimum gradient step (OGS) technique. This technique was repeated through five cycles. The first of these used the advanced patched conic model alone with initial conditions obtained from [22] and [24]. All successive cycles employed the perturbed conic model with the velocity offsets re-computed for each cycle. The cost function is defined by (2.13-.14) for the first cycle and by (3.31-.32) for successive cycles.

First Cycle: Iteration	Method	Cost Function (km^2/sec^2)
Initial Conditions	-	0.61931
1	OGS	0.41670
2	OGS	0.25163
3		
:		
198	OGS	0.0006968
199	OGS	0.0006964
200	OGS	0.0006961
Second Cycle: Iteration	**Method**	**Cost Function**
Initial Conditions	-	0.023412
1	OGS	0.013790
2	OGS	0.013629
3	OGS	0.013415
:		
49	OGS	0.012933
50	OGS	0.012926
Third Cycle: Iteration	**Method**	**Cost Function**
Initial Conditions	-	0.012836
1	OGS	0.012824
2	OGS	0.012816
:		
79	OGS	0.012250
80	OGS	0.012241
Fourth Cycle: Iteration	**Method**	**Cost Function**
Initial Conditions	-	0.012155
1	OGS	0.012140
2	OGS	0.012131

Fourth Cycle: Iteration	Method	Cost Function
:		
99	OGS	0.011551
100	OGS	0.011545

Fifth Cycle: Iteration	Method	Cost Function
Initial Conditions	-	0.011491

As the iteration approached a minimum the rate of convergence slowed down. The procedure was terminated at the fifth cycle due to

1) The small change in the solution point during the third and fourth cycles (the coordinates varied by 10^{-5} days and 10^{-3} degrees).
2) The small change in the cost function for each iteration (about 10^{-5} to 10^{-6} per iteration in the fourth cycle).
3) The small change in the cost function between the fourth and fifth cycles.

$$\delta J = 5.4\ (10^{-5})$$

4) Fluctuations in the components of the OGS weighting matrix indicating that the path of the iteration changes direction repeatedly.

Since the trajectory sequence found is not a free-fall solution, a velocity impulse is required at each SOI entry and exit point. The magnitudes of these impulses (in m/sec) for the last cycle are

Point	Impulse Required
1	-
2	0.181
3	9.935

Point	Impulse Required
4	10.380
5	69.168
6	70.561
7	0.607
8	2.240
9	27.545
10	27.402
11	2.515
12	-
Total Impulse	220.534 m/sec

Since they are boundary points and need not be matched with any other trajectory segments, points 1 and 12 do not have impulses required.

Total running time on the IBM 360/65 was about 450 seconds.

7.3 Perturbed Conic Results

The first step in the perturbed conic model is the calculation of the perturbations in the initial and final position and velocity for each leg due to the disturbing accelerations. The magnitudes of these perturbations (in km and m/sec) for the last cycle are

Leg	$\delta r(t_1)$	$\delta v(t_1)$	$\delta r(t_2)$	$\delta v(t_2)$
1-2	41,314.08	40.979	32,426.32	40.633
2-3	2614.02	26.988	4091.55	42.725
3-4	28,220.08	45.670	29,609.92	46.557
4-5	4237.34	44.509	2906.04	30.227
5-6	46,910.76	49.855	48,591.14	50.337
6-7	2821.81	29.843	2253.46	23.601
7-8	31,659.97	40.791	40,915.69	38.892
8-9	3542.84	21.977	5319.98	33.174

Leg	$\delta r(t_1)$	$\delta v(t_1)$	$\delta r(t_2)$	$\delta v(t_2)$
9-10	48,817.55	43.424	59,081.77	46.252
10-11	5558.97	34.485	4081.22	25.052
11-12	40,283.06	39.210	23,510.72	35.092

The next step is the calculation of the position and velocity perturbations at the mid-point that eliminate the position perturbations at the initial and final points. The magnitudes of these mid-point perturbations (in km and m/sec) for the last cycle are

Leg	$\delta\hat{r}(t_M)$	$\delta\hat{v}(t_M)$
1-2	200,104.06	13.023
2-3	4079.14	810.701
3-4	1,096,815.12	249.635
4-5	4147.93	1694.559
5-6	1,415,883.04	339.272
6-7	1170.26	224.513
7-8	184,637.38	10.833
8-9	4769.56	1010.601
9-10	1,845,405.84	271.268
10-11	5340.29	3490.696
11-12	242,051.23	12.239

The last step is the calculation of the offsets of the initial and final velocities. These offset magnitudes (in m/sec) for the last cycle are

Leg	$\delta\hat{v}(t_1)$	$\delta\hat{v}(t_2)$
1-2	18.892	47.168
2-3	23.658	36.195
3-4	136.154	137.953
4-5	36.352	22.588

Leg	$\delta\hat{v}(t_1)$	$\delta\hat{v}(t_2)$
5-6	179.485	180.798
6-7	19.858	17.587
7-8	36.508	26.500
8-9	18.928	25.041
9-10	168.229	145.449
10-11	25.288	19.274
11-12	37.285	43.667

7.4 Comparison with Numerically Integrated Results

The accuracy of the analytic procedure is evaluated by comparison with numerically integrated trajectory legs using the procedure described in Section 5.4. The quantities used to evaluate the accuracy of the analytic technique are the errors in the velocity offsets at the initial and final times and the position error at the final time due to the use of the analytically determined initial velocity. The magnitudes of these quantities (in km and m/sec) are

Leg	$\Delta v(t_1)$	$\Delta v(t_2)$	$\Delta r(t_2)$
1-2	0.265	0.397	6474.90
2-3	0.019	0.078	307.75
3-4	4.091	4.148	3645.73
4-5	0.072	0.020	453.86
5-6	8.757	8.830	7159.38
6-7	0.030	0.010	360.25
7-8	0.279	0.238	7305.56
8-9	0.007	0.052	143.39
9-10	5.489	5.574	5829.96
10-11	0.045	0.012	1849.09
11-12	0.388	0.240	8008.43

In order to fly the trajectory, it would be necessary to apply additional velocity corrections at each SOI entry and exit point to eliminate the above errors. The following table lists the magnitudes (in m/sec) of the impulse required at each SOI entry and exit point as predicted by the analytic technique and the magnitudes (in m/sec) of the errors in these predictions as determined by the numerical integrations.

Point	Impulse Required	Error
1	-	0.265
2	0.181	0.410
3	9.935	4.166
4	10.380	4.218
5	69.168	8.749
6	70.561	8.856
7	0.607	0.277
8	2.240	0.239
9	27.545	5.532
10	27.402	5.612
11	2.515	0.386
12	-	0.240
Totals	220.534	38.950

The differences in the periapse conditions between the numerically integrated trajectory legs and the two-body reference values for the planetocentric legs are

Leg	Δr_π	Δv_π	Δt_π
2-3	18.01 km	11.351 m/sec	7.997 minutes
4-5	19.81 km	6.743 m/sec	-6.991 minutes
6-7	38.27 km	5.371 m/sec	-2.307 minutes
8-9	66.57 km	14.038 m/sec	9.291 minutes
10-11	38.36 km	31.352 m/sec	7.879 minutes

7.5 Discussion of Results

Since the solution found is not a zero of the cost function, it may not be assumed to be a global minimum. The divergence of the GNR iteration indicates strongly that no zero of the cost function exists locally but this has not been proven. Similarly, the existence of other lower but non-zero minima has not been disproven. Some experimentation using different sets of initial conditions was conducted but no firm conclusions on the existence of multiple solutions were reached.

The calculation of the direct return trajectories in this example proved to be a most severe test of the trajectory determination technique. The initial and final velocity offsets required for these legs were an order of magnitude larger than those for previous trajectories. The source of these large offsets may be seen by examining the trajectories in Figures 7.1 to 7.3. The direct return trajectories obviously spend a large time in the vicinity of the planet with which they are associated leading to their somewhat extreme behavior.

The errors in the offset calculations associated with the direct return trajectories are also about an order of magnitude larger than those for previous heliocentric trajectories. This is due to two effects

1) The larger offsets put a greater strain on the linearity assumptions of the perturbed conic model.

2) The nearness of the associated planet over a large part of the trajectory causes significant differences between the two-body state transition matrix used and the actual many-body state transition matrix.

Of these two sources, the second is considered more significant. One point which is interesting to note is the fact that the final position

error due to using the analytically determined initial velocity is not significantly larger for the direct return trajectories. This indicates that the velocity errors for the direct returns are not in a critical direction.

The general accuracy of the trajectory determination procedure as applied to the periodic trajectory example appears to be compatible with the results of the preceding examples. For applications for which the accuracy of the direct return leg calculations proved unacceptable, a third stage using numerical integration to determine the velocity offsets for these legs could be added to the solution procedure.

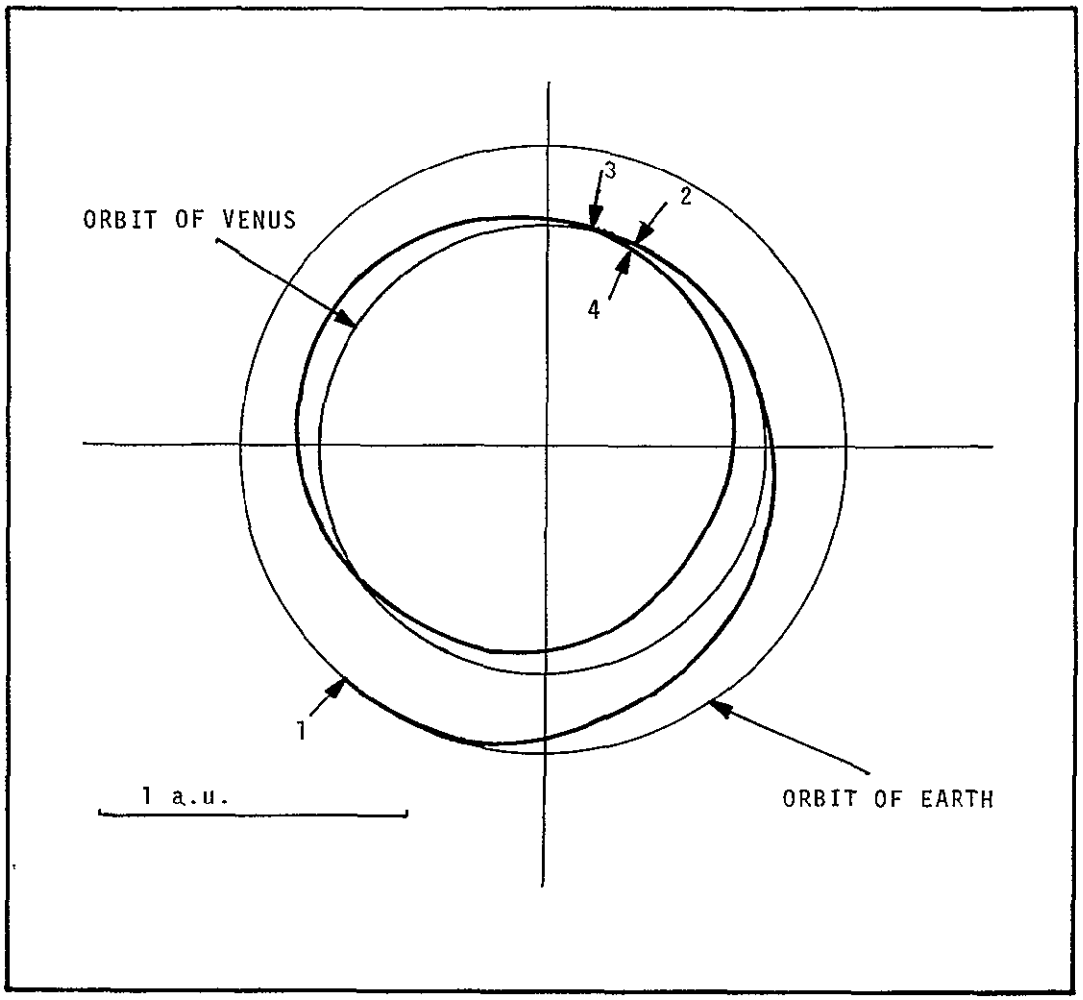

Figure 7.1 Periodic Trajectory Segment

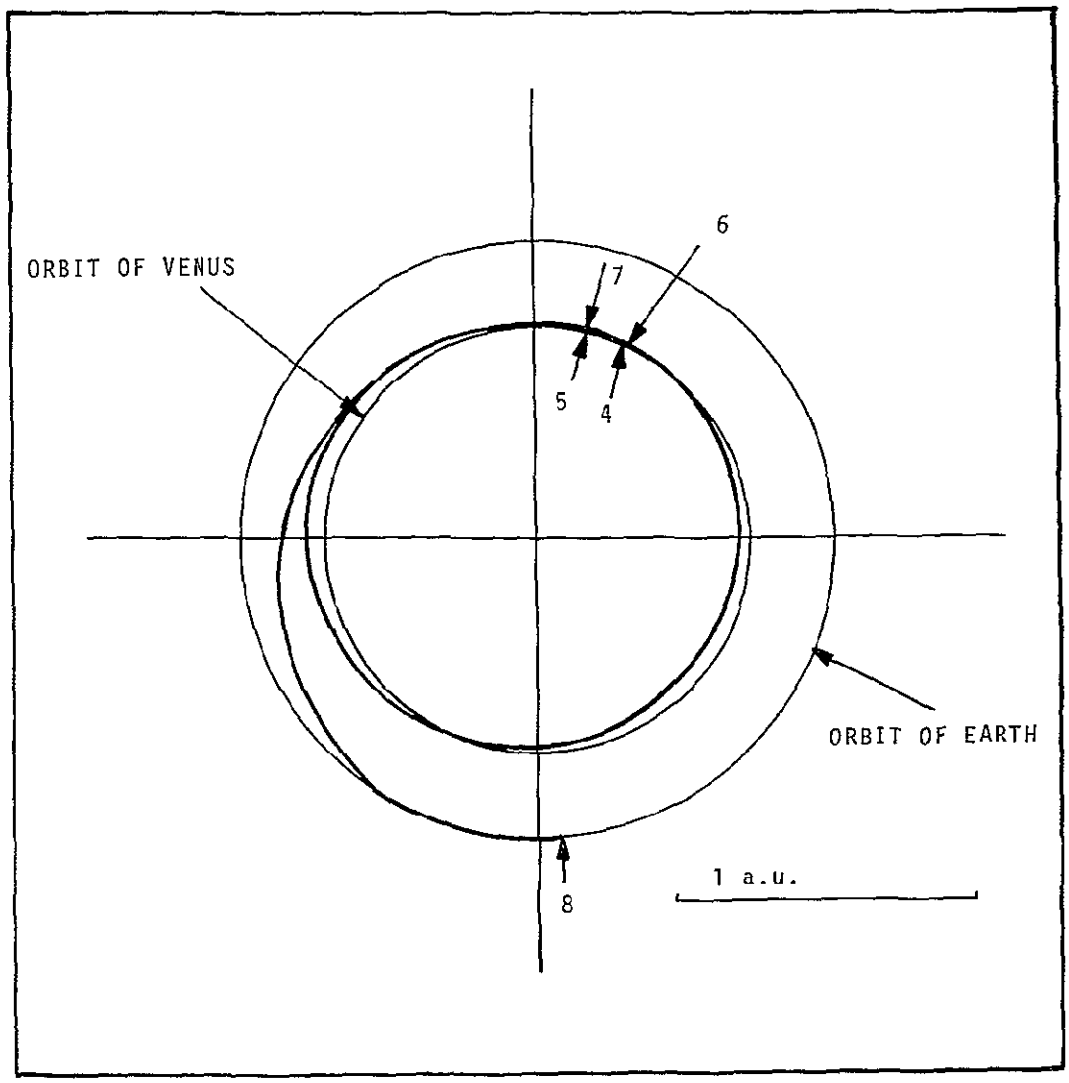

Figure 7.2 Periodic Trajectory Segment

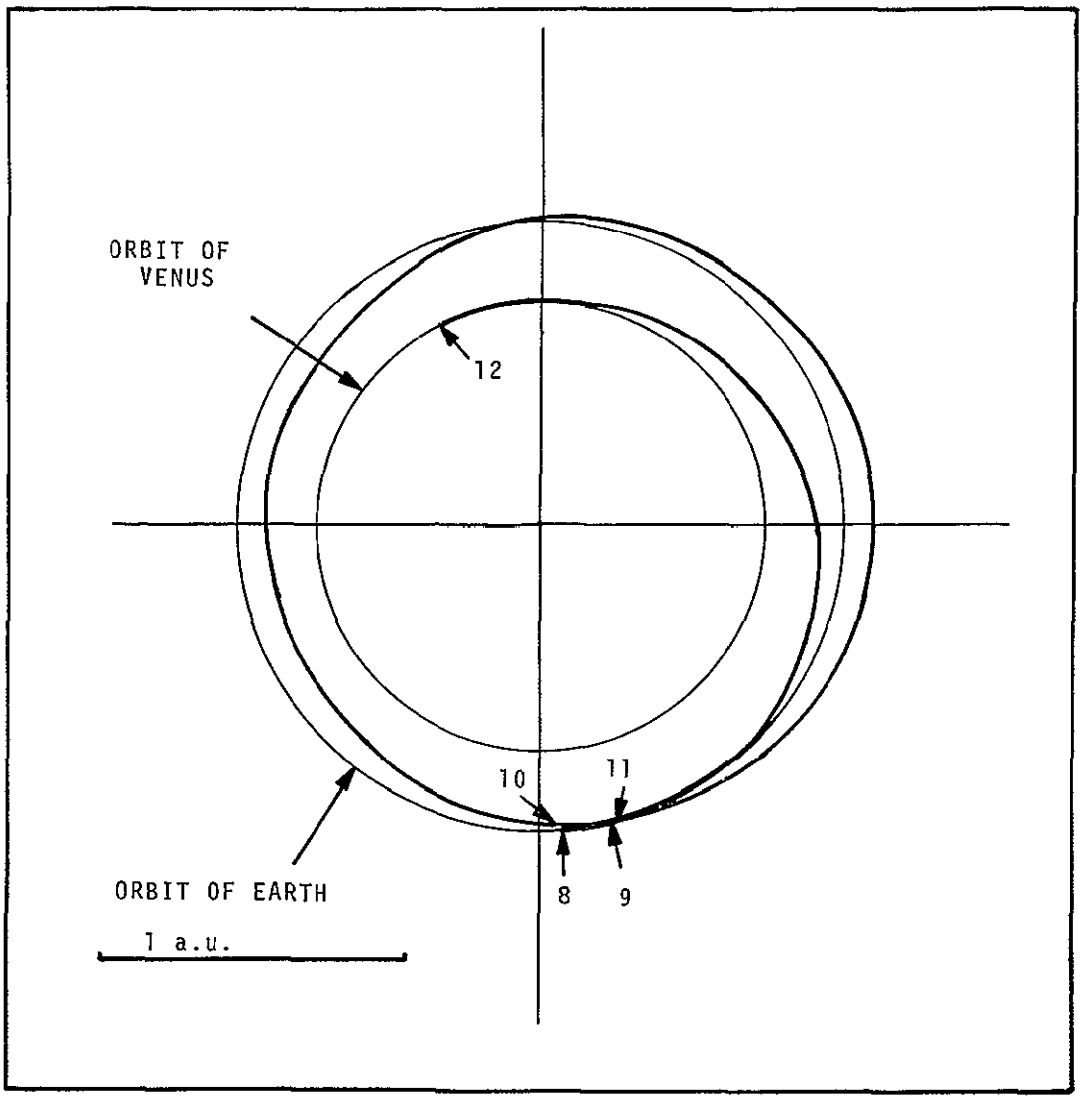

Figure 7.3 Periodic Trajectory Segment

Chapter 8

Summary, Conclusions, and Recommendations

8.0 Summary and Conclusions

The trajectory targeting technique developed in this thesis is intended for the pre-mission calculation of reference trajectories for multiple swingby interplanetary trajectories. The primary objective has been to develop a technique which

i) has a wide enough region of convergence such that the initial conditions for the trajectory determination process may be derived from a simple patched conic mission analysis,

ii) is largely analytic to minimize computational time required, and

iii) is accurate enough to eliminate or at least significantly reduce the need for numerical integration of trajectories.

The trajectory targeting technique developed is applied in the following manner. A simple patched conic model (consisting of a sequence of heliocentric conic arcs running from the center of one planet to the next matched in relative hyperbolic excess velocity at each planetary encounter) is used to calculate a set of initial conditions for an advanced patched conic model. This advanced patched conic model consists of a set of alternating heliocentric and planetocentric conic arcs joined at the planetary sphere of influence (SOI). These arcs are specified by the position and time of the entry and exit points of the trajectory through the SOI of each planet encountered (i.e. the heliocentric arcs run from the exit point on one SOI to the entry point on the next SOI while the planetocentric arcs run from the entry point to the exit point of a single SOI). Since the end points and the time of

flight for each arc are specified, the conic initial and final velocities may be calculated by solving Lambert's Problem.

Since the initial conditions for the SOI entry and exit points were determined using an approximate model, the conic arcs in the advanced patched conic model are not likely to match dynamically. Instead, velocity discontinuities occur at each SOI entry and exit point. Using the sum of the squares of the magnitudes of these velocity mis-matches as a cost function, the next step is to formulate the problem of varying the entry and exit points and times to minimize the total velocity mis-match as a parameter optimization problem. The expression for the gradient of the cost function with respect to the entry and exit point coordinates may be determined analytically from the relations for the Lambert Problem. Then, by applying first- or second-order iteration techniques, the velocity mis-match may be reduced to a minimum, which will be zero for a free-fall trajectory.

Once the velocity mis-match has been minimized for the advanced patched conic model the next step is to repeat the process using the perturbed conic model. Using the two-body conic arcs calculated for the advanced patched conic model as reference trajectories, perturbed conic segments (which include perturbations caused by the disturbing accelerations of the planets on the heliocentric legs and the disturbing acceleration of the sun on the planetocentric legs) which pass through the same end points and times as the advanced patched conic segments are calculated analytically. These perturbed conic segments differ from the advanced patched conic segments by velocity offsets at the initial and final times. The cost function is now modified to include these offsets and the iteration procedure to minimize the velocity mis-match (now including the offsets) is repeated. This process is repeated with the offsets re-calculated at each stage until convergence to a set of dynamically consistent (i.e. matching in position, velocity and time)

perturbed conic segments is achieved. If a free-fall trajectory is not found, the process determines a powered trajectory with the minimum velocity mis-match.

After the velocity mis-match has been minimized for the perturbed conic segments, the initial and final velocity offsets may be re-calculated using numerically integrated trajectory legs running between the same end points and times as the perturbed conic legs. At this point, two alternatives are possible. The first is to repeat the iteration process of the preceding steps using velocity offsets calculated by numerical integration at each stage. This will provide a trajectory whose accuracy is limited only by the numerical precision of the integration techniques used but will also consume a large amount of computer time. A second alternative is to accept the errors of the analytic technique as being well below the mid-course correction allowance and to use a single determination of each trajectory leg by numerical integration as a check of the accuracy of the analytic procedure and as a means of determining the velocity impulse needed at each SOI entry and exit point to fly the trajectory predicted.

The basic advantages of the trajectory targeting technique developed in this thesis are

1) The technique is basically analytic in nature, providing a great reduction in the computation required. Its convergence range is wide.

2) A continuous description of the entire trajectory is provided. The near-planet phases of the trajectory are approximated quite well by the planetocentric trajectory legs.

3) By specifying the trajectory as a sequence of individual legs matched in position, velocity, and time, the

determination of the trajectory is uniformly accurate along the trajectory. In addition, guidance objectives are given for each leg of the trajectory.

4) The effects of other disturbing forces (such as non-gravitational effects) may be easily included in the perturbed conic analysis.

5) A powered trajectory is provided for those cases which do not have a free-fall solution.

The main limitation of the analytic technique lies in its accuracy. The main assumption of the perturbation techniques employed is that each trajectory segment is basically two-body in nature. The presence of strong disturbing accelerations acting over extended periods of time can cause large perturbations from the two-body reference legs and lead to a degradation in the accuracy of the results (as seen in Chapter 7). In such cases, the use of a final step employing velocity offsets calculated by numerical integration for the strongly perturbed legs may be necessary.

The basic conclusion of this thesis is that the analytic targeting technique developed provides results sufficiently accurate for a wide variety of multiple swingby missions. Where its accuracy is not adequate, it may be supplemented by a final stage using numerical integration (with the associated penalty of increased computation) to provide any degree of accuracy required. For heliocentric arcs (with the exception of those discussed in Chapter 7), the initial and final velocities may be determined analytically to better than 0.4 m/sec. Errors in final position for a numerical integration of each leg using the calculated initial velocity range from 1300 km to 15,000 km with typical values falling in the region of 5000-8000 km. For planetocentric arcs, the initial and final velocities are determined generally

to within 0.1 m/sec. The exceptions to this occur at Jupiter and Saturn for the Grand Tour example where the neglected effects of the disturbing accelerations due to other planets proved significant. Errors in final position for numerical integrations of individual legs using the calculated initial velocity range from 1.6 km to 240,000 km with the bulk of the values in the interval 2-2000 km.

8.1 Contributions of the Thesis

The author considers the following items to constitute the original contributions of this thesis in the field of trajectory determination and targeting:

1) The development of a basically analytic technique for the precision targeting of multiple swingby reference trajectories. This technique has the following features:
    a) a wide range of convergence
    b) a uniformly high level of accuracy along the entire trajectory
    c) specification of guidance objectives along the entire trajectory
    d) fast and simple to apply
    e) easily adaptable to different disturbing force models.
2) Development of a method which provides an economical means of checking and refining the results of simple patched conic analyses of complicated trajectories.
3) Development of a simple means for determining powered solutions for multiple swingby trajectories in cases where free-fall solutions do not exist.
4) Determination of the first accurate many-body reference

trajectories for a multiple swingby trajectory having more than one intermediate swingby.

Contributions of a secondary nature to the objective of this thesis are 1) development of the optimum gradient step (OGS) modification to the steepest descent procedure, 2) derivation of analytic partial derivative matrices for variations about a solution to Lambert's Problem, and 3) development of a perturbed conic technique which improves the linear range for the perturbed two-body model.

8.2 Recommendations for Further Study

Several improvements and extensions of the results of this thesis are recommended. These are

1) Include the effects of other disturbing accelerations (such as planetary oblateness, solar radiation pressure, low thrust, etc) in the perturbed conic model.

2) Explore the feasibility of using the perturbed two-body state transition matrix (developed in Appendix D) in the perturbed conic model.

3) Study the possibility of determining (either analytically or numerically) the second partial derivative matrices for the Lambert Problem. This would allow the use of second order techniques to search for non-zero minima of the velocity mis-match cost function.

4) Extend the perturbed conic analysis to include the determination of injection and arrival conditions in the near-planet region.

Several areas for further research using the techniques developed in this thesis are

1) Apply the analytic partial derivative matrices and solution techniques developed to the simple patched conic model for use in preliminary mission planning.

2) Apply the targeting techniques developed to detailed mission analysis studies for the determination of launch windows, abort and inflight mission modification alternatives, midcourse guidance requirements, and the effects of guidance and navigation inaccuracies.

3) Apply the techniques for the matching of perturbed conic arcs to the optimization of multiple impulse orbit-to-orbit transfers. These transfers may be considered as sequences of perturbed conic coasting arcs with impulsive velocity changes at the matching points. The trajectory segment matching techniques developed here may be used to minimize the total impulse used for the given transfer.

Appendix A

Notation and Coordinate Systems

A.1 Notation

The following notation convention is used in this thesis. Examples are given for (3x1) vectors and (3x3) matrices but apply for any dimension quantities.

vector = column matrix

$$\underline{x} = \begin{bmatrix} x_1 \\ x_2 \\ x_3 \end{bmatrix}$$

vector transpose = row matrix

$$\underline{x}^T = [x_1 \; x_2 \; x_3]$$

vector magnitude

$$x = |\underline{x}| = \sqrt{x_1^2 + x_2^2 + x_3^2}$$

unit vector

$$\underline{i}_x = \underline{x} \; / \; x$$

inner (or dot) product

$$\underline{x} \cdot \underline{y} = \underline{x}^T \underline{y} = x_1 y_1 + x_2 y_2 + x_3 y_3$$

outer (or dyadic) product

$$\underline{x}\,\underline{y}^T = \begin{bmatrix} x_1y_1 & x_1y_2 & x_1y_3 \\ x_2y_1 & x_2y_2 & x_2y_3 \\ x_3y_1 & x_3y_2 & x_3y_3 \end{bmatrix}$$

cross product

$$\underline{x} \times \underline{y} = \begin{bmatrix} x_2y_3 - x_3y_2 \\ x_3y_1 - x_1y_3 \\ x_1y_2 - x_2y_1 \end{bmatrix}$$

vector derivatives

$$\frac{\partial \underline{x}}{\partial a} = \begin{bmatrix} \frac{\partial x_1}{\partial a} \\ \frac{\partial x_2}{\partial a} \\ \frac{\partial x_3}{\partial a} \end{bmatrix}$$

$$\frac{\partial \underline{x}}{\partial \underline{a}} = \begin{bmatrix} \frac{\partial x_1}{\partial a_1} & \frac{\partial x_1}{\partial a_2} & \frac{\partial x_1}{\partial a_3} \\ \frac{\partial x_2}{\partial a_1} & \frac{\partial x_2}{\partial a_2} & \frac{\partial x_2}{\partial a_3} \\ \frac{\partial x_3}{\partial a_1} & \frac{\partial x_3}{\partial a_2} & \frac{\partial x_3}{\partial a_3} \end{bmatrix}$$

Unit Matrix

$$I = \begin{bmatrix} 1 & 0 & 0 \\ 0 & 1 & 0 \\ 0 & 0 & 1 \end{bmatrix}$$

Zero Vector

$$\underline{0} = \begin{bmatrix} 0 \\ 0 \\ 0 \end{bmatrix}$$

A.2 Coordinate Systems

A.2.1 Heliocentric Coordinate System

The heliocentric coordinate system is a non-rotating cartesian coordinate system centered in the sun with

a) the positive x-axis along the line of intersection of the earth's equatorial plane and the ecliptic plane.
b) the positive z-axis in a direction perpendicular to the ecliptic plane and parallel to the angular momentum vector of the earth about the sun
c) the positive y-axis in the ecliptic plane located so as to form a right-handed coordinate system.

A.2.2 Planetocentric Coordinate System

The planetocentric coordinate system is a non-rotating cartesian coordinate system centered in a planet with its axes parallel to the heliocentric coordinate system.

Appendix B

Calculation of Conic Arcs and Their Partial Derivative Matrices

B.1 Calculation of Conic Trajectory Arcs

Referring to Figure B.1, the Lambert Problem is defined as follows:

Given: 1) Initial position $\underline{r}_1$ and time t_1

2) Final position $\underline{r}_2$ and time t_2

3) The number N of complete revolutions made about the central body.

Find the initial ($\underline{v}_1$) and final ($\underline{v}_2$) velocities for a two-body conic trajectory connecting these two points.

The problem is solved using the following steps:

1) Determine by some means

a) $G_1 = \text{sgn}\,[\pi^2 - \theta^2]$ (B.1)

where

θ = central angle traversed by the last incomplete revolution of the trajectory

b) whether the trajectory is an ellipse or a hyperbola

2) Calculate

$$\underline{c} = \underline{r}_2 - \underline{r}_1 \quad , \qquad c = |\underline{c}| \tag{B.2}$$

$$s = \frac{1}{2}(r_1 + r_2 + c) \tag{B.3}$$

3) For an ellipse, solve for λ in the transcendental equation

$$\sqrt{\mu}(t_2-t_1) = \tau = \left(\frac{s}{1-\cos\lambda}\right)^{\frac{3}{2}} \left[2\pi N + (\lambda-\sin\lambda)-G_1(\beta-\sin\beta)\right] \quad (B.4)$$

where

$$s(1-\cos\beta) = (s-c)\ (1-\cos\lambda) \quad (B.5)$$

and

$$0 \leq \lambda \leq 2\pi \quad ; \quad 0 \leq \beta \leq \lambda \quad ; \quad 0 \leq \beta \leq \pi$$

μ = gravitational parameter of central body

Calculate

$$a = s/(1-\cos\lambda) \quad (B.6)$$

$$G_2 = \text{sgn}\ [\pi^2 - \lambda^2] \quad (B.7)$$

For a hyperbola, solve for γ in the transcendental equation

$$\sqrt{\mu}(t_2-t_1) = \tau = \left(\frac{s}{\cosh\gamma-1}\right)^{\frac{3}{2}} \left[(\sinh\gamma-\gamma)-G_1(\sinh\delta-\delta)\right] \quad (B.8)$$

where

$$s(\cosh\delta-1) = (s-c)(\cosh\gamma-1) \quad (B.9)$$

and

$$0 \leq \delta \leq \gamma \leq \infty$$

Calculate

$$a = s/(1-\cosh\gamma) \quad (B.10)$$

and set

$$G_2 = +1 \tag{B.11}$$

4) Calculate the quantities

$$A = G_1 \sqrt{\frac{1}{s-c} - \frac{1}{2a}} \tag{B.12}$$

$$B = G_2 \sqrt{\frac{1}{s} - \frac{1}{2a}} \tag{B.13}$$

$$V_c = \sqrt{\frac{u}{2}} [A + B] \tag{B.14}$$

$$V_p = \sqrt{\frac{u}{2}} [A - B] \tag{B.15}$$

The initial and final velocities are given by

$$\underline{v}_1 = V_c \underline{i}_c + V_p \underline{i}_{r_1} \tag{B.16}$$

$$\underline{v}_2 = V_c \underline{i}_c - V_p \underline{i}_{r_2} \tag{B.17}$$

where

$$\underline{i}_{r_1} = \frac{\underline{r}_1}{r_1}$$

$$\underline{i}_{r_2} = \frac{\underline{r}_2}{r_2}$$

$$\underline{i}_c = \frac{1}{c} (\underline{r}_2 - \underline{r}_1) \tag{B.18}$$

The derivations for these equations may be found in [3].

B.2 Calculation of Conic Partial Derivative Matrices

This section deals with the derivation of the partial derivative matrices

$$\frac{\partial \underline{v}_1}{\partial \underline{r}_1} \quad , \quad \frac{\partial \underline{v}_1}{\partial \underline{r}_2} \quad , \quad \frac{\partial \underline{v}_2}{\partial \underline{r}_1} \quad , \quad \frac{\partial \underline{v}_2}{\partial \underline{r}_2}$$

and the partial derivative vectors

$$\frac{\partial \underline{v}_1}{\partial t_1} \quad , \quad \frac{\partial \underline{v}_1}{\partial t_2} \quad , \quad \frac{\partial \underline{v}_2}{\partial t_1} \quad , \quad \frac{\partial \underline{v}_2}{\partial t_2}$$

The notation

$$\frac{\partial \alpha}{\partial \underline{r}_k} = \nabla_k \alpha = \begin{bmatrix} \frac{\partial \alpha}{\partial x_k} \\ \frac{\partial \alpha}{\partial y_k} \\ \frac{\partial \alpha}{\partial z_k} \end{bmatrix} \qquad \text{for } \alpha = \text{scalar}$$

and

$$\frac{\partial \underline{\alpha}}{\partial \underline{r}_k} = \nabla_k \underline{\alpha} = \begin{bmatrix} \frac{\partial \alpha_1}{\partial x_k} & \frac{\partial \alpha_1}{\partial y_k} & \frac{\partial \alpha_1}{\partial z_k} \\ \frac{\partial \alpha_2}{\partial x_k} & \frac{\partial \alpha_2}{\partial y_k} & \frac{\partial \alpha_2}{\partial z_k} \\ \frac{\partial \alpha_3}{\partial x_k} & \frac{\partial \alpha_3}{\partial y_k} & \frac{\partial \alpha_3}{\partial z_k} \end{bmatrix} \qquad \text{for } \underline{\alpha} = \begin{bmatrix} \alpha_1 \\ \alpha_2 \\ \alpha_3 \end{bmatrix} = \text{vector}$$

will be used for k = 1 or 2

To find the desired partial derivatives using the chain rule, it is necessary to derive some intermediate results.

1) $$r_k = \left[x_k^2 + y_k^2 + z_k^2\right]^{\frac{1}{2}} \qquad k = 1, 2 \qquad \text{(B.19)}$$

$$\frac{\partial r_k}{\partial \alpha_k} = \frac{\alpha_k}{r_k} \qquad \alpha = x, y, z$$

$$\therefore \quad \nabla_k r_k = \underline{i}_{r_k} \tag{B.20}$$

2) $$c^2 = r_1^2 + r_2^2 - 2\,\underline{r}_1 \cdot \underline{r}_2$$

$$= r_1^2 + r_2^2 - 2\,(x_1x_2 + y_1y_2 + z_1z_2)$$

$$\therefore \quad \nabla_1 c = -\,\underline{i}_c \tag{B.21}$$

$$\nabla_2 c = \underline{i}_c$$

3) $$s = \tfrac{1}{2}\,(r_1 + r_2 + c)$$

$$\nabla_1 s = \tfrac{1}{2}\,(\underline{i}_{r_1} - \underline{i}_c)$$

$$\nabla_2 s = \tfrac{1}{2}\,(\underline{i}_{r_2} + \underline{i}_c \tag{B.22}$$

4) a) For an ellipse

$$\tau = \left(\frac{s}{1-\cos\lambda}\right)^{\frac{3}{2}} \left[2\pi N + \left(\lambda - \sin\lambda\right) - G_1\left(\beta - \sin\beta\right)\right] \tag{B.4}$$

Then,

$$\frac{\partial\tau}{\partial\alpha} = \left(\frac{s}{1-\cos\lambda}\right)^{\frac{3}{2}} \left[\left(1-\cos\lambda\right)\frac{\partial\lambda}{\partial\alpha} - G_1\left(1-\cos\beta\right)\frac{\partial\beta}{\partial\alpha}\right]$$

$$+\frac{3}{2}\left(\frac{s}{1-\cos\lambda}\right)^{\frac{1}{2}} \left\{ \frac{1}{(1-\cos\lambda)^2} \left[\left(1-\cos\lambda\right)\frac{\partial s}{\partial\alpha}\right.\right.$$

$$\left.\left. -s\,\sin\lambda\,\frac{\partial\lambda}{\partial\alpha}\right] \right\} \left[2\pi N + (\lambda - \sin\lambda) - G_1\,(\beta - \sin\beta)\right] \tag{B.23}$$

Using

$$s(1-\cos\beta) = (s-c)(1-\cos\lambda) \tag{B.5}$$

and its derivative

$$s \sin\beta \frac{\partial\beta}{\partial\alpha} + (1-\cos\beta) \frac{\partial s}{\partial\alpha} = (s-c)\sin\lambda \frac{\partial\lambda}{\partial\alpha} + \left(\frac{\partial s}{\partial\alpha} - \frac{\partial c}{\partial\alpha}\right) (1-\cos\lambda) \tag{B.24}$$

solve for

$$(1-\cos\beta) = \left(\frac{s-c}{s}\right) (1-\cos\lambda) \tag{B.25}$$

and

$$\frac{\partial\beta}{\partial\alpha} = \left(\frac{s-c}{s}\right)\left(\frac{\sin\lambda}{\sin\beta}\right) \frac{\partial\lambda}{\partial\alpha} + \frac{\cos\beta-\cos\lambda}{s \sin\beta} \frac{\partial s}{\partial\alpha} - \frac{(1-\cos\lambda)}{s \sin\beta} \frac{\partial c}{\partial\alpha} \tag{B.26}$$

Substitute (B.4), (B.25) and (B.26) into (B.23) to get

$$\begin{aligned}\frac{\partial\tau}{\partial\alpha} = \left(\frac{s}{1-\cos\lambda}\right)^{\frac{3}{2}} \Bigg\{ & (1-\cos\lambda) \frac{\partial\lambda}{\partial\alpha} \\ & - G_1\left(\frac{s-c}{s}\right) (1-\cos\lambda) \left[\left(\frac{s-c}{s}\right)\left(\frac{\sin\lambda}{\sin\beta}\right) \frac{\partial\lambda}{\partial\alpha} \right. \\ & \left. + \frac{(\cos\beta-\cos\lambda)}{s \sin\beta} \frac{\partial s}{\partial\alpha} - \frac{(1-\cos\lambda)}{s \sin\beta} \frac{\partial c}{\partial\alpha}\right]\Bigg\} \\ & + \frac{3}{2} \frac{\tau}{s} \left[\frac{\partial s}{\partial\alpha} - \frac{s \sin\lambda}{1-\cos\lambda} \frac{\partial\lambda}{\partial\alpha}\right]\end{aligned} \tag{B.27}$$

Grouping terms in (B.27)

$$\frac{\partial\tau}{\partial\alpha} = \left\{\left(\frac{s}{1-\cos\lambda}\right)^{\frac{3}{2}} (1-\cos\lambda)\left[1-G_1\left(\frac{s-c}{s}\right)^2 \frac{\sin\lambda}{\sin\beta}\right] - \frac{3}{2}\frac{\tau\sin\lambda}{1-\cos\lambda}\right\}\frac{\partial\lambda}{\partial\alpha}$$

$$- \left\{G_1\left(\frac{s}{1-\cos\lambda}\right)^{\frac{3}{2}}\left(\frac{s-c}{s}\right)(1-\cos\lambda)\left(\frac{\cos\beta-\cos\lambda}{s\sin\beta}\right) - \frac{3}{2}\frac{\tau}{s}\right\}\frac{\partial s}{\partial\alpha}$$

$$+ \left\{G_1\left(\frac{s}{1-\cos\lambda}\right)^{\frac{3}{2}}\left(\frac{s-c}{s}\right)(1-\cos\lambda)^2\left(\frac{1}{s\sin\beta}\right)\right\}\frac{\partial c}{\partial\alpha} \qquad (B.28)$$

Substituting

$$a = \frac{s}{1-\cos\lambda} \qquad (B.6)$$

into (B.28) where possible

$$\frac{\partial\tau}{\partial\alpha} = \left\{s\sqrt{a}\left[1-G_1\left(\frac{s-c}{s}\right)^2\frac{\sin\lambda}{\sin\beta}\right] - \frac{3}{2}\frac{a\tau}{s}\sin\lambda\right\}\frac{\partial\lambda}{\partial\alpha}$$

$$- \left\{G_1\sqrt{a}\left(\frac{s-c}{s}\right)\left(\frac{\cos\beta-\cos\lambda}{\sin\beta}\right) - \frac{3}{2}\frac{\tau}{s}\right\}\frac{\partial s}{\partial\alpha}$$

$$+ \left\{G_1\left(\frac{s-c}{\sqrt{a}}\right)\frac{1}{\sin\beta}\right\}\frac{\partial c}{\partial\alpha} \qquad (B.29)$$

Then, (B.29) may be written as

$$\frac{\partial\tau}{\partial\alpha} = \frac{1}{Q}\frac{\partial\lambda}{\partial\alpha} - H_1\frac{\partial s}{\partial\alpha} + H_2\frac{\partial c}{\partial\alpha} \qquad (B.30)$$

where

$$\frac{1}{Q} = s\sqrt{a}\left[1-G_1\left(\frac{s-c}{s}\right)^2\frac{\sin\lambda}{\sin\beta}\right] - \frac{3}{2}\frac{a\tau}{s}\sin\lambda \qquad (B.31)$$

$$H_1 = G_1\sqrt{a}\left(\frac{s-c}{s}\right)\left(\frac{\cos\beta-\cos\lambda}{\sin\beta}\right) - \frac{3}{2}\frac{\tau}{s} \tag{B.32}$$

$$H_2 = \frac{G_1(s-c)}{\sqrt{a}\sin\beta} \tag{B.33}$$

From (B.30) it can be seen that

$$\nabla_k\lambda = Q\left[H_1\,\nabla_k s - H_2\,\nabla_k c\right] \tag{B.34}$$

since

$$\nabla_k\tau = 0 \tag{B.35}$$

and that

$$\frac{\partial\lambda}{\partial\tau} = Q \tag{B.36}$$

since

$$\frac{\partial s}{\partial\tau} \equiv 0 \qquad \frac{\partial c}{\partial\tau} \equiv 0 \quad , \quad \frac{\partial\tau}{\partial\tau} \equiv 1$$

b) For a hyperbola, similar procedure may be followed.

$$\tau = \left(\frac{s}{\cosh\gamma-1}\right)^{\frac{3}{2}} \left[(\sinh\gamma-\gamma) - G_1(\sinh\delta-\delta)\right] \tag{B.8}$$

Taking the derivatives,

$$\frac{\partial\tau}{\partial\alpha} = \left(\frac{s}{\cosh\gamma-1}\right)^{\frac{3}{2}} \left[(\cosh\gamma-1)\frac{\partial\gamma}{\partial\alpha} - G_1(\cosh\delta-1)\frac{\partial\delta}{\partial\alpha}\right]$$
$$+ \frac{3}{2}\left(\frac{s}{\cosh\gamma-1}\right)^{\frac{1}{2}} \left\{\frac{1}{(\cosh\gamma-1)^2}\left[(\cosh\gamma-1)\frac{\partial s}{\partial\alpha} - s\sinh\gamma\frac{\partial\gamma}{\partial\alpha}\right]\right\}$$
$$\left[(\sinh\gamma-\gamma) - G_1(\sinh\delta-\delta)\right] \tag{B.37}$$

Using

$$s(\cosh\delta-1) = (s-c)(\cosh\gamma-1) \tag{B.9}$$

and its derivative

$$s\sinh\delta\frac{\partial\delta}{\partial\alpha} + (\cosh\delta-1)\frac{\partial s}{\partial\alpha} = (s-c)\sinh\gamma\frac{\partial\gamma}{\partial\alpha} + (\cosh\gamma-1)\left(\frac{\partial s}{\partial\alpha} - \frac{\partial c}{\partial\alpha}\right) \tag{B.38}$$

solve for

$$(\cosh\delta-1) = \left(\frac{s-c}{s}\right)(\cosh\gamma-1) \tag{B.39}$$

and

$$\frac{\partial\delta}{\partial\alpha} = \left(\frac{s-c}{s}\right)\left(\frac{\sinh\gamma}{\sinh\delta}\right)\frac{\partial\gamma}{\partial\alpha} + \left(\frac{\cosh\gamma-\cosh\delta}{s\sinh\delta}\right)\frac{\partial s}{\partial\alpha} - \left(\frac{\cosh\gamma-1}{s\sinh\delta}\right)\frac{\partial c}{\partial\alpha} \tag{B.40}$$

Substituting (B.8), (B.39), and (B.40) into (B.37) yields

$$\frac{\partial\tau}{\partial\alpha} = \left(\frac{s}{\cosh\gamma - 1}\right)^{\frac{3}{2}}\left\{(\cosh\gamma-1)\frac{\partial\gamma}{\partial\alpha} - G_1\left(\frac{s-c}{s}\right)(\cosh\gamma-1)\left[\left(\frac{s-c}{s}\right)\left(\frac{\sinh\gamma}{\sinh\delta}\right)\frac{\partial\gamma}{\partial\alpha}\right.\right.$$
$$\left.\left. + \left(\frac{\cosh\gamma-\cosh\delta}{s\sinh\delta}\right)\frac{\partial s}{\partial\alpha} - \left(\frac{\cosh\gamma-1}{s\sinh\delta}\right)\frac{\partial c}{\partial\alpha}\right]\right\}$$
$$+ \frac{3}{2}\frac{\tau}{s}\left[\frac{\partial s}{\partial\alpha} - \frac{s\sinh\gamma}{\cosh\gamma-1}\frac{\partial\gamma}{\partial\alpha}\right] \qquad (B.41)$$

Grouping terms,

$$\frac{\partial\gamma}{\partial\alpha} = \left\{\left(\frac{s}{\cosh\gamma-1}\right)^{\frac{3}{2}}(\cosh\gamma-1)\left[1-G_1\left(\frac{s-c}{s}\right)^2\left(\frac{\sinh\gamma}{\sinh\delta}\right)\right] - \frac{3}{2}\frac{\tau\sinh\gamma}{\cosh\gamma-1}\right\}\frac{\partial\gamma}{\partial\alpha}$$
$$- \left\{G_1\left(\frac{s}{\cosh\gamma-1}\right)^{\frac{3}{2}}\left(\frac{s-c}{s}\right)(\cosh\gamma-1)\left(\frac{\cosh\gamma-\cosh\delta}{s\sinh\delta}\right) - \frac{3}{2}\frac{\tau}{s}\right\}\frac{\partial s}{\partial\alpha}$$
$$+ \left\{G_1\left(\frac{s}{\cosh\gamma-1}\right)^{\frac{3}{2}}\left(\frac{s-c}{s}\right)(\cosh\gamma-1)^2\left(\frac{1}{s\sinh\delta}\right)\right\}\frac{\partial c}{\partial\alpha} \qquad (B.42)$$

Substituting

$$a = \frac{s}{1-\cosh\gamma} \qquad (B.10)$$

into (B.42) where possible

$$\frac{\partial\tau}{\partial\alpha} = \left\{s\sqrt{-a}\left[1 - G_1\left(\frac{s-c}{s}\right)^2\frac{\sinh\gamma}{\sinh\delta}\right] + \frac{3}{2}\frac{a\tau}{s}\sinh\gamma\right\}\frac{\partial\gamma}{\partial\alpha}$$
$$- \left\{G_1\sqrt{-a}\left(\frac{s-c}{s}\right)\left(\frac{\cosh\gamma-\cosh\delta}{\sinh\delta}\right) - \frac{3}{2}\frac{\tau}{s}\right\}\frac{\partial s}{\partial\alpha}$$
$$+ \left\{\frac{G_1(s-c)}{\sqrt{-a}\sinh\delta}\right\}\frac{\partial c}{\partial\alpha} \qquad (B.43)$$

Then, (B.43) may be written as

$$\frac{\partial \tau}{\partial \alpha} = \frac{1}{Q} \frac{\partial \gamma}{\partial \alpha} - H_1 \frac{\partial s}{\partial \alpha} + H_2 \frac{\partial c}{\partial \alpha} \tag{B.44}$$

where

$$\frac{1}{Q} = s\sqrt{-a}\left[1-G_1\left(\frac{s-c}{s}\right)^2 \frac{\sinh\gamma}{\sinh\delta}\right] + \frac{3}{2} \frac{a\tau}{s} \sinh\gamma \tag{B.45}$$

$$H_1 = G_1\sqrt{-a}\left(\frac{s-c}{s}\right)\left(\frac{\cosh\gamma-\cosh\delta}{\sinh\delta}\right) - \frac{3}{2}\frac{\tau}{s} \tag{B.46}$$

$$H_2 = G_1\left(\frac{s-c}{\sqrt{-a}}\right)\frac{1}{\sinh\delta} \tag{B.47}$$

From (B.44), it may be seen tha

$$\nabla_k\gamma = Q\,[H_1\,\nabla_k s - H_2\,\nabla_k c] \tag{B.48}$$

since

$$\nabla_k\tau \equiv 0 \tag{B.49}$$

and that

$$\frac{\partial \gamma}{\partial \tau} = Q \tag{B.50}$$

since

$$\frac{\partial s}{\partial \tau} \equiv 0 \quad , \quad \frac{\partial c}{\partial \tau} \equiv 0 \quad ; \quad \frac{\partial \tau}{\partial \tau} \equiv 1$$

5) From (B.4) or (B.8)

$$\tau = \sqrt{\mu}\ (t_2 - t_1) \tag{B.51}$$

Thus

$$\frac{\partial \alpha}{\partial t_1} = -\sqrt{\mu}\frac{\partial \alpha}{\partial \tau}$$

$$\frac{\partial \alpha}{\partial t_2} = \sqrt{\mu}\frac{\partial \alpha}{\partial \tau} \tag{B.52}$$

6) a) For an ellipse

$$a = \frac{s}{1-\cos\lambda} \tag{B.6}$$

Then,

$$\nabla_k a = \frac{1}{(1-\cos\lambda)^2}\ [(1-\cos\lambda)\ \nabla_k s - (s\ \sin\lambda)\ \nabla_k \lambda]$$

$$= \frac{1}{(1-\cos\lambda)^2}\ [(1-\cos\lambda)\ \nabla_k s - Qs\ \sin\lambda(H_1 \nabla_k s - H_2 \nabla_k c)]$$

$$= \left(\frac{a}{s}\right)^2\ [(\frac{s}{a} - QsH_1\ \sin\lambda)\ \nabla_k s + (QsH_2\ \sin\lambda)\ \nabla_k c]$$

Thus,

$$\nabla_k a = \left(\frac{a}{s}\right)^2\ [P_1 \nabla_k s - P_2 \nabla_k c] \tag{B.53}$$

where

$$P_1 = \frac{s}{a} - QsH_1 \sin\lambda \tag{B.54}$$

$$P_2 = - QsH_2 \sin\lambda \tag{B.55}$$

b) For a hyperbola

$$a = \frac{s}{1-\cosh\gamma} \tag{B.10}$$

Then

$$\nabla_k a = \frac{1}{(1-\cosh\gamma)^2} [(1-\cosh\gamma)\ \nabla_k s + s \sinh\gamma\ \nabla_k \gamma]$$

$$= \frac{1}{(1-\cosh\gamma)^2} [(1-\cosh\gamma)\ \nabla_k s + Qs \sinh\gamma (H_1 \nabla_k s - H_2 \nabla_k c)]$$

$$= \left(\frac{a}{s}\right)^2 [(\frac{s}{a} + QsH_1 \sinh\gamma)\ \nabla_k s - (QsH_2 \sinh\gamma)\ \nabla_k c]$$

Thus

$$\nabla_k a = \left(\frac{a}{s}\right)^2 [P_1 \nabla_k s - P_2 \nabla_k c] \tag{B.56}$$

where

$$P_1 = \frac{s}{a} + QsH_1 \sinh\gamma \tag{B.57}$$

$$P_2 = QsH_2 \sinh\gamma \tag{B.58}$$

7) For

$$A = G_1 \sqrt{\frac{1}{s-c} - \frac{1}{2a}} \tag{B.12}$$

$$\nabla_k A = \nabla_k \left[G_1 \sqrt{\frac{1}{s-c} - \frac{1}{2a}} \right]$$

$$= \frac{1}{2A} \nabla_k \left[\frac{1}{s-c} - \frac{1}{2a} \right]$$

$$= \frac{1}{2A} \left[- \frac{1}{(s-c)^2} (\nabla_k s - \nabla_k c) + \frac{1}{2a^2} \nabla_k a \right]$$

Substituting for $\nabla_k a$ yields

$$\nabla_k A = \frac{1}{2A} \left[- \frac{1}{(s-c)^2} (\nabla_k s - \nabla_k c) + \frac{1}{2s^2} (P_1 \nabla_k s - P_2 \nabla_k c) \right]$$

Collecting terms,

$$\nabla_k A = \frac{1}{2A} \left[\left(\frac{P_1}{2s^2} - \frac{1}{(s-c)^2} \right) \nabla_k s - \left(\frac{P_2}{2s^2} - \frac{1}{(s-c)^2} \right) \nabla_k c \right] \tag{B.59}$$

For

$$B = G_2 \sqrt{\frac{1}{s} - \frac{1}{2a}} \tag{B.13}$$

$$\nabla_k B = \nabla_k \left[G_2 \sqrt{\frac{1}{s} - \frac{1}{2a}} \right]$$

$$= \frac{1}{2B} \nabla_k \left[\frac{1}{s} - \frac{1}{2a} \right]$$

$$= \frac{1}{2B} \left[- \frac{1}{s^2} \nabla_k s + \frac{1}{2a^2} \nabla_k a \right]$$

$$= \frac{1}{2B}\left[-\frac{1}{s^2}\nabla_k s + \frac{1}{2s^2}(P_1\nabla_k s - P_2\nabla_k c)\right]$$

Thus, collecting terms

$$\nabla_k B = \frac{1}{2B}\left[\left(\frac{P_1}{2s^2} - \frac{1}{s^2}\right)\nabla_k s - \frac{P_2}{2s^2}\nabla_k c\right] \tag{B.60}$$

8) For

$$V_c = \sqrt{\frac{\mu}{2}}\,[A + B] \tag{B.13}$$

$$\nabla_k V_c = \sqrt{\frac{\mu}{2}}\,[\nabla_k A + \nabla_k B]$$

$$= \sqrt{\frac{\mu}{2}}\left\{\left[\frac{1}{2A}\left(\frac{P_1}{2s^2} - \frac{1}{(s-c)^2}\right) + \frac{1}{2B}\left(\frac{P_1}{2s^2} - \frac{1}{s^2}\right)\right]\nabla_k s\right.$$

$$\left. - \left[\frac{1}{2A}\left(\frac{P_2}{2s^2} - \frac{1}{(s-c)^2}\right) + \frac{1}{2B}\left(\frac{P_2}{2s^2}\right)\right]\nabla_k c\right\}$$

$$= \sqrt{\frac{\mu}{2}}\left\{\left[\frac{P_1}{4s^2}\left(\frac{1}{A} + \frac{1}{B}\right) - \frac{1}{2A(s-c)^2} - \frac{1}{2Bs^2}\right]\nabla_k s\right.$$

$$\left. - \left[\frac{P_2}{4s^2}\left(\frac{1}{A} + \frac{1}{B}\right) - \frac{1}{2A(s-c)^2}\right]\nabla_k c\right\}$$

Thus,

$$\nabla_k V_c = \sqrt{\frac{\mu}{2}}\,[2D_1\nabla_k s - D_2\nabla_k c] \tag{B.61}$$

where

$$D_1 = \frac{P_1}{8s^2}\left(\frac{1}{A} + \frac{1}{B}\right) - \frac{1}{4A(s-c)^2} - \frac{1}{4Bs^2} \tag{B.62}$$

$$D_2 = \frac{P_2}{4s^2} \cdot \left(\frac{1}{A} + \frac{1}{B}\right) - \frac{1}{2A(s-c)^2} \tag{B.63}$$

Similarly, for

$$V_p = \sqrt{\frac{\mu}{2}} [A - B] \tag{B.14}$$

$$\nabla_k V_p = \sqrt{\frac{\mu}{2}} [\nabla_k A - \nabla_k B]$$

$$= \sqrt{\frac{\mu}{2}} \left\{ \left[\frac{P_1}{4s^2} \left(\frac{1}{A} - \frac{1}{B}\right) - \frac{1}{2A(s-c)^2} + \frac{1}{2Bs^2}\right] \nabla_k s \right.$$

$$\left. \left[\frac{P_2}{4s^2} \left(\frac{1}{A} - \frac{1}{B}\right) - \frac{1}{2A(s-c)^2}\right] \nabla_k c \right\}$$

Thus

$$\nabla_k V_p = \sqrt{\frac{\mu}{2}} [2D_3 \nabla_k s - D_4 \nabla_k c] \tag{B.64}$$

where

$$D_3 = \frac{P_1}{8s^2} \left(\frac{1}{A} - \frac{1}{B}\right) - \frac{1}{4A(s-c)^2} + \frac{1}{4Bs^2} \tag{B.65}$$

$$D_4 = \frac{P_2}{4s^2} \left(\frac{1}{A} - \frac{1}{B}\right) - \frac{1}{2A(s-c)^2} \tag{B.66}$$

9) For

$$\underline{i}_c = \underline{c}/c \tag{B.18}$$

$$\nabla_k(\underline{i}_c) = \nabla_k\left(\frac{\underline{c}}{c}\right)$$

$$= \frac{1}{c^2}\left[c\nabla_k\underline{c} - \underline{c}(\nabla_k c)^T\right]$$

$$= \frac{1}{c}\left[\nabla_k\underline{c} - \underline{i}_c(\nabla_k c)^T\right] \qquad \text{(B.67)}$$

Since

$$\underline{c} = \underline{r}_2 - \underline{r}_1 = \begin{bmatrix} x_2 - x_1 \\ y_2 - y_1 \\ z_2 - z_1 \end{bmatrix}$$

$$\nabla_1\underline{c} = -I \quad ; \quad \nabla_2\underline{c} = I \qquad \text{(B.68)}$$

From (B.21)

$$\nabla_1 c = -\underline{i}_c \quad ; \quad \nabla_2 c = \underline{i}_c \qquad \text{(B.21)}$$

Substituting (B.21) and (B.68) into (B.67) yields

$$\nabla_1(\underline{i}_c) = -\frac{1}{c} I + \frac{1}{c}\underline{i}_c\,\underline{i}_c^T$$

$$\nabla_2(\underline{i}_c) = \frac{1}{c} I - \frac{1}{c}\underline{i}_c\,\underline{i}_c^T \qquad \text{(B.69)}$$

Similarly,

$$\nabla_1(\underline{i}_{r_1}) = \frac{1}{r_1} I - \frac{1}{r_1}\underline{i}_{r_1}\,\underline{i}_{r_1}^T \qquad \text{(B.70)}$$

$$\nabla_2(\underline{i}_{r_2}) = \frac{1}{r_2} I - \frac{1}{r_2}\underline{i}_{r_2}\,\underline{i}_{r_2}^T \qquad \text{(B.71)}$$

$$\nabla_1(\underline{i}_{r_2}) \equiv 0 \tag{B.72}$$

$$\nabla_2(\underline{i}_{r_1}) \equiv 0 \tag{B.73}$$

The above intermediate partials may be used for the calculation of the desired partial derivative matrices. From

$$\underline{v}_1 = V_c \, \underline{i}_c + V_p \, \underline{i}_{r_1} \tag{B.16}$$

$$\underline{v}_2 = V_c \, \underline{i}_c - V_p \, \underline{i}_{r_2} \tag{B.17}$$

calculate

$$\nabla_1 \underline{v}_1 = \underline{i}_c \, (\nabla_1 V_c)^T + V_c \nabla_1(\underline{i}_c) + \underline{i}_{r_1} (\nabla_1 V_p)^T + V_p \nabla_1(\underline{i}_{r_1})$$

$$= \underline{i}_c (\nabla_1 V_c)^T + \frac{V_c}{c} \left[- I + \underline{i}_c \, \underline{i}_c^T \right] + \underline{i}_{r_1} (\nabla_1 V_p)^T$$

$$+ \frac{V_p}{r_1} \left[I - \underline{i}_{r_1} \, \underline{i}_{r_1}^T \right]$$

Thus

$$\nabla_1 \underline{v}_1 = \left[\frac{V_p}{r_1} - \frac{V_c}{c} \right] I + \underline{i}_c \left[\nabla_1 V_c + \frac{V_c}{c} \, \underline{i}_c \right]^T \tag{B.74}$$

$$+ \underline{i}_{r_1} \left[\nabla_1 V_p - \frac{V_p}{r_1} \, \underline{i}_{r_1} \right]^T$$

Similarly,

$$\nabla_2 \underline{v}_1 = \left[\frac{1}{c} V_c\right] I + \underline{i}_c \left[\nabla_2 V_c - \frac{V_c}{c} \underline{i}_c\right]^T + \underline{i}_{r_1} \left[\nabla_2 V_p\right]^T \qquad (B.75)$$

$$\nabla_1 \underline{v}_2 = \left[-\frac{1}{c} V_c\right] I + \underline{i}_c \left[\nabla_1 V_c + \frac{V_c}{c} \underline{i}_c\right]^T - \underline{i}_{r_2} \left[\nabla_1 V_p\right]^T \qquad (B.76)$$

$$\nabla_2 \underline{v}_2 = \left[\frac{1}{c} V_c - \frac{1}{r_2} V_p\right] I + \underline{i}_c \left[\nabla_2 V_c - \frac{V_c}{c} \underline{i}_c\right]^T$$

$$- \underline{i}_{r_2} \left[\nabla_2 V_p - \frac{V_p}{r_2} \underline{i}_{r_2}\right]^T \qquad (B.77)$$

Substitute (B.13), (B.14), (B.61), and (B.64) into (B.74)-(B.77) to get

$$\nabla_1 \underline{v}_1 = \sqrt{\frac{\mu}{2}} \left\{\left[\frac{1}{r_1}(A - B) - \frac{1}{c}(A + B)\right] I + \underline{i}_c \left[2D_1 \nabla_1 s - D_2 \nabla_1 c + \frac{A + B}{c} \underline{i}_c\right]^T + \underline{i}_{r_1} \left[2D_3 \nabla_1 s - D_4 \nabla_1 c - \frac{A - B}{r_1} \underline{i}_{r_1}\right]^T \right\}$$

$$= \sqrt{\frac{\mu}{2}} \left\{ (E_0 - E_1) I + \underline{i}_c \left[D_1(\underline{i}_{r_1} - \underline{i}_c) + D_2 \underline{i}_c + E_1 \underline{i}_c\right]^T + \underline{i}_{r_1} \left[D_3(\underline{i}_{r_1} - \underline{i}_c) + D_4 \underline{i}_c - E_0 \underline{i}_{r_1}\right]^T \right\}$$

$$\nabla_1 \underline{v}_1 = \sqrt{\frac{\mu}{2}} \left\{ (E_0 - E_1) I + (D_3 - E_0) \underline{i}_{r_1} \underline{i}_{r_1}^T + (D_4 - D_3) \underline{i}_{r_1} \underline{i}_c^T + D_1 \underline{i}_c \underline{i}_{r_1}^T + (D_2 + E_1 - D_1) \underline{i}_c \underline{i}_c^T \right\} \qquad (B.78)$$

Similarly,

$$\nabla_2 \underline{v}_1 = \sqrt{\frac{\mu}{2}} \left\{ E_1 \, I + D_3 \, \underline{i}_{r_1} \, \underline{i}_{r_2}^T + (D_3 - D_4) \, \underline{i}_{r_1} \, \underline{i}_c^T \right.$$

$$\left. + D_1 \, \underline{i}_c \, \underline{i}_{r_2}^T + (D_1 - D_2 - E_1) \, \underline{i}_c \, \underline{i}_c^T \right\} \tag{B.79}$$

$$\nabla_1 \underline{v}_2 = \sqrt{\frac{\mu}{2}} \left\{ - E_1 \, I - D_3 \, \underline{i}_{r_2} \, \underline{i}_{r_1}^T - (D_4 - D_3) \, \underline{i}_{r_2} \, \underline{i}_c^T \right.$$

$$\left. + D_1 \, \underline{i}_c \, \underline{i}_{r_1}^T + (D_2 + E_1 - D_1) \, \underline{i}_c \, \underline{i}_c^T \right\} \tag{B.80}$$

$$\nabla_2 \underline{v}_2 = \sqrt{\frac{\mu}{2}} \left\{ (E_1 - E_2) \, I + (E_2 - D_3) \, \underline{i}_{r_2} \, \underline{i}_{r_2}^T \right.$$

$$\left. + (D_4 - D_3) \, \underline{i}_{r_2} \, \underline{i}_c^T + D_1 \, \underline{i}_c \, \underline{i}_{r_2}^T + (D_1 - D_2 - E_1) \, \underline{i}_c \, \underline{i}_c^T \right\} \tag{B.81}$$

where

$$E_0 = \frac{A - B}{r_1} \tag{B.82}$$

$$E_1 = \frac{A + B}{c} \tag{B.83}$$

$$E_2 = \frac{A - B}{r_2} \tag{B.84}$$

Define the matrices

$$M_1 = \underline{i}_{r_1} \, \underline{i}_{r_1}^T \qquad\qquad M_4 = \underline{i}_{r_2} \, \underline{i}_{r_1}^T$$

$$M_2 = \underline{i}_{r_1} \underline{i}_c^T \qquad M_5 = \underline{i}_{r_2} \underline{i}_c^T \tag{B.85}$$

$$M_3 = \underline{i}_c \underline{i}_c^T \qquad M_6 = \underline{i}_{r_2} \underline{i}_{r_2}^T$$

Substituting (B.85) into (B.78)-(B.81) yields

$$\nabla_1 \underline{v}_1 = \sqrt{\frac{\mu}{2}} \left[(E_0 - E_1) I + (D_3 - E_0) M_1 + (D_4 - D_3) M_2 \right.$$

$$\left. + D_1 M_2^T + (D_2 + E_1 - D_1) M_3 \right] \tag{B.86}$$

$$\nabla_2 \underline{v}_1 = \sqrt{\frac{\mu}{2}} \left[E_1 I + D_3 M_4^T + (D_3 - D_4) M_2 + D_1 M_5^T \right.$$

$$\left. + (D_1 - D_2 - E_1) M_3 \right] \tag{B.87}$$

$$\nabla_1 \underline{v}_2 = \sqrt{\frac{\mu}{2}} \left[- E_1 I - D_3 M_4 - (D_4 - D_3) M_5 + D_1 M_2^T \right.$$

$$\left. + (D_2 + E_1 - D_1) M_3 \right] \tag{B.88}$$

$$\nabla_2 \underline{v}_2 = \sqrt{\frac{\mu}{2}} \left[(E_1 - E_2) I + (E_2 - D_3) M_6 + (D_4 - D_3) M_5 \right.$$

$$\left. + D_1 M_5^T + (D_1 - D_2 - E_1) M_3 \right] \tag{B.89}$$

The partial derivatives with respect to time

$$\frac{\partial \underline{v}_1}{\partial \tau} \quad , \quad \frac{\partial \underline{v}_2}{\partial \tau}$$

may be gotten by the chain rule using

1) a) For an ellipse

$$a = \frac{s}{1-\cos\lambda} \tag{B.6}$$

$$\frac{\partial a}{\partial \tau} = - \frac{s \sin\lambda}{(1-\cos\lambda)^2} \frac{\partial \lambda}{\partial \tau}$$

$$= - \frac{a^2}{s} \sin\lambda \frac{\partial \lambda}{\partial \tau}$$

Using

$$\frac{\partial \lambda}{\partial \tau} = Q \tag{B.36}$$

$$\frac{\partial a}{\partial \tau} = - \frac{a^2 Q}{s} \sin\lambda \tag{B.90}$$

b) For a hyperbola

$$a = \frac{s}{1-\cosh\gamma} \tag{B.10}$$

$$\frac{\partial a}{\partial \tau} = \frac{s \sinh\gamma}{(1-\cosh\gamma)^2} \frac{\partial \gamma}{\partial \tau}$$

$$= \frac{a^2}{s} \sinh\gamma \frac{\partial \gamma}{\partial \tau}$$

Using

$$\frac{\partial \gamma}{\partial \tau} = Q \tag{B.50}$$

$$\frac{\partial a}{\partial \tau} = \frac{a^2 Q}{s} \sinh\gamma \tag{B.91}$$

2) From (B.12) - (B.15)

$$\frac{\partial A}{\partial \tau} = \frac{1}{4Aa^2} \frac{\partial a}{\partial \tau} \tag{B.92}$$

$$\frac{\partial B}{\partial \tau} = \frac{1}{4Ba^2} \frac{\partial a}{\partial \tau} \tag{B.93}$$

$$\frac{\partial V_c}{\partial \tau} = \sqrt{\frac{\mu}{2}} \left[\frac{\partial A}{\partial \tau} + \frac{\partial B}{\partial \tau}\right] \tag{B.94}$$

$$\frac{\partial V_p}{\partial \tau} = \sqrt{\frac{\mu}{2}} \left[\frac{\partial A}{\partial \tau} - \frac{\partial B}{\partial \tau}\right] \tag{B.95}$$

Substituting (B.90) - (B.93) into (B.94) and (B.95) yields

$$\frac{\partial V_c}{\partial \tau} = \sqrt{\frac{\mu}{2}} W \left[\frac{1}{A} + \frac{1}{B}\right] \tag{B.96}$$

$$\frac{\partial V_p}{\partial \tau} = \sqrt{\frac{\mu}{2}} W \left[\frac{1}{A} - \frac{1}{B}\right] \tag{B.97}$$

where

$$W = -\frac{Q}{45} \sin\lambda \qquad \text{(ellipse)}$$
$$= \frac{Q}{45} \sinh\gamma \qquad \text{(hyperbola)} \tag{B.98}$$

Using the above relations with (B.16) and (B.17) yields

$$\frac{\partial \underline{v}_1}{\partial \tau} = W \cdot \sqrt{\frac{\mu}{2}} \left[\left(\frac{1}{A} + \frac{1}{B} \right) \underline{i}_c + \left(\frac{1}{A} - \frac{1}{B} \right) \underline{i}_{r_1} \right] \tag{B.99}$$

$$\frac{\partial \underline{v}_2}{\partial \tau} = W \sqrt{\frac{\mu}{2}} \left[\left(\frac{1}{A} + \frac{1}{B} \right) \underline{i}_c - \left(\frac{1}{A} - \frac{1}{B} \right) \underline{i}_{r_2} \right] \tag{B.100}$$

Using (B.52),

$$\frac{\partial \underline{v}_1}{\partial t_1} = - \frac{\partial \underline{v}_1}{\partial t_2} = - \sqrt{\mu} \frac{\partial \underline{v}_1}{\partial \tau} \tag{B.101}$$

$$\frac{\partial \underline{v}_2}{\partial t_1} = - \frac{\partial \underline{v}_2}{\partial t_2} = - \sqrt{\mu} \frac{\partial \underline{v}_2}{\partial \tau} \tag{B.102}$$

B.3 Equation Summary for Partial Derivative Matrices

$$\nabla \underline{v}_1 = \sqrt{\frac{\mu}{2}} \left[(E_0 - E_1) I + (D_3 - E_0) M_1 + (D_4 - D_3) M_2 + D_1 M_2^T + (D_2 - D_1 + E_1) M_3 \right]$$

$$\nabla_2 \underline{v}_1 = \sqrt{\frac{\mu}{2}} \left[E_1 I + D_3 M_4^T - (D_4 - D_3) M_2 + D_1 M_5^T - (D_2 - D_1 + E_1) M_3 \right]$$

$$\nabla_1 \underline{v}_2 = \sqrt{\frac{\mu}{2}} \left[-E_1 I - D_3 M_4 - (D_4 - D_3) M_5 + D_1 M_2^T + (D_2 - D_1 + E_1) M_3 \right]$$

$$\nabla_2 \underline{v}_2 = \sqrt{\frac{\mu}{2}} \left[(E_1 - E_2)\, I - (D_3 - E_2)\, M_6 + (D_4 - D_3)\, M_5 + D_1\, M_5^T - (D_3 - D_1 + E_1)\, M_3 \right]$$

$$M_1 = \underline{i}_{r_1}\, \underline{i}_{r_1}^T \qquad M_3 = \underline{i}_c\, \underline{i}_c^T \qquad M_5 = \underline{i}_{r_2}\, \underline{i}_c^T$$

$$M_2 = \underline{i}_{r_1}\, \underline{i}_c^T \qquad M_4 = \underline{i}_{r_2}\, \underline{i}_{r_1}^T \qquad M_6 = \underline{i}_{r_2}\, \underline{i}_{r_2}^T$$

$$E_0 = \frac{A-B}{r_1} \qquad E_1 = \frac{A+B}{c} \qquad E_2 = \frac{A-B}{r_2}$$

$$D_1 = \frac{P_1}{8s^2}\left(\frac{1}{A} + \frac{1}{B}\right) - \frac{1}{4A(s-c)^2} - \frac{1}{4Bs^2}$$

$$D_2 = \frac{P_2}{4s^2}\left(\frac{1}{A} + \frac{1}{B}\right) - \frac{1}{2A(s-c)^2}$$

$$D_3 = \frac{P_1}{8s^2}\left(\frac{1}{A} - \frac{1}{B}\right) - \frac{1}{4A(s-c)^2} + \frac{1}{4Bs^2}$$

$$D_4 = \frac{P_2}{4s^2}\left(\frac{1}{A} - \frac{1}{B}\right) - \frac{1}{2A(s-c)^2}$$

<u>Ellipse</u>

$$P_1 = \frac{s}{a} - QsH_1 \sin\lambda$$

$$P_2 = - QsH_2 \sin\lambda$$

$$H_1 = G_1 \sqrt{a}\left(\frac{s-c}{s}\right)\left(\frac{\cos\beta - \cos\lambda}{\sin\beta}\right) - \frac{3}{2}\frac{\tau}{s}$$

$$H_2 = G_1 \left(\frac{s-c}{\sqrt{a}}\right)\frac{1}{\sin\beta}$$

$$\frac{1}{Q} = s\sqrt{a}\left[1 - G_1\left(\frac{s-c}{s}\right)^2 \frac{\sin\lambda}{\sin\beta}\right] - \frac{3}{2}\frac{a\tau}{s}\sin\lambda$$

<u>Hyperbola</u>

$$P_1 = \frac{s}{a} + QsH_1 \sinh\gamma$$

$$P_2 = QsH_2 \sinh\gamma$$

$$H_1 = G_1\sqrt{-a}\left(\frac{s-c}{s}\right)\left(\frac{\cosh\gamma - \cosh\delta}{\sinh\delta}\right) - \frac{3}{2}\frac{\tau}{s}$$

$$H_2 = G_1 \left(\frac{s-c}{\sqrt{-a}}\right)\frac{1}{\sinh\delta}$$

$$\frac{1}{Q} = s\sqrt{-a}\left[1 - G_1\left(\frac{s-c}{s}\right)^2 \frac{\sinh\gamma}{\sinh\delta}\right] + \frac{3}{2}\frac{a\tau}{s}\sinh\gamma$$

$$\frac{\partial \underline{v}_1}{\partial t_1} = -\frac{\partial \underline{v}_1}{\partial t_2} = -\sqrt{\mu}\frac{\partial \underline{v}_1}{\partial \tau}$$

$$\frac{\partial \underline{v}_2}{\partial t_1} = -\frac{\partial \underline{v}_2}{\partial t_2} = -\sqrt{\mu}\frac{\partial \underline{v}_2}{\partial \tau}$$

$$\frac{\partial \underline{v}_1}{\partial \tau} = W\sqrt{\frac{\mu}{2}}\left[\left(\frac{1}{A} + \frac{1}{B}\right)\underline{i}_c + \left(\frac{1}{A} - \frac{1}{B}\right)\underline{i}_{r_1}\right]$$

$$\frac{\partial \underline{v}_2}{\partial \tau} = W\sqrt{\frac{\mu}{2}}\left[\left(\frac{1}{A} + \frac{1}{B}\right)\underline{i}_c - \left(\frac{1}{A} - \frac{1}{B}\right)\underline{i}_{r_2}\right]$$

Ellipse	Hyperbola
$W = -\frac{Q \sin\lambda}{4s}$	$W = \frac{Q \sinh\gamma}{4s}$

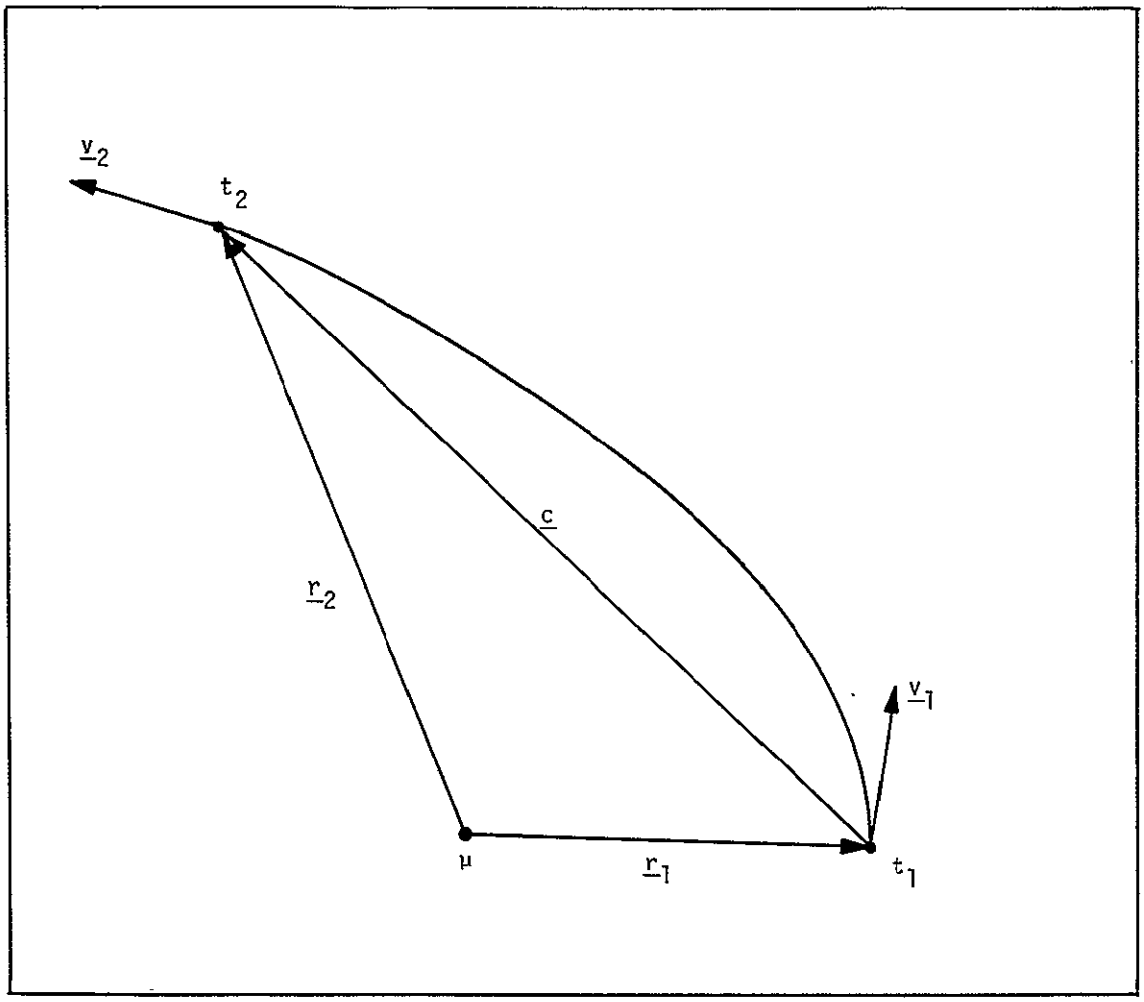

Figure B.1 Lambert Problem Geometry

Appendix C

Calculation of Planetary Data

C.1 Ephemeris Generation

Expressions for the mean elements of the eight inner planets were obtained from [35]. The elements obtained from the calculations are

Ω = longitude of ascending node

ω = argument of perihelion

M = mean anomaly

L = mean longitude = $\Omega + \omega + M$

$\tilde{\omega}$ = longitude of perihelion = $\Omega + \omega$

e = orbital eccentricity

i = orbital inclination to ecliptic plane

a = semi-major axis (in astronomical units)

The six elements L, $\tilde{\omega}$, Ω, e, i, a are given as expansions in the time in centuries

$$T = \frac{(J.D.) - (J.D.)_0}{36525.0} \tag{C.1}$$

measured from the epoch Julian date for January 0.5, 1900

$$(J.D.)_0 = 2415020.0 \text{ days} \tag{C.2}$$

The term (J.D.) is the current Julian date in days. The expansions, as determined empirically from observational astronomy are as follows.

Mercury

$a = 0.3870984$

$e = 0.20561421 + 0.00002046T - 0.000000030T^2$

$i = 7°0'10".37 + 6".699T - 0".066T^2$

$\Omega = 47°8'45".40 + 4266".75T + 0".626T^2$

$\tilde{\omega}$ = 75°53'58".91 + 5599".76 T + 1".061 T^2

L = 178°10'44".68 + 538106654".80 T + 1".084 T^2

Venus

a = 0.72333015

e = 0.00682069 - 0.00004774 T + 0.000000091 T^2

i = 3°23'37".07 + 3".621 T - 0".0035 T^2

Ω = 75°46'46".73 + 3239".46 T + 1".476 T^2

$\tilde{\omega}$ = 130°9'49".8 + 5068".93 T - 3".515 T^2

L = 342°46'1".39 + 210669162".88 T + 1".1148 T^2

Earth

a = 1.00000013

e = 0.01675104 - 0.00004180 T - 0.000000126 T^2

i = 0.0°

Ω = 0.0°

$\tilde{\omega}$ = 101°13'15".0 + 6189".03T + 1".63 T^2 + 0".012 T^3

L = 99°41'48".04 + 129602768".13 T + 1".089 T^2

Mars

a = 1.52368839

e = 0.09331290 + 0.000092064 T - 0.000000077 T^2

i = 1°51'1".20 - 2".430 T + 0".0454 T^2

Ω = 48°47'11".19 + 2775".57 T - 0".005 T^2 - 0".0192 T^3

$\tilde{\omega}$ = 334°13'5".53 + 6628".73 T + 0.4675 T^2 - 0".0043 T^3

L = 293°44'51".46 + 68910117".33 T + 1".1184 T^2

Jupiter

a = 5.202561

e = 0.04833475 + 0.000164180 T - 0.0000004676 T^2 - 0.0000000017 T^3

i = 1°18'31".45 - 20".506 T + 0.014" T^2

Ω = 99°26'36".19 + 3637.908" T + 1".2680 T^2 - 0".03064 T^3

$\tilde{\omega} = 12°43'15".34 + 5795".862\ T + 3".80258\ T^2 - 0".01236\ T^3$

$L = 238°2'57".32 + 10930687".148\ T + 1".20486\ T^2 - 0.005936\ T^3$

Saturn

$a = 9.554747$

$e = 0.05589232 - 0.0003455\ T - 0.000000728\ T^2 + 0.00000000074\ T^3$

$i = 2°29'33".07 - 14".108\ T - 0".05576\ T^2 + 0.00016\ T^3$

$\Omega = 112°47'25".40 + 3143".5025\ T - 0".54785\ T^2 - 0".0191\ T^3$

$\tilde{\omega} = 91°5'53".38 + 7050".297\ T + 2".9749\ T^2 + 0".0166\ T^3$

$L = 266°33'51".76 + 4404635".5810\ T + 1".16835\ T^2 - 0".021\ T^3$

Uranus

$a = 19.21814$

$e = 0.0463444 - 0.00002658\ T + 0.000000077\ T^2$

$i = 0°46'20".87 + 2".251\ T + 0".1422\ T^2$

$\Omega = 73°28'37".55 + 1795".204\ T + 4".722\ T^2$

$\tilde{\omega} = 171°32'55".14 + 5343".958\ T + 0".8539\ T^2 - 0".00218\ T^3$

$L = 244°11'50".89 + 1547508".765\ T + 1".16835\ T^2 - 0".021\ T^3$

Neptune

$a = 30.10957$

$e = 0.00899704 + 0.00000633\ T - 0.000000002\ T^2$

$i = 1°46'45".27 - 34".357\ T - 0".0328\ T^2$

$\Omega = 130°40'52".89 + 3956".166\ T + 0.89952\ T^2 - 0".016984\ T^3$

$\tilde{\omega} = 46°43'38".37 + 5128".468\ T + 1".40694\ T^2 - 0".002176\ T^3$

$L = 84°27'28".78 + 791589".291\ T + 1".15374\ T^2 - 0".002176\ T^3$

The other elements are found using

$$\omega = \tilde{\omega} - \Omega$$

$$M = L - \tilde{\omega} \qquad \text{(C.3)}$$

A listing of the gravitational parameter used for the planets and the sun is given in Table C.1.

Once the orbital elements of a planet have been calculated for a given time, its position and velocity may be calculated using the following relations (see [3] for derivations).

$$\underline{r}_p = a\,(\cos E - 1)\,\underline{i}_1 + \sqrt{ap}\,\sin E\,\underline{i}_2$$

$$\underline{v}_p = \frac{1}{r_p}\left[-\sqrt{\mu a}\,\sin E\,\underline{i}_1 + \sqrt{\mu p}\,\cos E\,\underline{i}_2\right] \tag{C.4}$$

where

E = eccentric anomaly

p = semilatus rectum

$= a(1-e^2)$

μ = gravitational parameter of the central body (in this case, of the sun)

The coordinate system defined by the unit vectors, $\underline{i}_1$, $\underline{i}_2$, $\underline{i}_3$ is shown in Figure C.1. It can be seen that these unit vectors may be expressed in the ecliptic frame as

$$\underline{i}_1 = \begin{bmatrix} \cos\Omega\cos\omega - \sin\Omega\sin\omega\cos i \\ \sin\Omega\cos\omega + \cos\Omega\sin\omega\cos i \\ \sin\omega\sin i \end{bmatrix}$$

$$\underline{i}_2 = \begin{bmatrix} -\cos\Omega\sin\omega - \sin\Omega\cos\omega\cos i \\ -\sin\Omega\sin\omega + \cos\Omega\cos\omega\cos i \\ \cos\omega\sin i \end{bmatrix} \tag{C.5}$$

$$\underline{i}_3 = \begin{bmatrix} \sin\Omega \sin i \\ -\cos\Omega \sin i \\ \cos i \end{bmatrix}$$

The eccentric anomaly E is related to the mean anomaly M by Kepler's equation

$$M = E - e \sin E \tag{C.6}$$

This equation is transcendental and may not be solved analytically. The solution technique used here is a Newton-Rapheson iteration which sets

$$E_{k+1} = E_k - \frac{\left[E_k - M - e \sin E_k\right]}{\left[1 - e \cos E_k\right]} \tag{C.7}$$

with the initial condition

$$E_0 = M \tag{C.8}$$

This iteration converges rapidly for orbits with small eccentricity.

C.2 Calculation of Sphere of Influence Radius

In this thesis, a somewhat larger sphere of influence (SOI) is used than the classical Laplace SOI. This enlarged SOI is the surface on which the direct acceleration due to the planet equals the perturbing acceleration due to the gradient of the solar gravitational field. Referring to Figure C.2 it can be shown (see [3]) that an approximate expression (good to first order in r/ℓ) for the acceleration on a point mass m due to a planet P and the sun S is

$$\ddot{\underline{r}} = - \frac{\mu_P + \mu_m}{r^2} \underline{i}_r + \frac{\mu_S}{\ell^2} \frac{r}{\ell} \left(3 \cos\alpha \, \underline{i}_\ell - \underline{i}_r \right) \tag{C.9}$$

where

$\underline{r}$ = position of mass m with respect to the planet P

$\underline{\ell}$ = position of the sun S with respect to the planet P

α = angle between $\underline{\ell}$ and $\underline{r}$

μ_S, μ_P, μ_m = gravitational parameters of the sun, planet, and mass m respectively.

Equating the direct and perturbing accelerations yields

$$\frac{r}{\ell} = \left(1 + 3 \cos^2\alpha \right)^{-\frac{1}{6}} \left(\frac{\mu_P + \mu_m}{\mu_S} \right)^{\frac{1}{3}} \tag{C.10}$$

Since

$$0.7937 \leq \left(1 + 3 \cos^2\alpha \right)^{-\frac{1}{6}} \leq 1.0$$

and

$$\mu_m << \mu_P \text{ or } \mu_S$$

the locus of these points may be approximated by a sphere of radius

$$r \approx \ell \left(\frac{\mu_P}{\mu_S} \right)^{\frac{1}{3}} \tag{C.11}$$

For computational purposes, ℓ is assumed equal to the semi-major axis of the orbit of the planet under consideration.

The Laplace SOI is a somewhat smaller surface defined approximately (see [3]) as

$$r = \ell \left(\frac{\mu_P}{\mu_S} \right)^{\frac{2}{5}} \tag{C.12}$$

This surface is the locus of points where the ratio of disturbing acceleration to primary acceleration is equal for the equations of motion referred to either the sun or the planet.

Numerical experiments by the author and by Carlson [29] show that a better trajectory approximation is obtained by using the enlarged sphere of influence. Carlson also shows that the theory of matched asymptotic expansion predicts an overlap of the region of validity of the heliocentric and planetocentric trajectory representations in the vicinity of this enlarged sphere of influence. A listing of the size of both the Laplace and the enlarged spheres of influence is given in Table C.2

Table C.1 Gravitational Parameters

Body	μ (km^3/sec^2)
Sun	0.1327154456 (10^{12})
Mercury	0.2211924093 (10^5)
Venus	0.32528295482(10^6)
Earth	0.39802852025(10^6)
Mars	0.4290138858 (10^5)
Jupiter	0.12671486322(10^9)
Saturn	0.3790137239 (10^8)
Uranus	0.580329029 (10^7)
Neptune	0.68714634755(10^7)

Table C.2 Sphere of Influence Radius

Body	Laplace Sphere (km)	Enlarged Sphere (km)
Mercury	113,455.7	318,688.4
Venus	616,362.0	1,458,966.1
Earth	923,738.2	2,157,378.4
Mars	574,520.1	1,564,377.2
Jupiter	48,177,614.0	76,638,659.8
Saturn	54,505,381.7	94,129,489.7
Uranus	51,742,213.6	101,287,919.7
Neptune	86,747,707.2	167,883,945.9

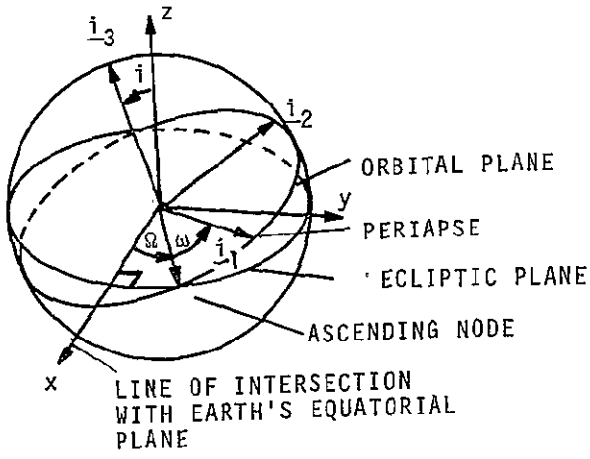

Figure C.1 Coordinate System Geometry

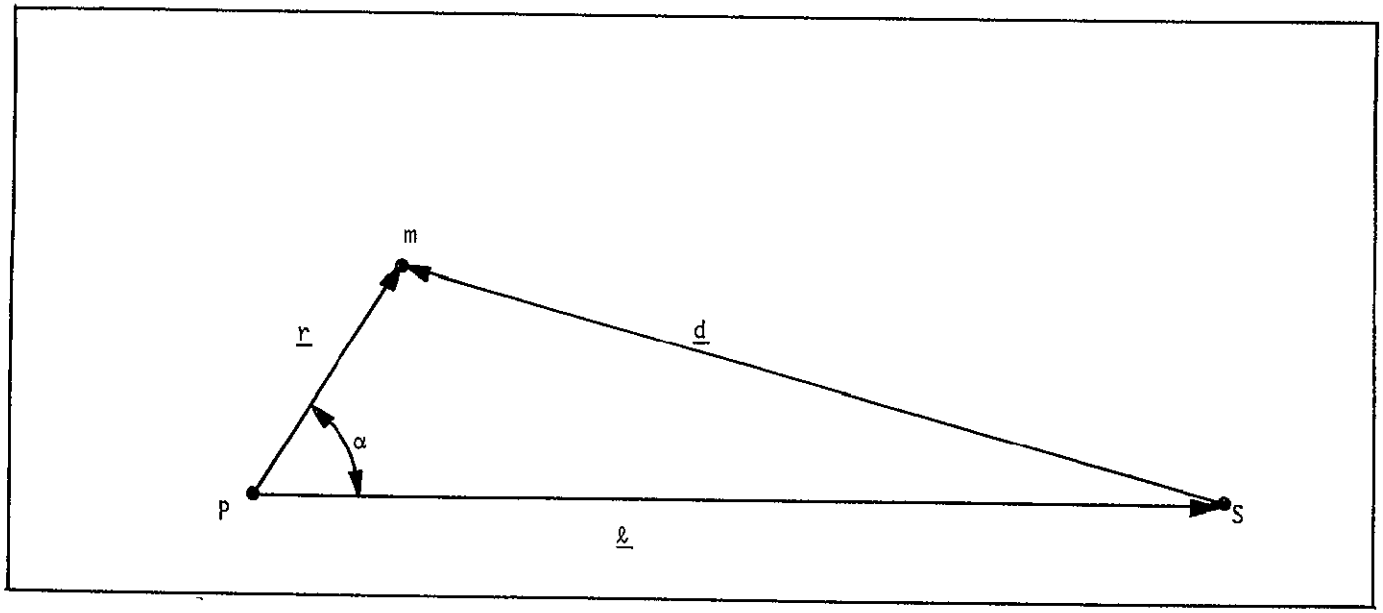

Figure C.2 Geometry of Perturbing Acceleration

Appendix D

Properties and Application of the Two-Body State Transition Matrix

D.1 Properties of the Two-Body State Transition Matrix

This section summarizes some of the more important properties of the two-body state transition matrix. For a more complete discussion, see [36] or [3].

The equation of motion for two-body flight is

$$\ddot{\underline{r}} = -\frac{\mu}{r^3}\,\underline{r} \tag{D.1}$$

The variational equation for small perturbations about the nominal trajectory is

$$\delta\ddot{\underline{r}} = G(\underline{r})\delta\underline{r} = G(t)\,\delta\underline{r} \tag{D.2}$$

where

$$G(\underline{r}) = \frac{\mu}{r^3}\left[3\,\underline{i}_r\,\underline{i}_r^T - I\right] \tag{D.3}$$

$$\underline{r} = \underline{r}(t)$$

Equations (D.1) and (D.2) may be put into first-order form by defining

$$\underline{x}(t) = \begin{bmatrix} \underline{r}(t) \\ \underline{v}(t) \end{bmatrix} \tag{D.4}$$

$$\delta\underline{x} = \begin{bmatrix} \delta\underline{r}(t) \\ \delta\underline{v}(t) \end{bmatrix} \tag{D.5}$$

Then

$$\dot{\underline{x}} = \begin{bmatrix} 0 & I \\ -\frac{\mu}{r^3} & 0 \end{bmatrix} \underline{x} \tag{D.6}$$

and

$$\delta\dot{\underline{x}} = F(t)\underline{x} \tag{D.7}$$

where

$$F(t) = \begin{bmatrix} 0 & I \\ G(t) & 0 \end{bmatrix} \tag{D.8}$$

The solution to (D.7) is given by

$$\delta\underline{x}\ (t) = \Phi_0(t,\ t_0)\ \delta\underline{x}(t_0) \tag{D.9}$$

where

$\Phi_0(t,t_0)$ = state transition matrix from time t_0 to time t for the two-body trajectory.

It may be shown [3] that the state transition matrix satisfies the same differential equation as the state

$$\dot{\Phi}_0(t,t_0) = F(t)\Phi_0(t,t_0) \tag{D.10}$$

with the initial conditions

$$\Phi_0(t_0,t_0) = I \tag{D.11}$$

A number of analytic solutions to (D.10) in different coordinate systems exist (see [3], [36], [37]). The one used in this thesis is by Goodyear [37], which provides a solution in generalized cartesian coordinates.

The state transition matrix is a member of a class known as symplectic matrices. These matrices satisfy the relation

$$Q^T J Q = J \tag{D.12}$$

where

$$J = \begin{bmatrix} 0 & I \\ -I & 0 \end{bmatrix} \qquad Q = \text{symplectic matrix}$$

Post-multiply (D.12) by Q^{-1} and pre-multiply by J to get

$$Q^{-1} = - J Q^T J \tag{D.13}$$

If the state transition matrix is partitioned into

$$\Phi_0(t,t_0) = \begin{bmatrix} A_0(t,t_0) & B_0(t,t_0) \\ C_0(t,t_0) & D_0(t,t_0) \end{bmatrix} \tag{D.14}$$

then

$$\Phi_0^{-1}(t,t_0) = \begin{bmatrix} D_0{}^T(t,t_0) & -B_0{}^T(t,t_0) \\ -C_0{}^T(t,t_0) & A_0(t,t_0) \end{bmatrix} \tag{D.15}$$

may be calculated using (D.13).

If (D.7) includes a disturbing term

$$\delta\dot{\underline{x}}(t) = F(t)\ \delta\underline{x}(t) + \underline{f}_0(t) \tag{D.16}$$

where

$\underline{f}_0(t)$ = disturbing vector

$$= \begin{bmatrix} \underline{0} \\ \underline{a}_d(t) \end{bmatrix}$$

$\underline{a}_d(t)$ = disturbing acceleration evaluated along the reference orbit

the solution to the perturbed motion is given by

$$\delta\underline{x}(t) = \Phi_0(t,t_0)\ \delta\underline{x}(t_0) + \int_{t_0}^{t} \Phi_0(t,\tau)\underline{f}_0(\tau)d\tau \qquad (D.17)$$

See [30] for a derivation of this relation.

D.2 Evaluation of Perturbation Integrals by Quadrature

In the calculation of the perturbed conic trajectory segments, it is necessary to evaluate the integral

$$\underline{s}(t) = \int_{t_0}^{t} \Phi_0(t,\tau)\underline{f}_0(\tau)d\tau \qquad (D.18)$$

in (D.17) Since both terms in the integrand are known functions of time along the reference trajectory, the integral may be evaluated by quadrature. The quadrature method chosen was Simpson's Rule [38], which states that

$$I = \int_{a}^{a+nh} u(t)dt = \frac{h}{3}\Big[u_0 + 4u_1 + 2u_2 + 4u_3 + \ldots + 4u_{n-3} + 2u_{n-2} + 4u_{n-1} + u_n\Big] + R_n \qquad (D.19)$$

where

h = step-size

n = number of steps (even)

u_k = u(a+kh)

$$R_n = - \frac{nh^5}{180} u^{IV}(\xi) \quad ; \quad (a \leq \xi \leq a + n\,h) \qquad (D.20)$$

= truncation error

The integral (D.18) always runs from the mid-point t_M of a trajectory segment to its end point t_2 or its initial point t_1 (see (3.12) and (3.13)). To take into account the fact that the integrand varys more rapidly with time near t_1 or t_2 than it does near t_M, the integral is evaluated over four sub-intervals with different step-sizes. These four intervals are

I_1: $h_1 = T_s$, $n_1 = 8$

I_2: $h_2 = 2T_s$, $n_2 = 8$

I_3: $h_3 = 4T_s$, $n_3 = 8$

I_4: The values of n and h for the fourth sub-interval are calculated using

$d = 8\,T_s$

$T_r = |t_i - t_M| - n_1h_1 - n_2h_2 - n_3h_3$

$= |t_i - t_M| - 56\,T_s \qquad (i = 1 \text{ or } 2)$

$n_4 = 2\,\text{Integer}\left[T_R/2d\right]$

$h_4 = T_R/n_4$

This method insures that the interval for I_4 is divided into an even number of steps approximately d in length.

For a small planet (Mercury, Venus, Earth, Mars) the parameter T_s is assigned the values

$T_s = 0.5$ days (heliocentric leg)

$T_s = 0.02$ days (planetocentric leg) (D.21)

while for a large planet (Jupiter, Saturn, Uranus, Neptune) it has the values

$$\begin{aligned} T_s &= 2.5 \text{ days} \quad \text{(heliocentric leg)} \\ T_s &= 0.5 \text{ days} \quad \text{(planetocentric leg)} \end{aligned} \tag{D.22}$$

These values are picked to provide a balance between running time and accuracy.

The value of the integral in (D.18) is given by the sum of the integrals over the sub-intervals.

$$I = I_1 + I_2 + I_3 + I_4 \tag{D.23}$$

To illustrate the accuracy of this procedure, a comparison between the perturbations obtained by quadrature and those found by numerical integration is given for

1) Heliocentric Ellipse (Earth to Venus)

t_1 = 2441478.8 days $\qquad$ t_M = 2441556.4599 days

t_2 = 2441634.11977 days

	Quadrature	Numerical Integration	Difference
$\delta r(t_1)$	35,164.67 km	35,267.35 km	102.78 km
$\delta v(t_1)$	39.723 m/sec	40.237 m/sec	.514 m/sec

2) Planetocentric Hyperbola (about Venus)

t_1 = 2441634.11977 days $\qquad$ t_M = 2441636.0597 days

t_2 = 2441637.99955 days

	Quadrature	Numerical Integration	Difference
$\delta r(t_1)$	1482.11 km	1512.57 km	30.46 km
$\delta v(t_1)$	26.470 m/sec	26.489 m/sec	.190 m/sec

3) Heliocentric Ellipse (Earth to Jupiter)

t_1 = 2443787.0 days t_M = 2444040.0151 days

t_2 = 2444293.03027 days

	Quadrature	Numerical Integration	Difference
$\delta r(t_2)$	687,602.28 km	689,394.07 km	1791.79 km
$\delta v(t_2)$	116.409 m/sec	117.202 m/sec	.793 m/sec

4) Planetocentric Hyperbola (about Jupiter)

t_1 = 2444293.03027 days t_M = 2444376.7112 days

t_2 = 2444460.39204 days

	Quadrature	Numerical Integration	Difference
$\delta r(t_1)$	355,455.46 km	356,310.0 km	854.54 km
$\delta v(t_1)$	147.690 m/sec	148.114 m/sec	0.424 m/sec

Errors in the calculation of the perturbations by the analytic quadrature method are on the order of 1% or less. Position perturbations tend to be more accurate than the velocity perturbations. This is due to the fact that the true A and B sub-matrices in the state transition matrix (see (D.14)) are more accurately approximated by their value on the two-body reference trajectory than are the C and D sub-matrices.

D.3 Calculation of Perturbed State Transition Matrix

It was stated in (D.7) and (D.10) that the state variation $\delta\underline{x}$ and the state transition matrix both satisfy the same differential equation.

$$\delta\dot{\underline{x}}(t) = F(t)\delta\underline{x}(t) \tag{D.7}$$

$$\dot{\Phi}(t,t_0) = F(t)\Phi(t,t_0) \tag{D.10}$$

Furthermore, if a perturbing term $\underline{f}$ is added to (D.7), its solution becomes

$$\delta\underline{x}(t) = \Phi(t,t_0)\delta\underline{x}(t) + \int_{t_0}^{t} \Phi(t,\tau)\underline{f}(\tau)d\tau \tag{D.17}$$

for

$$\delta\dot{\underline{x}}(t) = F(t)\delta\underline{x}(t) + \underline{f}(t) \tag{D.16}$$

A similar form may be derived for the perturbed state transition matrix. Let

$$\dot{\Phi}_0(t,t_0) = F_0(t)\ \Phi_0(t,t_0) \tag{D.24}$$

be the differential equation for the pure two-body problem while

$$\dot{\Phi}(t,t_0) = F(t)\Phi(t,t_0) \tag{D.25}$$

is the differential equation for the perturbed two-body problem. Note that

$$F(t) = F_0(t) + F_d(t)$$

$$= \begin{bmatrix} 0 & I \\ G & 0 \end{bmatrix} + \begin{bmatrix} 0 & 0 \\ G_d & 0 \end{bmatrix}. \tag{D.26}$$

where

$$G_d = \left.\frac{\partial \underline{a}_d}{\partial \underline{x}}\right|_0 \tag{D.27}$$

Substituting (D.26) into (D.25) yields

$$\dot{\Phi}(t,t_0) = F_0(t)\Phi(t,t_0) + F_d(t)\Phi(t,t_0) \tag{D.28}$$

Let

$$\Phi(t,t_0) = \Phi_0(t,t_0) + \delta\Phi(t,t_0) \tag{D.29}$$

(D.29)

Then, (D.28) becomes

$$\dot{\Phi}_0(t,t_0) + \delta\dot{\Phi}(t,t_0) = F_0(t)\Phi_0(t,t_0) + F_0(t)\delta\Phi(t,t_0) + F_d(t)\Phi_0(t,t_0) + F_d(t)\delta\Phi(t,t_0) \tag{D.30}$$

Eliminating the two-body terms and neglecting the product $F_d(t)\delta\Phi(t,t_0)$ leaves

$$\delta\dot{\Phi}(t,t_0) = F_0(t)\delta\Phi(t,t_0) + F_d(t)\Phi_0(t,t_0) \tag{D.31}$$

By comparing (D.31) with (D.16), the solution analogous to (D.17) is

$$\delta\Phi(t,t_0) = \Phi_0(t,t_0)\delta\Phi(t_0,t_0) + \int_{t_0}^{t} \Phi_0(t,\tau)F_d(\tau)\Phi_0(\tau,t_0)\,d\tau \tag{D.32}$$

Inserting (D.32) into (D.29) and recognizing that

$$\delta\Phi(t_0,t_0) = 0$$

yields

$$\Phi(t,t_0) = \Phi_0(t,t_0) + \int_{t_0}^{t} \Phi_0(t,\tau)F_d(\tau)\Phi_0(\tau,t_0)d\tau \qquad (D.33)$$

which is an approximate solution for a many-body state transition matrix.

The errors associated with the use of the pure two-body state transition matrix rather than the actual many body matrix were the major source of inaccuracy in the perturbed conic analysis. However, since these errors were not excessive, it was felt that the increased computation time associated with the above calculation of an approximate many-body state transition matrix was not justified. No numerical studies on the accuracy of the above technique were performed.

Appendix E

Trajectory Description Data

E.1 Description of Tables

This appendix presents the detailed data needed for the specification of the trajectories determined in Chapter 5-7. The following sections contain tables of

1) Planetary position in the heliocentric ecliptic coordinate system at each sphere of influence (SOI) entry and exit time.

2) Planetary velocity in the heliocentric ecliptic coordinate system at each SOI entry and exit time.

3) Position of SOI entry and exit points in the planetocentric ecliptic coordinate frame.

4) True heliocentric velocity at each SOI entry and exit point.

5) True planetocentric velocity at each SOI entry and exit point.

The true velocities at each SOI entry and exit point are determined by numerical integration of each trajectory leg as described in Section 5.4. The time of passage through each SOI entry and exit point may be found in Chapters 5-7. Planets are referred to by number in the tables in the following manner

Number	Planet	Number	Planet
1	Mercury	5	Jupiter
2	Venus	6	Saturn
3	Earth	7	Uranus
4	Mars	8	Neptune

E.2 Dual Planet Reconnaissance Trajectory

Planetary Position (km)

Point	Planet	x	y	z
1	3	-27,683,569	-149,351,633	0
2	2	-85,946,304	64,291,179	5,849,706
3	2	-92,494,950	54,464,844	6,090,584
4	4	9,298,184	-216,541,101	-4,783,633
5	4	20,235,530	-214,917,173	-5,017,472
6	3	150,071,922	1,341,038	0

Planetary Velocity (km/sec)

Point	Planet	v_x	v_y	v_z
1	3	28.803850	-5.536705	0.0
2	2	-21.115118	-28.219406	0.824872
3	2	-17.916849	-30.347939	0.610865
4	4	25.142150	3.112230	-0.550617
5	4	25.057758	4.344065	-0.522634
6	3	-0.752478	29.680227	0.0

Planetocentric Coordinates of SOI Entry and Exit Points (km)

Point	Planet	x	y	z
1	3	-1,618,847	1,228,772	-723,696
2	2	1,289,792	-678,612	-67,123
3	2	-1,457,233	56,086	43,682
4	4	1,139,936	1,065,458	112,352
5	4	-1,151,504	-1,053,602	1,060,012
6	3	2,124,226	309,891	214,270

True Heliocentric Velocity at SOI Entry and Exit Points (km/sec)

Point	Planet	V_x	V_y	V_z
1	3	25.411804	-3.308020	-1.496488
2	2	-28.702396	-24.100878	1.225602
3	2	-26.543009	-30.113072	0.865247
4	4	19.925562	-1.771693	-1.114716
5	4	19.783087	-0.479968	0.012257
6	3	-11.562989	27.887921	0.623309

True Planetocentric Velocity at SOI Entry and Exit Points (km/sec)

Point	Planet	V_x	V_y	V_z
1	3	-	-	-
2	2	-7.587318	4.118546	0.400726
3	2	-8.626212	0.234868	0.254384
4	4	-5.216591	-4.883929	-0.564099
5	4	-5.274674	-4.824036	0.534891
6	3	-	-	-

E.3 Grand Tour Trajectory

Planetary Position (km)

Point	Planet	x	y	z
1	3	146,373,093	30,840,193	0
2	5	-730,966,280	341,268,726	14,992,492
3	5	-793,050,422	172,374,356	17,066,856
4	6	-1,392,750,100	-367,498,888	61,896,089
5	6	-1,351,245,940	-523,607,941	62,947,475
6	7	-508,598,411	-2,816,199,860	-3,939,139
7	7	-417,872,638	-2,835,394,500	-5,185,687
8	8	825,783,251	-4,452,305,730	72,635,448

Planetary Velocity (km/sec)

Point	Planet	v_x	v_y	v_z
1	3	-6.627671	29.040716	0.0
2	5	-5.683434	-11.237136	0.172861
3	5	-2.929249	-12.166462	0.114945
4	6	1.929444	-9.356882	0.085318
5	6	2.952499	-9.024942	0.038810
6	7	6.653486	-1.521178	-0.091945
7	7	6.689117	-1.304052	-0.091596
8	8	5.299626	1.020036	-0.143199

Planetocentric Coordinates of SOI Entry and Exit Points (km)

Point	Planet	x	y	z
1	3	-422,358	2,090,193	327,087
2	5	52,179,576	-56,112,733	1,461,922
3	5	-76,427,535	-88,025	5,684,043
4	6	90,303,036	25,960,699	-5,635,961
5	6	18,853,800	-92,130,386	-4,109,294
6	7	-7,355,051	100,977,635	2,943,333
7	7	36,980,520	-94,149,082	5,256,825
8	8	-68,924,481	152,861,419	-8,235,400

True Heliocentric Velocity at SOI Entry and Exit Points (km/sec)

Point	Planet	v_x	v_y	v_z
1	3	-8.729043	38.773437	1.658246
2	5	-12.546516	-3.447447	0.060104
3	5	-13.280658	-12.488954	0.910924
4	6	-8.652141	-12.357576	0.746294
5	6	5.181211	-19.749870	-0.442043
6	7	7.716297	-16.446444	-0.533078

Point	Planet	v_x	v_y	v_z
7	7	12.174013	-15.208984	0.691257
8	8	12.136149	-14.246205	0.684301

True Planetocentric Velocity at SOI Entry and Exit Points (km/sec)

Point	Planet	v_x	v_y	v_z
1	3	-	-	-
2	5	-6.862569	7.789369	-0.232962
3	5	-10.351326	-0.322564	0.795978
4	6	-10.581829	-3.000683	0.660993
5	6	2.228758	-10.724730	-0.480851
6	7	1.062830	-14.925182	-0.441132
7	7	5.484978	-13.904982	0.782847
8	8	-	-	-

E.4 Periodic Trajectory

Planetary Position (km)

Point	Planet	x	y	z
1	3	115,517,131	-98,137,483	0
2	2	-98,406,259	42,926,751	6,271,195
3	2	-104,690,651	24,078,614	6,371,004
4	2	-97,993,845	43,854,474	6,260,237
5	2	-104,439,345	25,127,936	6,371,140
6	2	-97,465,377	45,010,278	6,245,750
7	2	-104,152,073	26,274,532	6,370,544
8	3	149,582,514	10,210,861	0
9	3	144,544,696	38,009,310	0
10	3	149,721,363	8,463,429	0
11	3	145,020,497	36,278,351	0
12	2	-96,870,027	-47,526,925	4,924,934

Planetary Velocity (km/sec)

Point	Planet	V_x	V_y	V_z
1	3	18.800505	22.595294	0.0
2	2	-14.161646	-32.263762	0.367108
3	2	-8.029999	-34.286904	-0.014566
4	2	-14.463523	-32.130379	0.386568
5	2	-8.371178	-34.206640	0.006423
6	2	-14.839637	-31.959383	0.410832
7	2	-8.744011	-34.114777	0.029399
8	3	-2.515094	29.612395	0.0
9	3	-8.062106	28.702144	0.0
10	3	-2.167525	29.633935	0.0
11	3	-7.715572	28.790893	0.0
12	2	15.182219	-31.602193	-1.314630

Planetocentric Coordinates of SOI Entry and Exit Points (km)

Point	Planet	x	y	z
1	3	247,388	-639,293	-2,045,577
2	2	726,703	511,959	-1,156,885
3	2	-1,279,966	527,150	460,850
4	2	1,283,436	-547,542	-426,113
5	2	-770,819	372,484	-1,181,388
6	2	748,191	-351,377	1,202,217
7	2	9,682	-767,274	-1,240,878
8	3	337,614	1,396,334	-1,609,518
9	3	1,614,003	107,287	1,427,503
10	3	1,637,219	-113,046	-1,400,362
11	3	1,107,649	-1,140,039	-1,458,666
12	2	-538,663	296,754	-1,323,012

True Heliocentric Velocity at SOI Entry and Exit Points (km/sec)

Point	Planet	V_x	V_y	V_z
1	3	17.323915	20.157965	-3.267526
2	2	-16.616974	-34.071864	4.356735
3	2	-12.484461	-32.404149	1.506887
4	2	-18.920016	-30.231828	1.908059
5	2	-11.046420	-32.921844	-4.047927
6	2	-17.512140	-30.658423	-3.641063
7	2	-8.650968	-36.809919	-4.202766
8	3	-3.262805	26.747620	3.254240
9	3	-4.699129	28.972881	2.858207
10	3	1.194127	29.890394	2.857028
11	3	-5.477269	26.475428	-2.992208
12	2	16.261390	-33.864871	3.969588

True Planetocentric Velocity at SOI Entry and Exit Points (km/sec)

Point	Planet	V_x	V_y	V_z
1	3	-	-	-
2	2	-2.455124	-1.807893	3.989942
3	2	-4.455058	1.883022	1.531741
4	2	-4.457173	1.899298	1.532338
5	2	-2.631615	1.269900	-4.102211
6	2	-2.625721	1.284945	-4.097597
7	2	0.093025	-2.694363	-4.232504
8	3	-0.746902	-2.862650	3.253536
9	3	3.351399	0.267886	2.882569
10	3	3.348385	0.253327	2.879679
11	3	2.239589	-2.317191	-2.991828
12	2	-	-	-

REFERENCES

1. Minovitch, M.A., "The Determination and Characteristics of Ballistic Interplanetary Trajectories under the Influence of Multiple Planetary Attractions" Jet Propulsion Laboratory Technical Report TR32-464, 1964

2. Hunter, M.W., "Future Unmanned Exploration of the Solar System" Aeronautics and Astronautics, Vol. 2, No. 5, May, 1964

3. Battin, R.H., Astronautical Guidance, McGraw Hill Book Co., New York, 1964

4. Battin, R.H., " The Determination of Round-Trip Interplanetary Trajectories", Journal of Aerospace Sciences, Vol. 26, No. 9, Sept. 1959

5. Minovitch, M.A., "Utilizing Large Planetary Perturbations for the Design of Deep-Space, Solar Probe, and Out-of-Ecliptic Trajectories", Jet Propulsion Laboratory Report TR32-849, Dec., 1965

6. Myers, K., "Gravity-Assisted Trajectories for Solar Probe Missions in the Ecliptic Plane", AIAA Journal of Spacecraft and Rockets, Vol. 6, No. 6, June, 1969

7. Sturms, F. and Cutting, E., "Trajectory Analysis of a 1970 Mission to Mercury via a Close Encounter with Venus", AIAA Paper 65-90, 1965

8. Sturms, F., "Trajectory Analysis of an Earth-Venus-Mercury Mission in 1973", Jet Propulsion Laboratory Report TR32-1062, January, 1967

9. VanderVeen, A., "The 1978 Venus-Swingby-to-Mercury Mission", Bellcomm Technical Memo TM-69-1013-2, February, 1969

10. Young, R.E., "The Two-Planet Flyby Problem", MIT Experimental Astronomy Laboratory Progress Report PR-3, January, 1967

11. VanderVeen, A., "Triple Planet Ballistic Flybys of Mars and Venus" AAS Paper No. 68-114, Sept. 1968 (Also Journal of Spacecraft and Rockets, Vol.6, No. 4, April, 1969)

12. Hollister, W.M., "The Mission for a Manned Expedition to Mars", Sc.D. Thesis in Instrumentation, M.I.T., May, 1963

13. Hollister, W.M., "Mars Transfer via Venus", AIAA Paper 64-647, August, 1964

14. Sohn, R.L., "Venus Swingby Mode for Manned Mars Missions", Journal of Spacecraft and Rockets, Vol. 1, No. 5, Sept.-Oct., 1964

15. Crocco, G.A., "One Year Exploration Trip, Earth-Mars-Venus-Earth", Proceedings of the VIIth International Astronomical Conference, Rome, 1956

16. Silver, B., "Grand Tours of the Jovian Planets", AIAA Paper 67-613, August, 1967

17. Friedlander, A.L., "Guidance Analysis of the Multiple Outer Planet (Grand Tour) Mission", Journal of Spacecraft and Rockets, Vol. 3, No. 10, Oct., 1966

18. Deerwester, J., "Jupiter Swingby Missions to Non-Specific Locations in Interplanetary Space", NASA TN D-5271, June, 1969

19. Deerwester, J., "Jupiter Swingby Missions to the Outer Planets", AIAA Journal of Spacecraft and Rockets, Vol. 3, No. 10, Oct. 1966

20. Kingsland, L., "Trajectory Analysis of a Grand Tour Mission to the Outer Planets", AIAA Paper 68-1055, 1968

21. Long, J.E., "To the Outer Planets", Aeronautics and Astronautics, Vol. 7, No. 6, June 1969

22. Hollister, W.M., "Periodic Orbits for Interplanetary Flight", Measurement Systems Laboratory Report RE-36, 1968

23. Menning, M.D., "Free-Fall Periodic Orbits Connecting Earth and Venus", S.M. Thesis in Dept. of Aeronautics and Astronautics, M.I.T., July, 1968

24. Hickman, D.E., "Guidance Requirements for Periodic Orbits", S.M. Thesis in Dept. of Aeronautics and Astronautics, M.I.T., July, 1968

25. Rall, C.S., "Free-Fall Periodic Orbits Connecting Earth and Mars", Sc.D. Thesis in Department of Aeronautics and Astronautics, M.I.T., October, 1969

26. McDonald, W.T., "A Special Purpose Interplanetary Trajectory Computation Program for Guidance and Navigation Studies", MIT Experimental Astronomy Laboratory Report RE-19, 1965

27. Breakwell, J. and Perko, L., "Matched Asymptotic Expansions, Patched Conics, and the Computation of Interplanetary Trajectories", Progress in Astronautics and Aeronautics, Vol. 17, R.L. Duncombe, ed., Academic Press, New York, 1966

28. Slater, G. and Stern, R., "Simplified Midcourse Guidance Techniques", M.I.T. Experimental Astronomy Laboratory Report RE-18, February, 1966

29. Carlson, N., "Analytic Guidance Formulation for Many-Body Space Trajectories", Ph.D. Thesis in Dept. of Aeronautics and Astronautics, M.I.T., May, 1969

30. Zadeh, L. and Desoer, C., Linear System Theory, McGraw Hill Book Company, New York, 1963

31. Danby, J.M.A., "Matrix Methods in the Calculation and Analysis of Orbits", AIAA Journal, Vol. 2, No. 1, January, 1964

32. Fletcher, R. and Reeves, C., "Function Minimization by Conjugate Gradients", Computer Journal, Issue 2, 1964

33. ————, "System /360 Scientific Subroutine Package, (360A-CM-03X) Version III Programmer's Manual", IBM H20-205-3, 1968

34. Shak, B.V., Buehler, R.S. and Kempthorne, O., "Some Algorithms for Minimizing a Function of Several Variables", Journal of the SIAM, Vol. 12, No. 1, March, 1964

35. Escobal, P.R., Methods of Astrodynamics, Academic Press, New York, 1968

36. Stern, R.G., "Interplanetary Midcourse Guidance Analysis", Sc.D. Thesis in the Dept. of Aeronautics and Astronautics, M.I.T., May, 1963

37. Goodyear, W., "A General Method for the Computation of Cartesian Coordinates and Partial Derivatives of the Two-Body Problem", NASA CR-522, Sept. 1966

38. Hildebrand, F., Introduction to Numerical Analysis, McGraw Hill Book Company, New York, 1956

BIOGRAPHICAL NOTE

Stephen Summers Bayliss was born in Buffalo, New York on September 15, 1943. He lived in Hamburg, New York until the age of 10 when his family moved to western Massachusetts. He attended school in Pittsfield, Massachusetts and graduated from Pittsfield High School in 1961. He attended M.I.T. and received the degree of Bachelor of Science in Aeronautics and Astronautics in June, 1965. He was elected to Tau Beta Pi and Sigma Gamma Tau in his junior year.

Mr. Bayliss entered the graduate program in the Department of Aeronautics and Astronautics at M.I.T. in September, 1965. He received the degree of Master of Science in June, 1966. His S.M. thesis was entitled "Navigational Satellite Systems". Through September, 1969, his graduate program was supported by a National Science Foundation Graduate Fellowship. In September, 1969, Mr. Bayliss became a research assistant in the Measurement Systems Laboratory.

During summers Mr. Bayliss has been employed by the MIT Instrumentation Laboratory (now the Charles Stark Draper Laboratory) (1962, 1963), NASA Manned Spacecraft Center (1964), NASA Electronics Research Center (1965), TRW Systems, Inc. (1966), Aerospace Corporation (1967), and Bellcomm, Inc. (1968).

Mr. Bayliss is a member of the American Institute of Aeronautics and Astronautics. He is married to the former Miss Diane Davidson of Quincy, Massachusetts.